AD-A056 218 CONSTRUCTION ENGINEERING RESEARCH LAB (ARMY) CHAMPAI--ETC F/G 9/5
DEVELOPMENT OF CONDUIT DESIGN ANALYTICAL PROCEDURE.(U)
JUN 78 W CROISANT, P NIELSEN, D SIEBER

UNCLASSIFIED CERL-IR-M-234 NL

1 OF 2
AD A056218

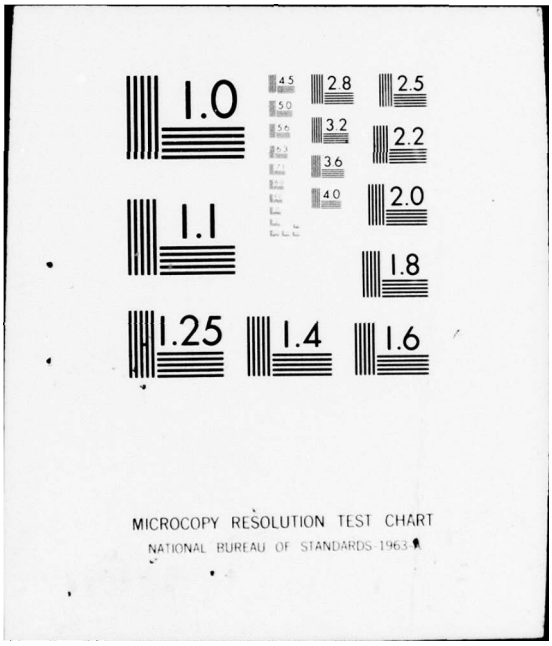
1.0
1.1
1.25
1.4
1.6
1.8
2.0
2.2
2.5
2.8
3.2
3.6
4.0
4.5
5.0
5.6
MICROCOPY RESOLUTION TEST CHART
NATIONAL BUREAU OF STANDARDS-1963-A

construction engineering research laboratory

LEVEL II

INTERIM REPORT M-234
June 1978
EMI Shielding of Conduit Systems

DEVELOPMENT OF CONDUIT DESIGN ANALYTICAL PROCEDURE

12

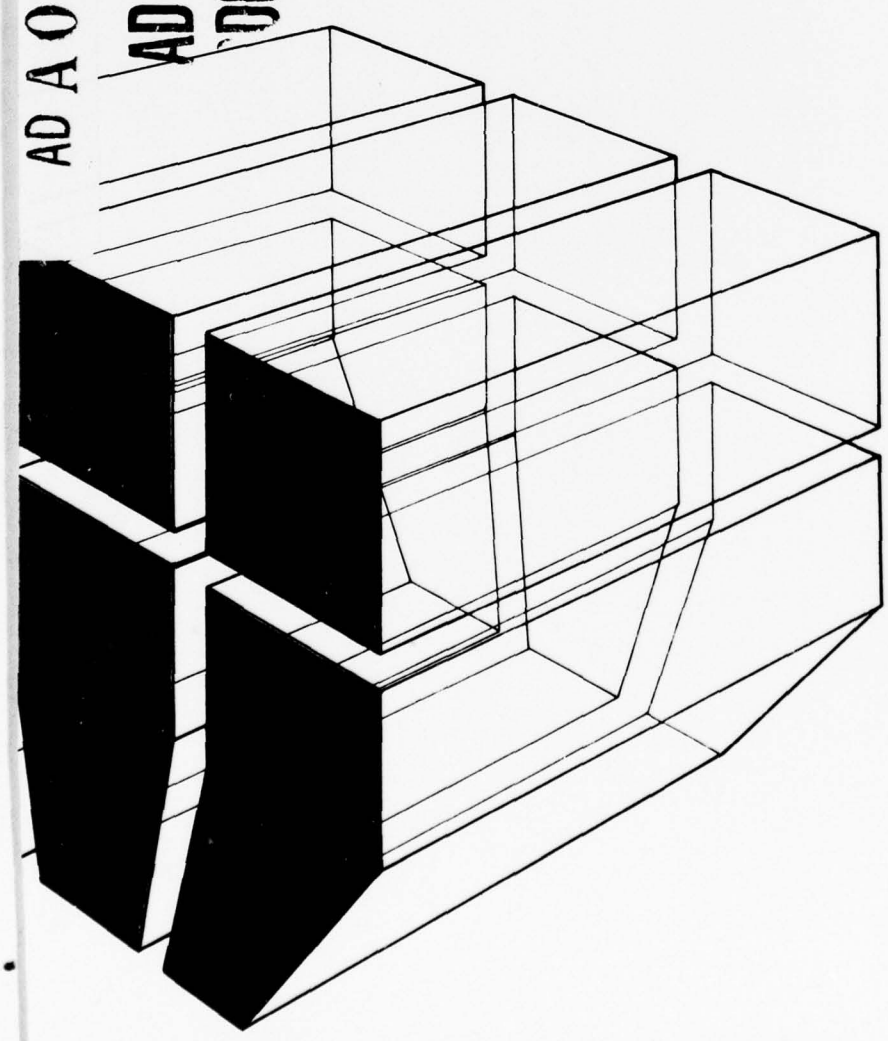

by
W. Croisant
P. Nielsen
D. Sieber
R. McCormack

CERL

The contents of this report are not to be used for advertising, publication, or promotional purposes. Citation of trade names does not constitute an official indorsement or approval of the use of such commercial products. The findings of this report are not to be construed as an official Department of the Army position, unless so designated by other authorized documents.

DESTROY THIS REPORT WHEN IT IS NO LONGER NEEDED
DO NOT RETURN IT TO THE ORIGINATOR

SECURITY CLASSIFICATION OF THIS PAGE (When Data Entered)

REPORT DOCUMENTATION PAGE

READ INSTRUCTIONS BEFORE COMPLETING FORM

1. REPORT NUMBER: CERL-IR-M-234	2. GOVT ACCESSION NO.
3. RECIPIENT'S CATALOG NUMBER	
4. TITLE (and Subtitle): DEVELOPMENT OF CONDUIT DESIGN ANALYTICAL PROCEDURE	5. TYPE OF REPORT & PERIOD COVERED: INTERIM rept.
	6. PERFORMING ORG. REPORT NUMBER
7. AUTHOR(s): W. Croisant, P. Nielsen, D. Sieber, Raymond G. R. McCormack	8. CONTRACT OR GRANT NUMBER(s)
9. PERFORMING ORGANIZATION NAME AND ADDRESS: CONSTRUCTION ENGINEERING RESEARCH LABORATORY, P.O. Box 4005, Champaign, IL 61820	10. PROGRAM ELEMENT, PROJECT, TASK AREA & WORK UNIT NUMBERS: 4A762719AT40 A1 020
11. CONTROLLING OFFICE NAME AND ADDRESS	12. REPORT DATE: June 1978
	13. NUMBER OF PAGES: 147 (149 P.)
14. MONITORING AGENCY NAME & ADDRESS (if different from Controlling Office)	15. SECURITY CLASS. (of this report): Unclassified
	15a. DECLASSIFICATION/DOWNGRADING SCHEDULE

16. DISTRIBUTION STATEMENT (of this Report)

Approved for public release; distribution unlimited.

17. DISTRIBUTION STATEMENT (of the abstract entered in Block 20, if different from Report)

18. SUPPLEMENTARY NOTES

Copies are obtainable from National Technical Information Service
Springfield, VA 22151

19. KEY WORDS (Continue on reverse side if necessary and identify by block number)

models
EMP analysis
conduit shielded circuits

20. ABSTRACT (Continue on reverse side if necessary and identify by block number)

This report presents proposed models for analysis of the electromagnetic pulse (EMP) signals in conduit shielded circuits. The models are intended for use in an analytical procedure for evaluating conduit system designs currently being developed.

The development of preliminary models for calculating (1) EMP penetration in solid conduit, (2) EMP leakage through defects, and (3) the effect of

DD FORM 1 JAN 73 1473 EDITION OF 1 NOV 65 IS OBSOLETE

Block 20 continued.

circuit impedances on EMP induced signals is presented. EMP properties and conduit physical properties important to the conduits shielding characteristics are examined. Both time domain and frequency domain analyses are presented.

FOREWORD

This investigation was performed for the Directorate of Military Construction, Office of the Chief of Engineers (OCE), under Project 4A762719AT40, "Mobility, Soils, and Weapons Effects," Technical Area A1, "Weapons Effects and Protective Structures," Work Unit 020, "EMI Shielding of Conduit Systems." The applicable QCR is 1.03.010. The OCE Technical Monitor was Mr. H. McCauley, DAEN-MCE-D.

This investigation was performed by the Engineering and Materials Division (EM), U.S. Army Construction Engineering Research Laboratory (CERL). Dr. G. R. Williamson is Chief of EM.

Appreciation is expressed to Dr. D. J. Leverenz and Messrs. D. Hannum, M. J. Pollock, J. Hall, and M. Hsu of CERL for their contributions to the study. Appreciation is also expressed to Dr. J. Verdeyen of the University of Illinois at Urbana-Champaign, who provided technical guidance in his capacity as an expert consultant.

COL J. E. Hays is Commander and Director of CERL, and Dr. L. R. Shaffer is Technical Director.

CONTENTS

TABLES

TABLES (Cont'd)

FIGURES

FIGURES (Cont'd)

FIGURES (Cont'd)

FIGURES (Cont'd)

DEVELOPMENT OF CONDUIT DESIGN
ANALYTICAL PROCEDURE

1 INTRODUCTION

Background

Electromagnetic shielding is often required in the design of Army facilities in order to protect electronic or electrical systems or components from the effects of unwanted electromagnetic energy.* These effects range from equipment malfunction to actual component damage. Although many sources of electromagnetic interference (EMI)† generate sufficient energy in stray or unwanted electromagnetic fields to cause malfunction of electronic equipment, damage from these sources is unlikely. The possibility of damage is greatest from the high energy contained in an electromagnetic pulse (EMP) resulting from a nuclear detonation[1] or the high currents associated with a lightning stroke.

The most common method of providing protection against EMP is to place the equipment in electromagnetically shielded zones within the hardened facility. In large, complex facilities, shielding is required in several locations or zones, which require electrical interconnections for electrical power and data transmission, monitor and control signals, and other general communication needs. The most practical way to make the electrical interconnections is by conventional wiring or cabling. However, if these wires and cables are routed through unshielded zones, any EMP which occurs will induce potentially damaging pulses on these wires.[2] It is therefore essential

*Two recent examples are the SAFEGUARD BMD site, which required 80-dB EMP shielding in addition to EMI shielding of certain portions of the facility, and the STTF (Systems Technology Test Facility), Kwajalein, which required 40- to 76-dB EMI shielding.

†"Electromagnetic interference" is a general term commonly used to describe any type of radiated electromagnetic energy which may interfere with operation of electrical or electronic equipment or instrumentation. Nuclear electromagnetic pulse is a specific type of EMI having the form of a single pulse of electromagnetic energy. The shape and magnitude of the pulse (which determines its spectral energy density content) is predictable for various threats. Radio frequency interference is another specific kind of EMI within the radio frequency spectrum.

[1]B. D. Favaudo and L. C. Martin, *Review of Factors for Application in Component Damage Analysis*, Protection Engineering and Management (PEM) note, PEM-52 (September 1976).

[2]E. F. Vance, *Coupling to Cables*, DNA Handbook Revision, Chapter 11, ADB001204 (Defense Nuclear Agency, December 1974); and E. F. Vance, *Design Guidelines for the Treatment of Penetrations Entering Communications Facilities*, ADB007076 (Defense Nuclear Agency, August 1975).

that all wiring and cabling penetrating the shielded zones also be shielded against EMP. Such shielding can be accomplished by using individually shielded wires or cables or by routing the wiring and cabling through metal conduits. Physical protection and shielding can be provided by these conduits, which are typically used for electrical entry[3] and have been used for signal cable routing in EMP-protected systems.[4]

The facility designer must therefore be aware of the shielding properties of the various components which make up a conduit system so that an adequate shield for the wiring and cabling will be provided. The components of the conduit system may include the conduit, conduit fittings, and other conduit-related hardware items such as couplings, unions, junction boxes, pull boxes, cast fittings, and flexible joints. Most of these related items are standard electrical items, since few items have been developed specifically for EMP-hardened applications.[5] The conduit system does not provide infinite shielding, but is compromised by the limited shielding of the conduit itself, by deficiencies inherent in some standard hardware items, and in some cases by improper installation practices.[6]

To date, conduit design has been accomplished without adequate guidance which would enable accurate determination of the conduit system shielding and prediction of induced pulse energy on conduit-housed circuits. The overall EMP protection acceptability determination has been accomplished after design and construction by extensive analysis and field and laboratory testing. These extensive evaluations and other studies in this technological area have generated a wealth of technical data, but using these data requires the designer to review an excessive amount of literature, not all of which is readily available. Although TM5-855-5[7] contains a variety of EMP design information, it does not contain the detailed information required for conduit system design and evaluation.

---

[3]E. F. Vance, *Electromagnetic - Pulse Handbook for Electric Power Systems,* ADA009228 (Defense Nuclear Agency, February 1975), p 145.

[4]D. J. Leverenz, R. G. McCormack, and P. H. Nielsen, *EMP Shielding Properties of Conduit Systems and Related Hardware,* Technical Report C-19/ADA012729 (U. S. Army Construction Engineering Research Laboratory [CERL], June 1975), p 11.

[5]*As-Built Survey and Evaluation of EMP/RFI Protective Features,* Vol. 2, HND-SP-72-145-ED-R (Huntsville Division [HND] of the U. S. Army Corps of Engineers, August 1973); and *SAFEGUARD EMP/RFI Lessons Learned (SAFEGUARD Ground Facilities),* HND-SP-75-350-ED-SR (HND, 31 December 1975).

[6]D. J. Leverenz, R. G. McCormack, and P. H. Nielsen, *Development and Evaluation of Repairs and EMP Leaks in Conduit Systems,* Technical Report C-17/ADA011223 (CERL, April 1975).

[7]*Nuclear Electromagnetic Pulse Protection,* TM 5-855-5 (Department of the Army, February 1974).

An analytical design procedure which can be used to theoretically predict the shielding of complex conduit systems is therefore needed. Such a procedure would allow the conduit system designer to systematically assess the EMP hardness of conduit systems and assure a cost-effective design which provides adequate EMP protection of sensitive electronic/electrical equipment.

Objective

The objective of this study is to develop a model of conduit system shielding behavior for use in an analytical procedure which is to be included in TM 5-855-5. The procedure, which will be used in the design of EMP-hardened conduit systems, is intended to provide District engineer personnel with a practical basis for evaluating the potential EMP penetration (and hence shielding effectiveness) of the more common conduit configurations, and for predicting the induced signals on conductors within conduit systems.

Scope

This report presents preliminary models for EMP leakage into electrical conduits. These models are intended for use in an analytical procedure for conduit system design under development at CERL. The analytical procedure will enable a designer to predict the EMP shielding performance on EMP hardness of proposed conduit systems. The model developed represents a significant portion of the final procedure; however, for actual determination of signal levels induced on conduit protected conductors, the following additional information is necessary: (a) the current induced on the conduit, (b) cross-coupling between conductors in the same conduit, (c) EMP leakage characterization (analytical and/or empirical) of conduit-related hardware items. This information can either be derived from the literature or further experimental and mathematical studies. The final analytical procedure will include enough of this information to be independent and not rely on external sources of information.

The model developed can be applied to shielded cables; however, since braided cables have additional coupling mechanisms not present in solid shields, the model will not give an accurate representation of the shielding behavior of braided cables.

Approach

Development of the leakage model for conduit systems involved three major efforts: (a) literature search, (b) mathematical analysis, and (c) empirical studies. The detailed literature search was performed to provide a summary of previous efforts directed toward development of

mathematical models or procedures for predicting conduit system shielding. Analysis of existing data then permitted determination of the form for general models for predicting the signals on various circuits within conduits for specific conduit defects and for the inherent conduit shielding. Mathematical analysis was performed to expand and refine the models and show expected conduit circuit signals for a generalized pulse threat. Both time domain and frequency domain analyses were investigated. Empirical work utilizing pulse current injection testing was then performed to verify the time domain models and determine values for mathematical model coefficients for the various conduit hardware items.

Organization of Report

Chapter 2 describes the model for conduit leakage. The appendices provide detailed information on the development of the model. Pertinent characteristics of EMP are discussed in Appendix A. Appendix B describes the general experimental procedures used to obtain conduit and related hardware parameters necessary for the calculations used in the model. Appendix C presents the theoretical model of EMP penetration of solid conduit and the experimental verifications. Appendices D and E describe typical values of design dimensions and material properties of conduit, respectively. Appendices F through H detail the theoretical analyses and experimental evaluations used in developing the models. The annotated bibliography presents references which, although not required for use of the model, provide a source of additional information.

2 DESCRIPTION OF THE CONDUIT LEAKAGE MODEL

Overview

Efforts were directed toward developing and verifying mathematical techniques for determining the EMP field penetration into conduit systems and the level of induced signals on lines within the conduit resulting from such penetration. Although the analytical procedure occasionally involves complicated mathematical operations, computer calculations have held to a minimum. The proposed procedure uses simplified mathematical models which describe the major features of the induced signals, supplemented with empirical data from injected-current EMP tests of various hardware items. The procedure consists of the following steps:

a. Determination of conduit current and the acceptable signal levels (degree of hardness to be maintained). The conduit current, including magnitude and time variation, must be established. The actual nature of the conduit current depends on a number of factors--often in a rather complicated manner. It is beyond the scope of this study to detail the calculation of EMP pickup by conduit systems. Appendix A describes some general characteristics of EMP and the bibliography contains some references on the topic which can be used by the designer. Alternatively, the threat current may be supplied by the basic construction specification or may be assumed to have a peak magnitude of 500 to 10,000 amperes[8] with a waveshape similar to the incident EMP radiation. The degree of hardness required depends on the components and equipment connected to the conduit protected wires and cables. This information should be provided in the installation specifications.

b. Establishing the basic conduit design configuration and identifying the type and quantity of system components, including sections of conduit, conduit size, and conduit material; couplings; unions; unilets, condulets, etc; pull boxes; and junction boxes. Any defects such as openings or electrical discontinuities must also be identified.

c. Calculation of the EMP penetration of the conduit for the specified current. Because the basic shielding is provided by the solid conduit, the analyses start by considering the EMP penetration through the conduit wall itself. The procedure for this calculation can use either time domain or frequency domain analysis. This calculation is discussed in greater detail in the section of this chapter entitled Calculation of EMP Penetration of Solid Conduit.

[8] E. F. Vance, *Treatment of Penetrations Entering Communications Facilities*, ADB007076 (Defense Nuclear Agency, August 1975), p 2.

d. Determination of the effects of defects and components for specified current. In developing the mathematical model for the EMP penetration of some defects and hardware items, emphasis was placed on coordinating simple mathematical models with results of empirical evaluations of these items. This was done because the limited use of some of these items did not warrant a detailed mathematical analysis based on electromagnetic field theory. Although testing every type and variation of every hardware item was not possible, a representative selection has been tested and their properties tabulated. The procedure for this calculation can use either time domain or frequency domain analysis. This step is discussed further in the section of this chapter entitled Calculation of EMP Penetration of Defects, Conduit Fittings, and Related Hardware.

e. Accounting for propagation characteristics of the signal. For rapidly varying EMP-induced signals, the propagation must be analyzed using transmission line theory. The onset of the signal at the end of a conduit system will be delayed by the time it takes the signal to travel the distance from the location of the defect to the end of the conduit. Furthermore, possible reflections due to mismatch in termination of a transmission line may also arise.

For slowly varying signals, the transmission line properties become less significant, and in the limit, such problems approach the equivalent circuit problem with lumped parameters. The time delay due to propagation time becomes negligible for slowly varying signals, since the velocity of propagation is nearly that of the speed of light.

f. Accounting for the effect of circuit impedances and wire and cable type. A general mathematical model was developed for expressing the short circuit current in terms of inherent resistance (R) and inductance (L). This model can be modified to show the effects of increasing R and/or L. This step is discussed in the section of this chapter entitled Effects of Circuit Configuration on EMP-Induced Signals.

g. Accounting for possible signal summation. Development of methods for performing this step is planned for future studies.

h. Comparison of the composite EMP signal with the equipment susceptibility.

i. Redesign of the conduit system as required, based on problem areas identified in step h.

Calculation of EMP Penetration of Solid Conduit

This step involves determining the electromagnetic signal induced in the interior of a hollow circular cylinder because of a current

pulse* on the outer surface. Since the current pulse can take various forms, all of varying frequency content, a general solution (assuming constant permeability and conductivity) can be determined by calculating the time response of the conduit due to an impulse of electromagnetic energy, and then convoluting this response with any given input. Similarly, the Fourier transform of the internal electric field resulting from an impulse current (referred to in the literature as the surface transfer impedance) can be multiplied by the Fourier transform of the current pulse to obtain the frequency domain solution for the electric field.

To simplify calculation of the electric field inside the conduit, the modified Bessel functions appearing in the Laplace transform of the electric field are replaced in this model by their asymptotic expansions. The results obtained using the asymtotic form of the Bessel functions are valid for cylindrical shields that have inner radii which are large compared to the skin depth of the lowest frequency of interest in the surface current pulse.+ Two infinite series solutions for the electric field due to current impulse have been developed (see Appendix C)--one which converges for early times (Eq 1) and one which converges for late times (Eq 2):

$$E(a, \theta) = Q \left[\frac{8}{\pi^{3/2}\sqrt{ab}\ \mu\sigma^2(b-a)^3}\right] \left\{ \sum_{n=0}^{\infty} \frac{\exp\left[-\frac{(2n+1)^2}{\theta}\right]}{\theta^{3/2}} \left[\frac{(2n+1)^2}{\theta} - 1/2\right] \right\} \qquad \text{[Eq 1]}$$

$$\theta \geq 0$$

*The term "pulse" is used to refer to an arbitrary current injection of short duration; the term "impulse" is reserved for a signal of negligible duration whose magnitude is sufficiently large to induce a finite change on the system.

+It is shown in Appendix C that a (radius) to δ (skin depth) ratio is 10 for a 1-in. steel conduit at a frequency of 200 kHz assuming values of 150 for the relative permeability and 20×10^{-8} ohm-m for the resistivity.

$$E(a, \theta) = Q\left[\frac{8}{\pi^{3/2}\sqrt{ab}\ \mu\sigma^2(b-a)^3}\right]\left\{\frac{\sqrt{\pi}}{2}\left[\sum_{n=0}^{\infty}(-1)^{n+1}\ \frac{n^2\pi^2}{4}\right.\right.$$

$$\left.\left.\exp\left(\frac{-n^2\pi^2}{4}\theta\right)\right]\right\},\ \theta > 0 \qquad \text{[Eq 2]}$$

where E = internal electric field

Q = injected charge

a = inner radius

b = outer radius

σ = conductivity

μ = permeability

θ = relative time expressed in units of a characteristic diffusion time $\theta = t/T$

$T = \frac{\mu\sigma(b-a)^2}{4}$

$E(a, \theta)$ can be put in the form

$$E(a, \theta) = QFS(\theta) \qquad \text{[Eq 3]}$$

where Q = charge passed along the cylinder

$$F = \frac{8}{\pi^{3/2}\sqrt{ab}\ \mu\sigma^2(b-a)^3}$$

$\theta = t/T$

$S(\theta)$ = the two series representations denoted by braces in Eqs 1 and 2.

Thus, the unit impulse response for a circular cylinder of a specified size and material can be defined by the shield parameters T and F, which depend on the dimensions and material properties of the cylinder. Investigation (Appendix C) showed that these two parameters can be easily determined experimentally, which is important since the material properties of conduits are not readily known. Experimentation also indicated that once the parameters for one size cylinder of a given material are known, the parameters for another size cylinder of the same material can be found.

The electric field for a current pulse (I_c) other than an impulse can be determined by convolution with the impulse response (Eq 1 or Eq 2):

$$E(a, t) = QF \int_0^t I_c\,(t-\lambda)S\,(\lambda/T)d\,\lambda \qquad \text{[Eq 4]}$$

where E = internal electric field

Q = injected charge

$F = \dfrac{8}{\pi^{3/2}\sqrt{ab}\;\mu\sigma^2\,(b-a)^3}$

I_c = current pulse

S = series representations of impulse response

t = time

T = diffusion time $\dfrac{\mu\sigma(b-a)^2}{4}$

λ = an integration variable

Appendix C provides the detailed theoretical analysis and experimental evaluation of the model. The model assumes linearity; however, some deviations may occur at high current levels (saturation effects). Several examples of the impulse response, as well as results for other than impulse currents, are presented and compared with the experimental results and are in excellent agreement.

Calculation of EMP Penetration of Defects, Conduit Fittings, and Related Hardware

As previously indicated, the basic shielding of a conduit system is provided by the solid conduit itself. However, defects in the conduit such as cracks and breaks may seriously compromise the shielding. In addition, because the many fittings and related hardware items (e.g., couplings, unions, case access fittings, pull boxes, junction boxes, flexible sections) used in conduit systems have not been designed for use in EMP-hardened structures, they may also compromise the EMP shielding of the system. Thus, assessing the EMP penetration of the entire conduit system requires that the contribution of various defects, conduit fittings, and hardware items be evaluated.

Because mathematical analysis of even relatively simple defects, conduit fittings, and hardware items is a very difficult (and in some

cases very nearly impossible) task, some reliance must be placed on empirical results. On the other hand, the signals resulting from defects quite often depend on the magnitude and waveshape of the applied current as well as the characteristics of the defect itself; thus complete reliance on empirical data would necessitate the acquisition of enormous amounts of data to account for the potential variations in waveshape and characteristics of defects which might occur in actual conduit systems. The resultant volume of data would be difficult if not impossible to use, and extrapolation to situations for which data were not taken would not be easy.

The approach used is therefore a compromise between the theoretical and empirical. It uses relatively simple mathematical models supplemented with experimental evaluation of certain parameters.

To a first approximation, the signals induced on a wire within a conduit due to a defect can be considered to result from the wire coupling with the electric and magnetic fields associated with the current in the vicinity of the defect. The general model for the direct field penetration of a defect is proposed to be

$$V_L = RI + M\frac{dI}{dt} \qquad \text{[Eq 5]}$$

where V_L = voltage on the wire

R and M = coupling coefficients between the wire and the electric and magnetic fields, respectively

I = current pulse.

Appendix F describes development and testing of the model, and Appendix G provides the coefficients for some selected defects, fittings, and related hardware determined through empirical testing.

Determining the Effects of Circuit Configuration on EMP-Induced Signals

The signals induced on a wire inside a solid conduit due to an EMP depend on the configuration of the circuit associated with that wire. This section describes two configurations--open and short circuits.

Open Circuit

The open circuit voltage induced on a wire within a conduit can be expressed as the EMP-induced electric field integrated along the length of the conduit. The relation for this voltage is

$$V_{oc}(t) = \ell\, E(a, \theta) = \ell Q \left[\frac{8}{\pi^{3/2} \sqrt{ab}\ \mu\sigma^2 (b-a)^3}\right]$$

[Eq 6]

$$\frac{\sqrt{\pi}}{2} \left[\sum_{n=o}^{\infty} (-1)^{n+1} \frac{n^2\pi^2}{4} \exp\left(\frac{-n^2\pi^2}{4}\theta\right)\right.$$

where ℓ = length

Q = injected charge

a = inner radius

b = outer radius

σ = conductivity

μ = permeability

$\theta = t/T$

$T = \mu\sigma \frac{(b-a)^2}{4}$

After this integration, all that was introduced to modify the expression for the internal electric field was the length of the conduit. Because this modification is time-independent, the Fourier transform of the open-circuit voltage expression is equivalent to the Fourier transform of the internal electric field. Thus, the open circuit voltage frequency response is equivalent to the induced electric field frequency response described in the section of this chapter entitled Calculation of EMP Penetration of Solid Conduit.

Short Circuit

The short circuit current response to an impulse current pulse can be described to a good approximation by considering a lumped parameter circuit being driven by the integral of the electric field over the length of exposed circuit. Eq 7 gives an infinite series expression developed using this model:

$$I(t) = A \left[\frac{\sqrt{\alpha}}{\sin 2\sqrt{\alpha}} \exp(-\alpha\theta) + \sum_{n=1}^{\infty} \frac{(-1)^n n^2 \exp\left(\frac{-n^2\pi^2}{4}\theta\right)}{n^2 - \frac{4}{\pi^2}\alpha}\right] \qquad \text{[Eq 7]}$$

where α = dimensionless parameter which is the ratio of the conduit diffusion time T and the L/R time constant

R = inherent resistance

L = inductance

ℓ = length

$\theta = t/T$

$$A = \frac{\ell Q}{2\pi\sqrt{ab}} \frac{\mu}{\sigma} \frac{1}{L} \frac{1}{\sqrt{T}}$$

Appendix H describes the theoretical analysis and experimental evaluation of these models, which were found to be in good agreement with experimental results. Appendix H also contains graphs which enable rapid determination of peak current and time to occurrence of the peak current.

Frequency Domain Analysis

The preliminary analytical procedure developed by CERL primarily uses time domain analysis. The analysis of EMP penetration of solid conduit and of some conduit defects can also be done in the frequency domain. Development of transfer impedances and transfer functions for use in frequency domain analysis has been done by others. The results of some of this recent work[9] are summarized in Appendices C and F.

[9]H. A. Roberts, J. Capobianco, and F. Agee, *SAFEGUARD Buried Conduit Studies* (Harry Diamond Laboratories [HDL], undated).

3 CONCLUSIONS

This report has presented a preliminary model for the design of EMP-hardened conduit systems which Corps of Engineers design personnel can use to evaluate the potential EMP penetration of the more common conduit configurations and to predict the induced signals on conductors within conduit systems. The model developed is an essential portion of an analytical procedure for conduit system design, but additional information is necessary for completion of the procedure.

This report has also detailed the development of the proposed model. During the development, the following conclusions were reached:

a. The penetration of conduit by a current pulse can be calculated directly from the equations which govern the propagation of electromagnetic fields through conducting media. An exact expression for the Laplace transform of the electric field due to an impulse current can be calculated in a straightforward manner using standard Laplace transform theory; however, inversion of the exact transform is somewhat tedious, as it involves finding the roots of an expression involving Bessel functions and their cross products. A good approximation which involves asymptotic expansion of the Bessel functions may be used in many cases. Two infinite series solutions for the electric field in this case are presented (one of which converges for early times whereas the other converges for late times). The electric field for a current pulse other than an impulse can be determined using the convolution theorem. The convolution can be accomplished using numerical integration. Several examples of the impulse response, as well as results for other than impulse currents, are presented and compared with experimental results with excellent agreement.

b. The current arising on a shorted wire due to the electric field penetration of rigid conduit was found to be described to a good approximation by considering a lumped parameter circuit being driven by the integral of the electric field over the length of exposed conduit. An infinite series expression using this model has been developed and found to be in good agreement with experimental results.

c. The material properties for construction grade conduit are not readily available.

d. Transfer impedances or transfer functions present an alternate analytic approach for conduit system design. Transfer functions for solid conduit and a limited number of conduit or related hardware defects are available from the literature (see the annotated bibliography) or from work by other agencies. If the frequency domain approach is pursued, measurements on additional items should be made. Since, in general, the transfer impedance may be a complicated function, computerized

numerical integration techniques may be necessary to obtain the system response in the time domain. Existing programs will need to be adapted or new programs developed for this requirement.

e. A mathematical model can be developed for conduits with aperture-type defects which will define to a first approximation the induced current on wires internal to the conduit. A table of coefficients for this model can be prepared through empirical work; development of such a table will enable a rapid general solution to EMP threat currents.

APPENDIX A:

CHARACTERISTICS OF EMP

The EMP is characterized by large magnitude electromagnetic fields with short rise times (a few nanoseconds) and somewhat longer fall times (a few microseconds). Most of the energy associated with the EMP lies within the radio-frequency spectrum with a range from a few hertz to the very high frequency (VHF) band.

The EMP differs from most other natural (e.g., lightning) or man-made (e.g., radar) EMI in that the EMP's time waveform shows a faster rise time and a higher amplitude. Normally, most natural and man-made sources are confined to a narrow portion of the frequency spectrum, whereas the EMP occupies a rather wide portion. In addition, high-intensity EMP fields can occur over a large area almost simultaneously. Intense natural and man-made electromagnetic fields seldom have such a wide simultaneous distribution.

EMP fields can have considerable variation of magnitude, time dependence, and direction. One can, however, define a typical field environment which possesses the major features. For the most part, a double-exponential approximation can be used to describe the most important features

$$E(t) = E_o[e^{-\alpha t} - e^{-\beta t}] \qquad \text{[Eq A1]}$$

where α = the pulse decay time constant

β = the rise time constant

With $\alpha >> \beta$, E_o is approximately the peak value of the incident electric field strength. The values of these quantities depend on weapon characteristics and the location of the observer relative to the burst point; however, the following values are representative and can be used for purposes of illustration:

$$E_o \simeq 5.2 \times 10^4 \text{ volts/meter}$$

$$\alpha \simeq \frac{1}{6.7 \times 10^{-7} \text{ sec}}$$

$$\beta \simeq \frac{1}{3.8 \times 10^{-9} \text{ sec}}$$

This waveform is shown in Figure A1. The Fourier transform of this pulse is

$$E(\omega) = E_o \frac{\alpha - \beta}{(1+j\omega\alpha)(1+j\omega\beta)} \qquad \text{[Eq A2]}$$

The magnitude of $E(\omega)$ is plotted in Figure A2. Thus, a typical EMP is characterized by a very fast rise time with a peak electric field strength on the order of magnitude of 50 kV/m and a duration of approximately 1 μsec. The pulse contains significant energy at frequencies up to 100 MHz.

The fields incident on the earth's surface from a high altitude nuclear explosion can be modeled as a plane wave. The magnitude of the electric field strength E (volts/meter) in free space is related to the magnetic field strength H (amperes/meter) by the impedance of free space.

$$E = \eta_o H = (377 \text{ ohms})\ H \text{ volts/meter} \qquad \text{[Eq A3]}$$

Since the incident local field is assumed to be a plane wave, the magnetic field H has a time variation similar to the electric field and has a peak value

$$H_{peak} = \frac{E_{peak}}{377} \text{ amperes/meter} \qquad \text{[Eq A4]}$$

The EMP will, of course, be modified by propagation through a material other than free space (or air).

The exact electrical transient induced on a line or conduit system by an incident EMP is a complex function of location (buried or aboveground), length, terminations, etc. This problem is analyzed in detail in the Defense Nuclear Agency *EMP Handbook*,[10] and is not covered in this report. The analysis presented in this report is not dependent on a particular waveshape and is applicable to any arbitrary function. Thus, while it is important to know the induced signal for any actual calculation of conduit system response, it is not necessary to know the exact characteristics of this signal for an explanation of the procedure for the calculations. A reasonable approximation to use for illustration purposes is a magnitude of 0.5 to 10 kA[11] with a pulse shape (rise time, duration) similar to that of the incident field. This general type of transient would be expected to appear on a fairly long aboveground line. A transient appearing on a buried line would be expected to be lower in magnitude with attenuation of the high frequency components, resulting in a slower rise-time pulse.

[10] E. F. Vance, *EMP (Electromagnetic Pulse) Handbook*, DNA-2114H-2 (Defense Nuclear Agency, December 1974), Chapter 11, ADB001204. The total document, DNA-2114H-2, is classified confidential; however, Chapter 11 is available in an unclassified version from the Defense Documentation Center using the referenced AD number.

[11] E. F. Vance, *Design Guidelines for the Treatment of Penetrations Entering Communications Facilities*, ADB007076 (Defense Nuclear Agency, August 1975).

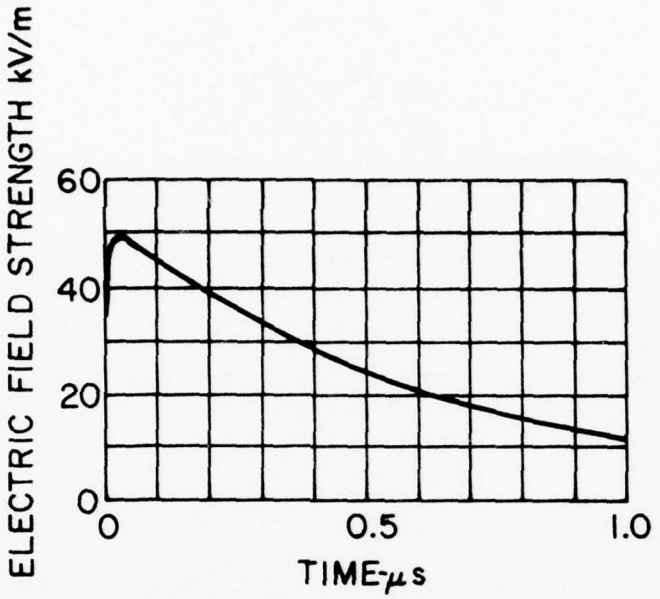

Figure A1. Two-exponential representation of the high-altitude EMP waveform. From E. F. Vance, *Electromagnetic-Pulse Handbook for Electric Power Systems*, ADA009228 (Defense Nuclear Agency, February 1975), p 26.

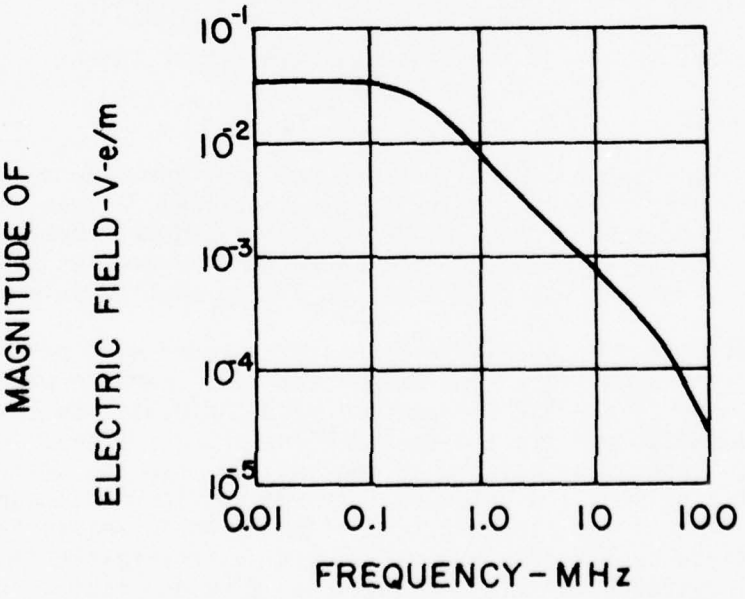

Figure A2. Magnitude of the spectrum of the two-exponential waveform. From E. F. Vance, *Electromagnetic-Pulse Handbook for Electric Power Systems*, ADA009228 (Defense Nuclear Agency, February 1975), p 26.

APPENDIX B:

EXPERIMENTAL PROCEDURE

As part of the development and evaluation of the analytical procedure, a program was developed to experimentally determine the EMP penetration of conduit with and without defects and of various conduit hardware items using injected-current tests. In addition, measuring fundamental material properties such as permeability and conductivity was necessary because these properties are not readily available for construction-grade materials.

Pulse Injection

Since the principal concern of this study is the effects of electromagnetic pulses, the experimental evaluation was primarily concerned with pulsed current. Two pulse-injection techniques were used to study the effects of EMP:

a. Capacitor discharge, for pulses of short duration

b. Battery discharge, for pulses of long duration.

The measurement setup for each was essentially the same.

Measurement Setup

Figure B1 shows a typical measurement configuration consisting of a pulse generator (see the following two sections), a test specimen composed of a section of conduit and conduit hardware items to be tested, a shielded enclosure to protect the measurement equipment used to measure the signals induced as a result of the applied pulse.

The test specimen was installed as the ground side of a parallel conduit transmission line. One end of the test specimen was closed with an end cap to prevent EMP leakage, and the other was inserted into a conduit stub fastened to the shielded enclosure. A sense wire of 12-gauge solid copper was fastened to the end cap, run the entire length of the test specimen, and extended into the shielded enclosure (see Figure B1). In some tests, each end of the sense wire was terminated in a resistance approximately equal to the characteristic impedance of the coaxial system consisting of the sense wire and test conduit.

The appropriate electronic equipment was selected according to the signal to be measured. The signals most often measured were (a) the voltage across the termination resistor of the sense wire, and (b) the current flowing in the sense wire with the sense wire shorted; i.e.,

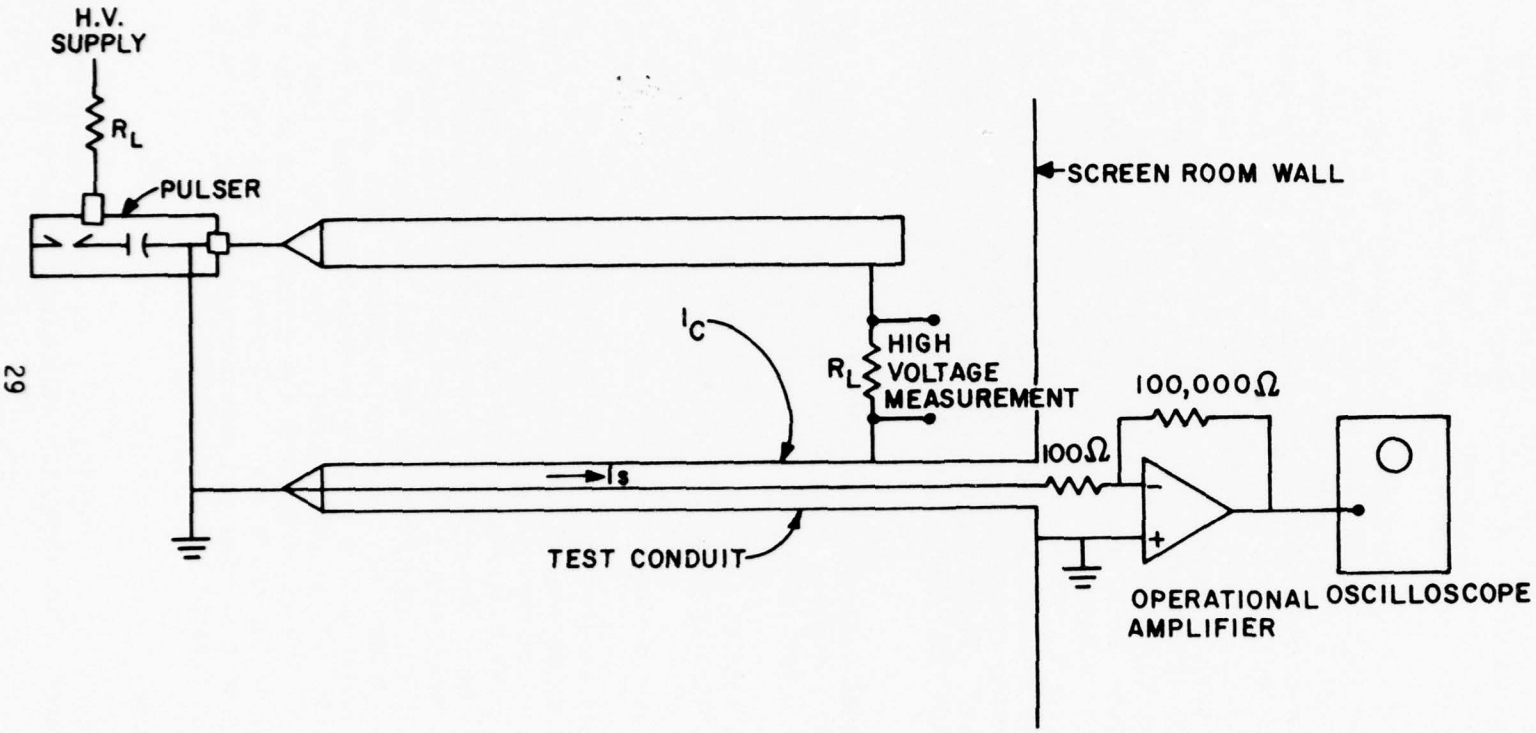

Figure B1. Parallel conduit transmission line. (Test configuration for fast risetime pulse injection.)

zero resistance termination. For low-level signals, an amplifier with a gain of 950 was used. A Pearson Model 411 current probe was used to detect the short circuit current. The signals were fed into an oscilloscope or an ERDAC III transient digitizer and recorder.

The ERDAC III is a digital recording oscilloscope with the capability of capturing and storing one-shot transients. It has a minimum sampling period of 1 μsec when sampling a single waveform. It also has up to four-channel measurement capability, but the sampling period per channel is multiplied by the number of channels used. Thus, for two-channel usage, as was common in deriving much of the data of this report, the sample interval per channel is once in 2 μsec. Each sample is stored with 10-bit resolution (1 part in 1024) and the overall amplitude accuracy is 0.5 percent of full scale. The ERDAC III has cathode ray tube (CRT) display of the stored signal and a movable cursor, the x and y coordinates of which are read out digitally. Thus, any point on a recorded curve may be quickly and accurately read out. The ERDAC III also includes a tape recording feature which enables recording of all stored transients on tape for later analysis by computer or other processor. Signals with rise times too fast to be sampled accurately with the ERDAC III were monitored and photographed on oscilloscopes.

The applied pulse was monitored with a Pearson Model 310 current probe, and the voltage across the transmission line termination was measured with a Tektronix 6015 high-voltage probe.

Modifications of this basic measurement configuration are described in the appropriate sections of this report.

Capacitor Discharge Current Injection

The source used for fast rise time pulse injection was a high voltage spark discharge pulser, as shown in Figure B1. A low inductance capacitor was charged up to the spark gap discharge voltage. When the gap fired, the capacitor was discharged into the parallel conduit transmission line. The rise time of the pulse produced was limited mainly by the inductance of the capacitor; the pulse length was determined by the value of the capacitor and the load resistance on the parallel conduit transmission line. The system used at CERL was a repetitive free-running pulser with a repetition rate determined by the voltage setting on the high voltage power supply. The firing voltage was controlled by adjustment of the spark gap and the concentration of the sulfur hexafluoride (SF_6) in the spark gap. Typical pulse peak values were 200 A with 5 to 10 nsec rise time and approximately 4 μsec e^{-1} fall time (where e is the base of natural logarithms).

Battery Discharge Setup

Slower rise time current injection was accomplished using the battery discharge setup shown schematically in Figure B2. Four

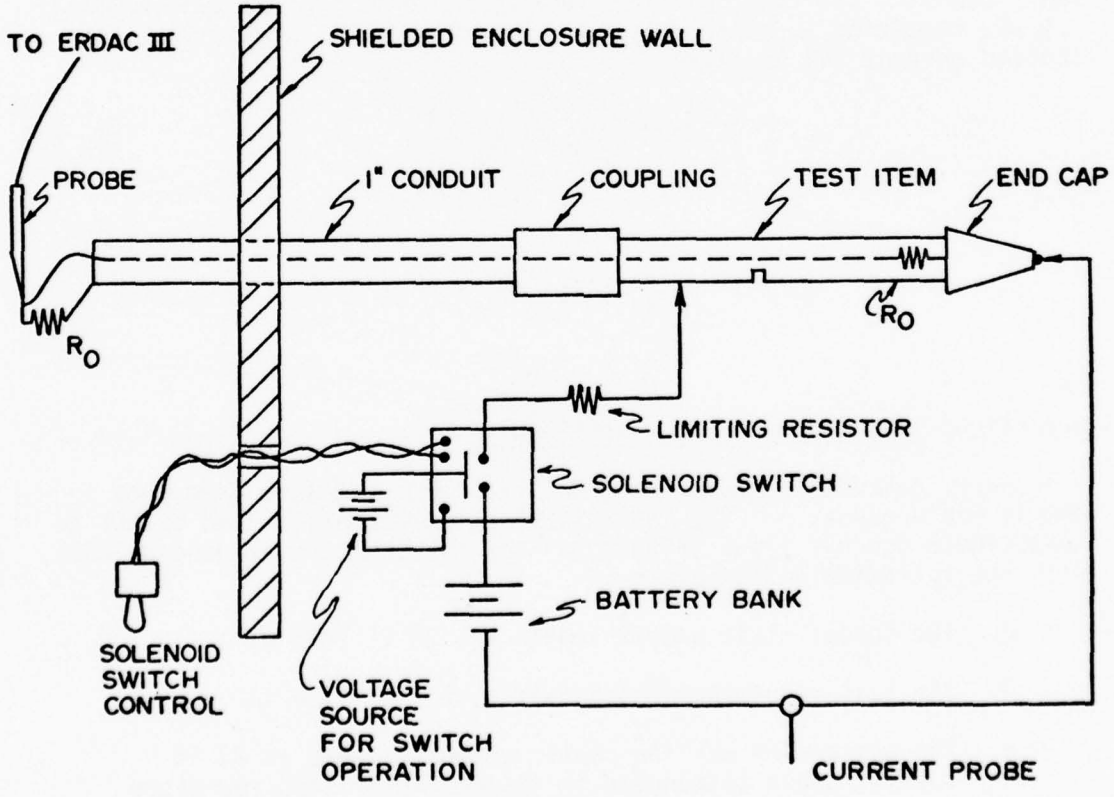

Figure B2. *Battery discharge setup for current-injection testing.*

automotive-type lead-acid storage batteries in series were used as the current source; they provided a capability for up to 250 A peak injection current. The current was switched by an automotive-type, engine-starter solenoid switch capable of switching several hundred amperes. The solenoid of this switch was controlled by a separate 12-V storage battery and a push-button switch. The push-button switch was electrically connected by means of a twisted pair of wires routed through a mechanical feed-through fitting to the interior of the shielded enclosure, thus providing simultaneous control of both the current switching and the measuring equipment.

The injection current was limited by means of a series resistor made from several parallel strands of nichrome wire. The thermal time constant of the nichrome wire was measured and found to be much greater than the time of occurrence of leakage and diffusion current phenomena within conduits. The room-temperature resistance of the limiting resistor was 0.22 ohms, thus establishing the peak current of approximately 225 A. The inductance of the loop consisting of the storage battery bank, conduit, limiting resistor, and solenoid switch was approximately 2.9 μH, resulting in a current rise time of about 13 μsec. Thus, the applied current had the form

$$I(t) = I_o \left(1 - e^{\frac{-t}{\gamma_o}}\right) \qquad \text{[Eq B1]}$$

with

$$I_o \approx 225 \text{ A}$$

$$\gamma_o \approx 13 \text{ μsec}$$

Experimental Procedure - Frequency Domain

Harry Diamond Laboratories (HDL) has performed some frequency domain measurements.[12] The laboratory test arrangement used by HDL to investigate conduit flaws (Figure B3) was similar to that used by CERL, with the following differences:

a. The conduit test sample length was 20 ft (6.1 m)

b. The test transmission line was a coaxial line

c. The sense wire was the center conductor from an RG 58 coaxial cable terminated in its characteristic impedance

[12]H. A. Roberts, J. Capobianco, and F. Agee, *SAFEGUARD Buried Conduit Studies* (HDL, undated).

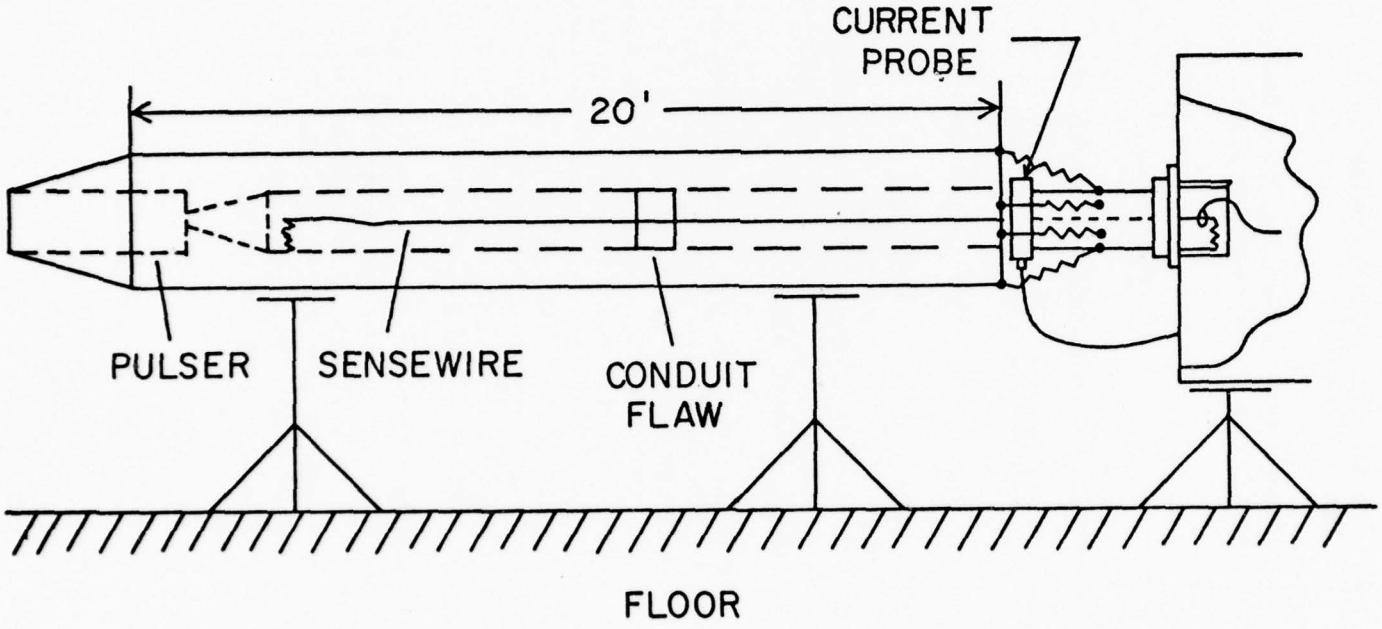

Figure B3. Laboratory arrangement for investigating conduit flaws. From H. A. Roberts, J. Capobianco, and F. Agee, *SAFEGUARD Buried Conduit Studies* (HDL, undated).

d. The shielded room to which the conduit sample was attached was a 1-m cube.

Flaw impedances were measured using a Hewlett Packard 8000 series spectrum analyzer. This instrument measured the amplitude, but not phase of

$$I_S(\omega) \; / \; I_C(\omega) = Z_f(\omega) \qquad \text{[Eq B2]}$$

where $I_S(\omega)$ = the cable (or sense wire) current

$I_C(\omega)$ = the conduit current

$Z_F(\omega)$ = the amplitude of the flaw impedance.

The data were plotted as a decibel plot of $I_S(\omega) \; / \; I_C(\omega)$ or equivalently as 20 log $[IZ_F(\omega)/2Z_o]$, where Z_o is the characteristic impedance of the sense wire-conduit transmission line. This is because Z_F is in parallel with two transmission lines in series, each with a characteristic impedance of Z_o (Figure B4).

The measurement of the flaw impedance consisted of replacing the pulser in Figure B3 with a signal source and measuring the ratio of the conduit current to the sense wire current at a sufficient number of frequencies to determine the shape of the flaw impedance curve. HDL measurements with the spectrum analyzer covered a frequency range from near DC to 100 MHz. This measurement technique provided a dynamic range of approximately 140 dB, which is sufficient to measure the flaw impedance or transfer function of flexible conduit (0.015 to 0.035 in. [0.381 to 0.899 mm] wall thickness), but not enough to measure the diffusion current transfer function for rigid-walled conduit.

Instrumentation to measure amplitude and phase information (both of which are necessary to transform from the frequency domain to the time domain) is available. This information can be continuously plotted by instruments such as the HP Model 3575A Gain/Phase Meter (1 Hz to 13 MHz) and HP Model 8407A Analyzer (100 Hz to 110 MHz). A vector voltmeter could be used for manual plotting of the amplitude and phase information.

Measurement of Material Properties

In the calculation of the penetration of conduit by EMP (and hence the calculation of the basic shielding provided by the conduit) presented in Appendix C, it is apparent that the specimen's electrical conductivity σ and magnetic permeability μ are two material properties of interest. The values of these properties are tabulated in a number of places for a variety of materials. The data reveal that the

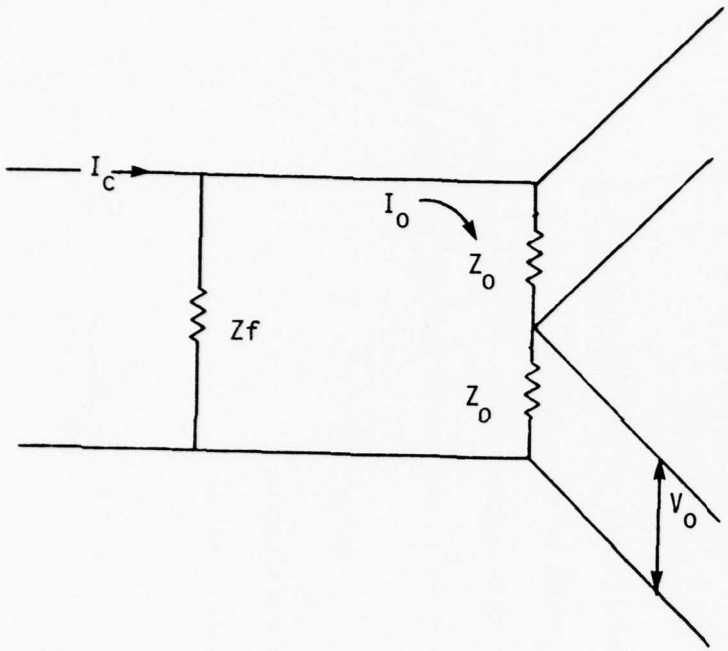

Z_f = flaw impedance

I_c = conduit current

I_o = current induced on transmission line

Z_o = transmission line impedance

V_o = induced voltage

$$I_o = \frac{I_c Z_f}{2Z_o + Z_f}$$

Figure B4. Conduit flaw impedance concept.

properties are strongly influenced by chemical composition as well as heat treatment. Unfortunately, values of these properties could not be readily obtained from conduit manufacturers. The importance of these properties in the calculations and the unavailability of the data made experimental determination of these properties for construction-grade conduit necessary.

Since measuring a specimen's resistance is often more convenient than measuring its conductivity, the electrical conductivity σ may be determined as

$$\sigma = \frac{1}{\rho} \frac{\text{mho}}{\text{meter}} \qquad \text{[Eq B3]}$$

where ρ = the resistivity (ohm-meter)

The resistivity is determined by passing a direct current through the specimen and measuring the voltage drop across the specimen. The voltage V, due to a current I, is given by

$$V = IR \qquad \text{[Eq B4]}$$

where R = the resistance of the specimen = $\rho \frac{\ell}{A}$

ℓ = the length of the specimen

A = the cross-sectional area of the specimen.

In the case of conduit, the cross section is given by

$$A = \pi (b^2 - a^2) \qquad \text{[Eq B5]}$$

where a = the inside radius

b = the outer radius

Hence,

$$V = I \frac{\rho \ell}{\pi(b^2 - a^2)} \qquad \text{[Eq B6]}$$

It follows that

$$\rho = \frac{\pi(b^2 - a^2)}{\ell} \frac{V}{I} \qquad \text{[Eq B7]}$$

Figure B5 shows a schematic of the measurement technique. Note that the points of measurement of the voltage are between the points of current injection. This eliminates the measurement of voltage due to contact resistance.

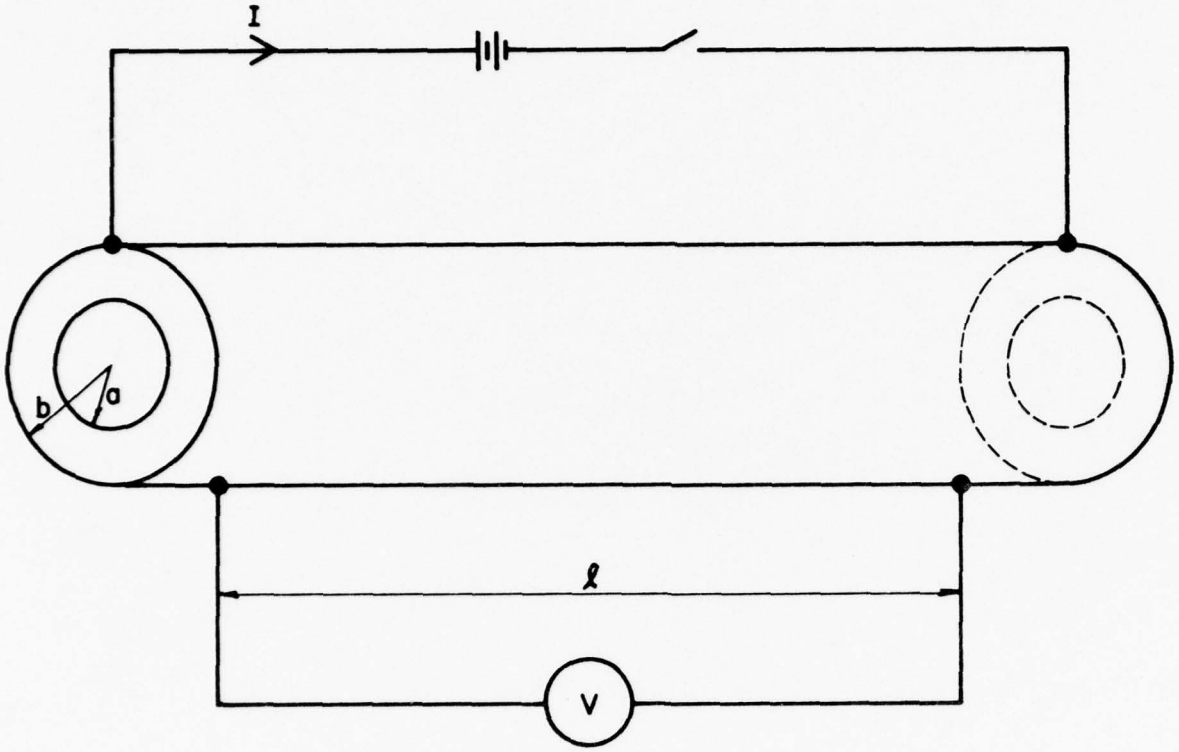

Figure B5. Schematic of the measurement setup for conductivity.

APPENDIX C:

EMP PENETRATION OF SOLID CONDUIT

Approach

This appendix describes the development and testing of a method for determining the electromagnetic signal induced in the interior of a hollow circular cylinder due to a current pulse* on the outer surface. Since the current pulse can take various forms--all of different frequency content--a general solution can be determined by calculating the time response of the conduit due to an impulse of electromagnetic energy and then convoluting this response with any given input. Similarly, the Fourier transform of the internal electric field due to an impulse current (referred to in the literature as the surface transfer impedance) can be multiplied by the Fourier transform of the current pulse to obtain the frequency domain solution for the electric field.

Determination of the electric field at the inner surface of a hollow circular cylinder of finite conductivity subjected to an external surface current impulse involves the solution of Maxwell's equations for the axial electric field inside the cylinder due to the current applied to the surface of the conduit. Straightforward application of the Laplace transform technique leads to a transform of the electric field which involves modified Bessel functions. Similarly, the Fourier transform of the electric field involves modified Bessel functions of complex arguments.

In the literature[13] concerning the electromagnetic shielding effectiveness of cylindrical structures under various transient conditions,

*The term "pulse" is used to refer to an arbitrary current injection of short duration; the term "impulse" is reserved for a signal of negligible duration whose magnitude is sufficiently large to induce a finite change on the system.

[13]S. A. Schelkunoff, "The Electromagnetic Theory of Co-axial Transmission Lines and Cylindrical Shields," *Bell System Technical Journal*, Vol XIII (1934), pp 532-579; Charles W. Harrison, "Transient Electromagnetic Field Propagation Through Infinite Sheets," *IEEE Transactions on Antenna and Propagation*, Vol AP-12, No. 3 (May 1964), pp 319-334; R.W.P. King and E. W. Harrison, "Cylindrical Shields," *IEEE Transactions on Antenna and Propagation*, Vol AP-9, No. 2 (1961), pp 166-170; D. A. Miller and P. P. Toulias, "Penetration of Co-axial Cables by Transient Fields," *IEEE Electromagnetic Compatibility Symposium Record* (1968), pp 414-423; E. F. Vance and J. E. Nanvicz, "Internal Voltages and Currents in Solid Shielded Cables," *IEEE Electromagnetic Compatibility Symposium Record* (1968), pp 198-209; and J. L. Erskine, "Calculations of the Fields in a Closed Cylinder Resulting from an Electromagnetic Pulse," *IEEE Electromagnetic Compatibility Symposium Record* (1968), pp 291-297.

the standard approaches lead to computational difficulties, since the presence of the modified Bessel functions makes direct inversion of the Laplace transform to obtain a time domain solution difficult. Evaluation of the Fourier transform to obtain a solution in the frequency domain is also difficult. Many of the techniques require extensive numerical calculations; however, a large class of problems exists for which accurate and rapidly converging series solutions in the time domain (and a relatively simple expression in the frequency domain) can be obtained by replacing the modified Bessel functions in the transform(s) with their asymptotic expansions for large arguments.[14] The results obtained using the asymptotic form of the Bessel functions are valid for cylindrical shields that have inner radii which are large compared to the skin depth of the lowest frequency of interest in the surface current pulse. For a given cylinder, the impulse response so calculated can then be convoluted with an arbitrary surface current to obtain the resultant electric field on the interior of the conduit.

The impulse response for a circular cylinder of a specified size and material can be defined by two shield parameters which depend on the cylinder's dimensions and material properties. These two parameters can be easily determined experimentally, which is important, since the properties of many materials are not readily available. Once the parameters for one size cylinder of a given material are known, the parameters for another size cylinder of the same material can be found.

The calculated impulse responses were checked experimentally. The application of the theoretical impulse response to the determination of the response for a complicated driving current was demonstrated by predicting the response to a damped sinusoid surface current and comparing it with the measured signal.

Theoretical Analysis

Time Domain

The calculations for the internal electric field refer to a hollow cylinder (Figure C1) of length ℓ, inner radius a, outer radius b, conductivity σ, permeability μ, and permittivity ε. It is assumed that σ, μ, and ε are isotropic constants.

The current, $I_c(t)$, applied to the cylinder is assumed to be flowing in the positive z-direction and is uniform with respect to z and ϕ. For the purpose of the analysis, it is assumed that the applied current is an impulse of the form

[14] D. J. Leverenz, W. Croisant, and J. Verdeyen, "Electromagnetic Induced Diffusion Signals on Conduit Protected Cables," *1974 IEEE-EMC Symposium Record*, IEEE CHO 803-7 EMC (1974).

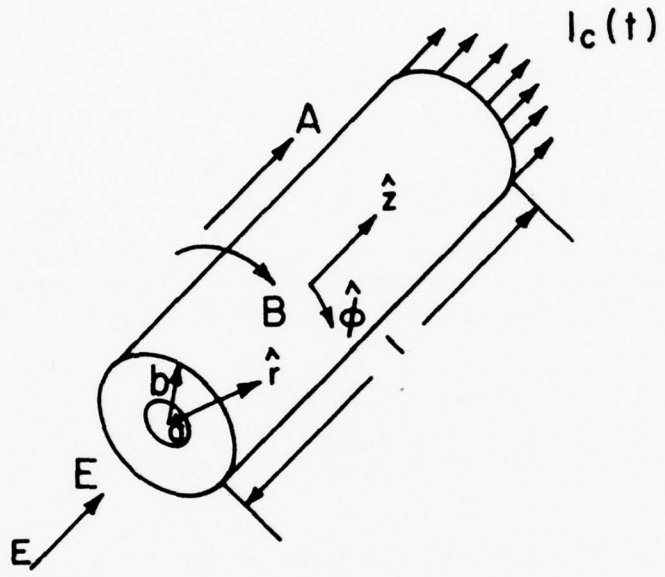

Figure C1. Model for electric field calculations.

$$I_c(t) = Q\,\delta(t) \qquad \text{[Eq C1]}$$

where Q = the injected charge

$\delta(t)$ = a unit impulse

Defining A(r,t) as the magnetic vector potential in the z-direction and applying Maxwell's equations for a conducting medium (a medium for which $\sigma >> \omega\varepsilon$) to this model yields the following differential equations:

$$\frac{\partial^2 A(r,t)}{\partial r^2} + \frac{1}{r}\frac{\partial A(r,t)}{\partial r} = \mu\sigma\frac{\partial A(r,t)}{\partial t} \qquad \text{[Eq C2]}$$

$$E(r,t) = -\frac{\partial A(r,t)}{\partial t} \qquad \text{[Eq C3]}$$

where the direction and field components are defined in Figure C1.

The initial condition A(r,0) = 0 and the boundary conditions:

$$\frac{\partial A(a,t)}{\partial r} = -B(a,t) = 0 \qquad \text{[Eq C4]}$$

$$\frac{\partial A(b,t)}{\partial r} = -B(b,t) = -\frac{\mu Q \delta(t)}{2\pi b} \qquad \text{[Eq C5]}$$

are to be imposed upon Eq C2.

Use of the Laplace transform for the time variable along with the specified spatial boundary conditions results in the following expression for the vector potential for the region $a \leq r \leq b$:

$$\tilde{A}(r,s) = -\frac{\mu Q}{2\pi b\sqrt{\mu\sigma s}} \left[\frac{K_1(\sqrt{\mu\sigma s}\, a)\, I_0(\sqrt{\mu\sigma s}\, r) + I_1(\sqrt{\mu\sigma s}\, a)\, K_0(\sqrt{\mu\sigma s}\, r)}{I_1(\sqrt{\mu\sigma s}\, b)\, K_1(\sqrt{\mu\sigma s}\, a) - K_1(\sqrt{\mu\sigma s}\, b)\, I_1(\sqrt{\mu\sigma s}\, a)} \right] \qquad \text{[Eq C6]}$$

where I and K = modified Bessel functions of the first and second kind, respectively.

The transform of the electric field is related to the above by

$$\tilde{E}(r,s) = -s\tilde{A}(r,s) \qquad \text{[Eq C7]}$$

However, for r = a, the exact relation (the Wronskian)--

$$I_\nu(w)K_{\nu+1}(w) + I_{\nu+1}(w)\cdot K_\nu(w) = \frac{1}{w} \qquad \text{[Eq C8]}$$

reduces the numerator of the bracketed expression in Eq C6 to $1/\sqrt{\mu\sigma s}\, a$, so that at the inner surface of the cylinder the transform of the interior electric field resulting from the current pulse on the outer surface is

$$\tilde{E}(a,s) = \frac{Q}{2\pi ab\sigma} \left[I_1(\sqrt{\mu\sigma s}\, b)\, K_1(\sqrt{\mu\sigma s}\, a) - K_1(\sqrt{\mu\sigma s}\, b)\, I_1(\sqrt{\mu\sigma s}\, a) \right]^{-1} \qquad \text{[Eq C9]}$$

Due to the modified Bessel functions, it is difficult to directly invert the exact transform (Eq C9); however, for large arguments, one can use the asymptotic form of the modified Bessel functions

$$I_\nu(w) \simeq \frac{\exp(w)}{\sqrt{2\pi w}} \left[1 - \frac{4\nu^2-1}{8w} + \frac{(4\nu^2-1)(4\nu^2-9)}{2!(8w)^2} - \ldots\right] \quad \text{[Eq C10]}$$

and

$$K_\nu(w) \simeq \sqrt{\frac{\pi}{2w}} \exp(w)\left[1 + \frac{4\nu^2-1}{8w} + \frac{(4\nu^2-1)(4\nu^2-9)}{2!(8w)^2} + \ldots\right] \quad \text{[Eq C11]}$$

In view of Eqs C10 and C11, it is apparent that for a sufficiently large argument, the series terms beyond the first may be neglected in the asymptotic expansions. The next section demonstrates that this approximation is valid provided the inner radius a is much larger than the skin depth for the lowest frequency* of interest, i.e.,

$$a >> \delta = (2/\omega\mu\sigma)^{1/2} \quad \text{[Eq C12]}$$

Thus, the results using this approximation apply to most problems--surely to the system considered in the experimental section. (However, note that this assumption does not place a restriction on the ratio of the wall thickness to the skin depth.) Within this framework, Eq C9 simplifies considerably:

$$\tilde{E}(a,s) = \frac{Q}{\pi\sqrt{ab}} \sqrt{\frac{\mu}{\sigma}} \frac{\sqrt{s}}{\exp[(b-a)\sqrt{\mu\sigma s}] - \exp[-(b-a)\sqrt{\mu\sigma s}]} \quad \text{[Eq C13]}$$

or

$$\tilde{E}(a,s) = \frac{Q}{2\pi\sqrt{ab}} \sqrt{\frac{\mu}{\sigma}} \frac{\sqrt{s}}{\sinh[(b-a)\sqrt{\mu\sigma s}]} \quad \text{[Eq C14]}$$

where the first term of the series Eqs C10 and C11 have been used instead of the Bessel functions.

The Laplace transforms (Eqs C13 and C14) can be inverted by two techniques to obtain two different series representations of the electric field:

*A more precise definition of this statement is considered in the next section of this appendix.

a. Expand the transform (Eq C13) in a Taylor series expansion and invert term by term

b. Invert the transform (Eq C14) directly using the method of residues to obtain a second series solution.

The details of these inversion schemes are shown in the annex along with tabular data on the time variation. For the first scheme, the time history of the electric field is given by

$$E(a,\theta) = Q\left[\frac{8}{\pi^{3/2}\sqrt{ab}\,\mu\sigma^2(b-a)^3}\right] \left\{\sum_{n=0}^{\infty} \frac{\exp\left[-\frac{(2n+1)^2}{\theta}\right]}{\theta^{3/2}}\left[\frac{(2n+1)^2}{\theta} - \frac{1}{2}\right]\right\}, \theta \geq 0 \qquad \text{[Eq C15]}$$

where θ = a relative time expressed in units of a characteristic diffusion time T

$T = \mu\sigma(b-a)^2/4$

$\theta = t/T$

t = time

The second inversion scheme yields an expression which converges well at late times

$$E(a,\theta) = Q\left[\frac{8}{\pi^{3/2}\sqrt{ab}\,\mu\sigma^2(b-a)^3}\right] \left\{\frac{\sqrt{\pi}}{2}\left[\sum_{n=0}^{\infty}(-1)^{n+1}\,\frac{n^2\pi^2}{4}\exp\left(-\frac{n^2\pi^2}{4}\theta\right)\right]\right\} (\theta > 0). \qquad \text{[Eq C16]}$$

$E(a,\theta)$ can be put in the form

$$E(a,\theta) = QF\,S(\theta) \qquad \text{[Eq C17]}$$

where Q = charge passed along the cylinder

$$F = \frac{8}{\pi^{3/2}\sqrt{ab}\,\mu\sigma^2\,(b-a)^3}$$

$\theta = t/T$

$S(\theta)$ = the two series representations denoted by braces in Eqs C15 and C16

A table of values of $S(\theta)$ is presented in the annex to this appendix, and a plot is shown in Figure C2.

It is apparent that Eq C15 converges rapidly for small values of θ, whereas Eq C16 converges rapidly for large values of θ, very slowly for small values of θ, and not at all for $\theta = 0$. Eq C15 is more convenient for generation of the impulse response, since the first term alone is dominant over most of the range of interest. For example, at the peak of $S(\theta)$, the first term alone accounts for 99.99 percent of the value of the peak. The second term in the series contributes an 8 percent correction to the first at $\theta = 1.4$, but, at this relative time, the field is only 10 percent of its peak value.

The peak of $S(\theta)$ occurs at a relative time given by

$$\theta_p = 0.36701 \qquad \text{[Eq C18]}$$

at which

$$S(\theta_p) = 0.65604 \qquad \text{[Eq C19]}$$

Therefore, the electric field attains a peak value

$$E(a,\theta_p) = 0.65604\ QF \qquad \text{[Eq C20]}$$

at

$$t = .36701T \qquad \text{[Eq C21]}$$

These two characteristics of the peak electric field are most useful in the experimental determination of the shield parameters T and F.

For an arbitrary current pulse $I_c(t)$, the electric field can be determined by convolution with the impulse response. Hence, the electric field for an arbitrary current pulse is

$$E(a,t) = QF \int_0^t I_c(t-\lambda)\ S(\lambda/T)\ d\lambda \qquad \text{[Eq C22]}$$

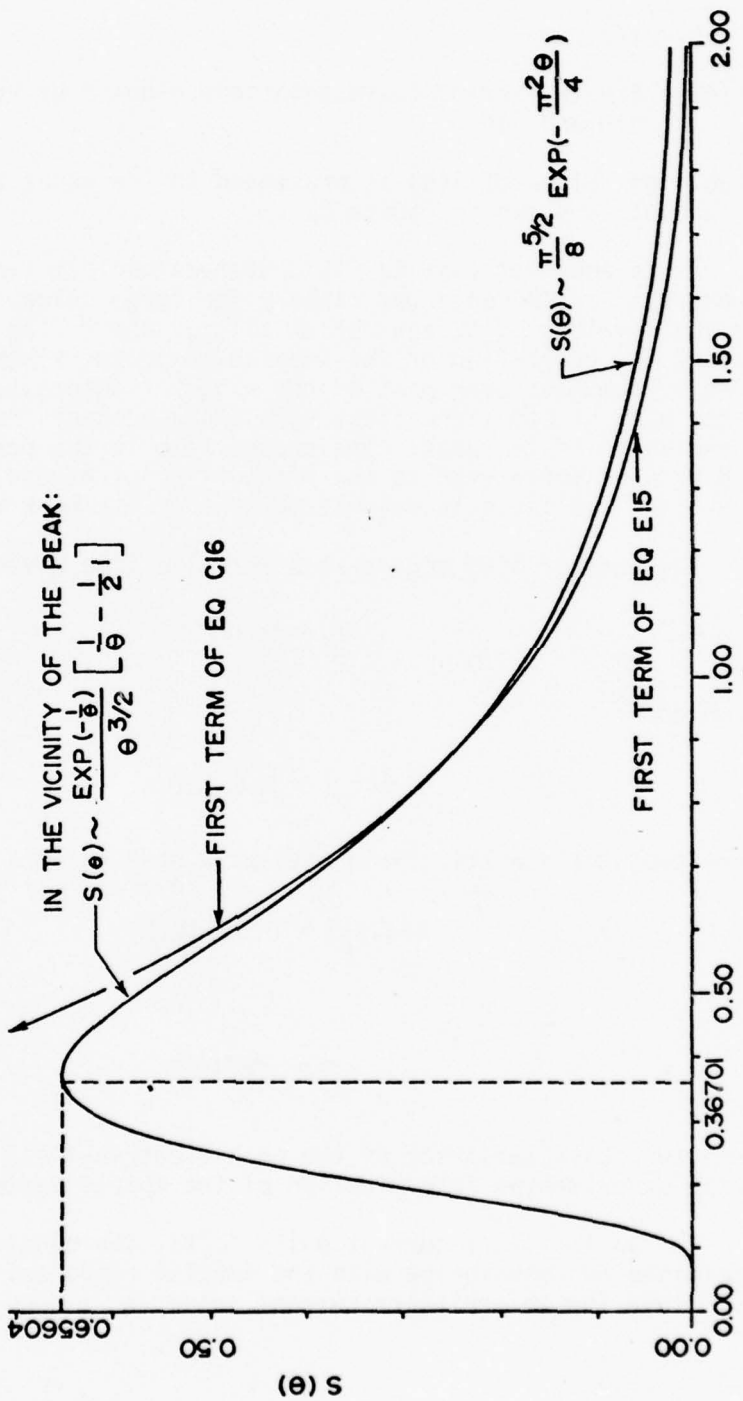

Figure C2. Impulse response function.

Frequency Domain

Although the main objective of this study is to examine the time variation of the electric field, it is useful to briefly consider the results obtained in the frequency domain using the asymptotic expansion of the Bessel functions.

From the definition of the Fourier transform, it is apparent that the Fourier transform of the electric field at the inner surface of the cylinder can be obtained from Eq C9 by letting s equal $j\omega$. Thus, at the inner surface of a conducting cylinder the Fourier transform of the electric field due to a surface current impulse on the outer surface is

$$\hat{E}(a,\omega) = \frac{Q}{2\pi ab\sigma}\{I_1[(1+j)b/\delta]K_1[(1+j)a/\delta] - I_1[(1+j)a/\delta]K_1[(1+j)b/\delta]\}^{-1} \qquad \text{[Eq C23]}$$

Evaluating this expression is difficult because of the modified Bessel functions of complex arguments; however, using the first terms of the asymptotic expansions Eqs C10 and C11, the Fourier transform can be expressed in terms of the dimensionles variable, ξ:

$$\xi = 8\mu\sigma\,(b-a)^2\omega/4 = 8(b-a)^2/\delta^2 \qquad \text{[Eq C24]}$$

so that the modulus is given by

$$|\hat{E}(a,\omega)| = Q\left[\frac{1}{2\pi\sqrt{ab}\,(b-a)\sigma}\right]\frac{\sqrt{\xi}}{\sqrt{\cosh\sqrt{\xi} - \cos\sqrt{\xi}}} \qquad \text{[Eq C25]}$$

and the phase by

$$\phi = \tan^{-1}\left[\frac{\tanh\,(\sqrt{\xi}/2) + \tan\,(\sqrt{\xi}/2)}{\tanh\,(\sqrt{\xi}/2) - \tan\,(\sqrt{\xi}/2)}\right] \qquad \text{[Eq C26]}$$

Figure C3 shows plots of $|\hat{E}(a,\omega)|$ and ϕ as functions of ξ. The low-pass filter characteristics of this response are best illustrated by examining the falloff at $\xi \geq 100$. For instance, the relative response at $\xi = 1000$ is 84 dB below that at $\xi = 100$.

To replace the Bessel functions I_1 and K_1 by the approximations which retain only the first term of the asymptotic expansions, the

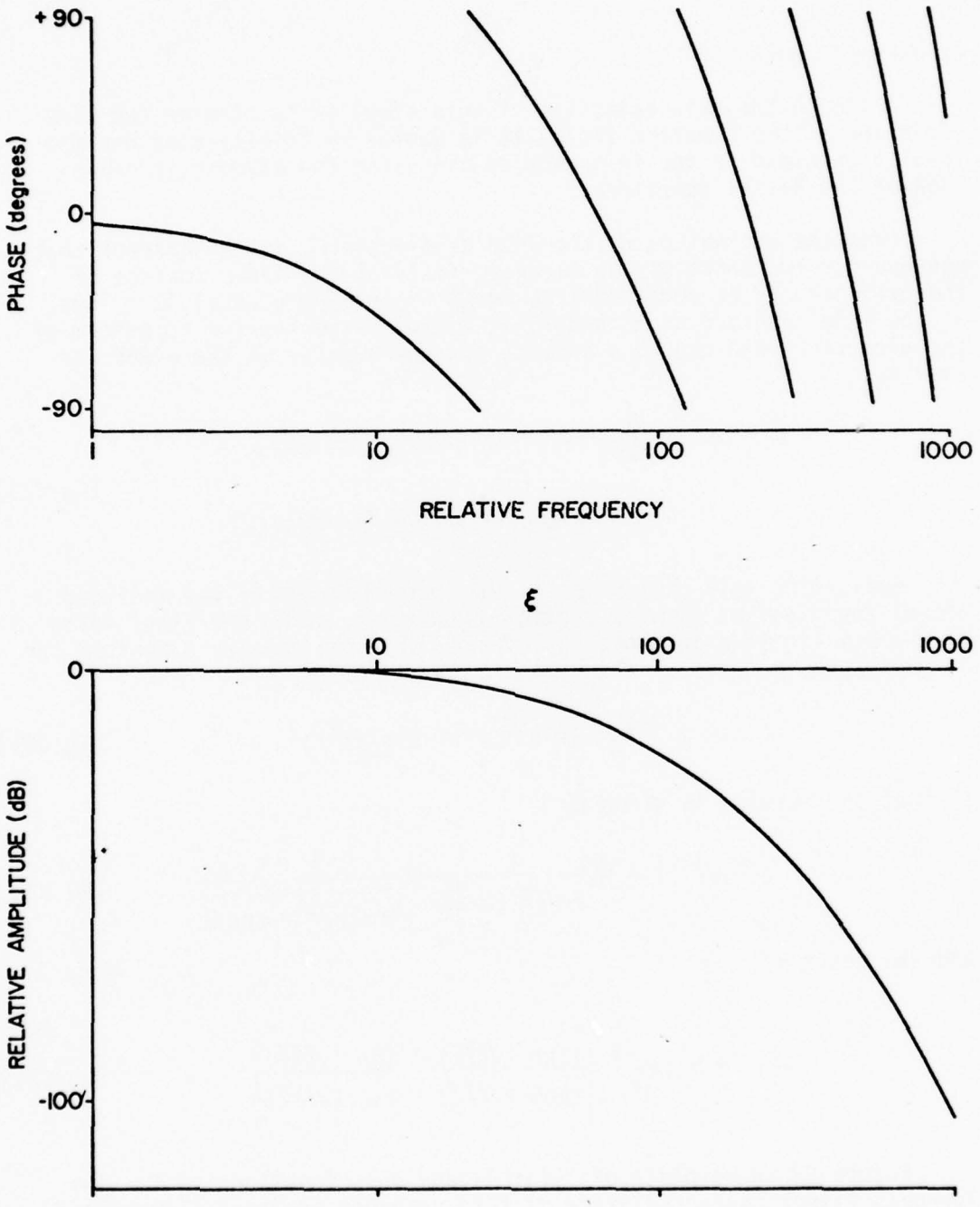

Figure C3. Phase and relative amplitude of the Fourier transform of the impulse response as functions of the relative frequency ξ. (Note that the phase is continuously lagging; however, to conserve space the curve is plotted between $\pm$ 90° since that is the interval over which $\tan^{-1}$ is usually defined.)

other terms must be negligible. The other terms will be negligible if $\sqrt{\mu\sigma\omega}\, a \gg 1$ or, if δ is the skin depth of the lowest frequency component of interest, then $a/\delta \gg 1/\sqrt{2}$. The exact degree to which the terms should be negligible depends somewhat on the particular problem being considered. For instance, if $a/\delta \geq 10$, then the magnitude of the second term is less than 5 percent of the first term. Assuming a relative permeability of 150 and a resistivity of 20×10^{-8} ohm-m for steel conduit, this corresponds to a frequency of 200 Hz for an $a/\delta = 10$ for a 1-in. (2.54-cm) conduit. However, note again that the restriction is on the radius of the air-filled core--not on metallic wall thickness.

Experimental Evaluation

Time Domain

The experiment depicted in Figure C4 was used to test the utility of the results of the previous section. The ground side of the transmission line was the test conduit, which was connected to a conduit stud welded into the side of a shielded room. The pulser consisted of a free-running adjustable spark gap and a low inductance capacitor mounted inside an aluminum cylinder pressurized with sulfur hexafluoride (SF_6) gas. This pulser was capable of producing up to 35-kV pulses with less than a 10-nsec rise time into a 100-ohm load.

The test conduit was a standard 10-ft (3.0-m) section and was thus electrically short (nanoseconds) compared to the decay time (microseconds) of the capacitor being discharged into the transmission line. Thus, even with a mismatch between the transmission line and the load resistor, R_o, the rise time of $I_c(t)$ was short compared to its decay time, which in turn was short compared to the time scales of response. For this reason, the conduit driving current, $I_c(t)$, can be expressed as

$$I_c(t) = \frac{Q}{\tau} \exp(-t/\tau) \qquad \text{[Eq C27]}$$

where $Q = V_o C$ = the charge on the capacitor

$\tau = R_o C$ = the time constant of the capacitor discharge

V_o = the breakdown voltage of the spark gap

R_o = the load resistor (conduit transmission line termination)

In the limit, as $\tau \to 0$, $I_c(t)$ yields

$$\lim_{\tau \to 0} I_c(t) = Q\delta(t) \qquad \text{[Eq C28]}$$

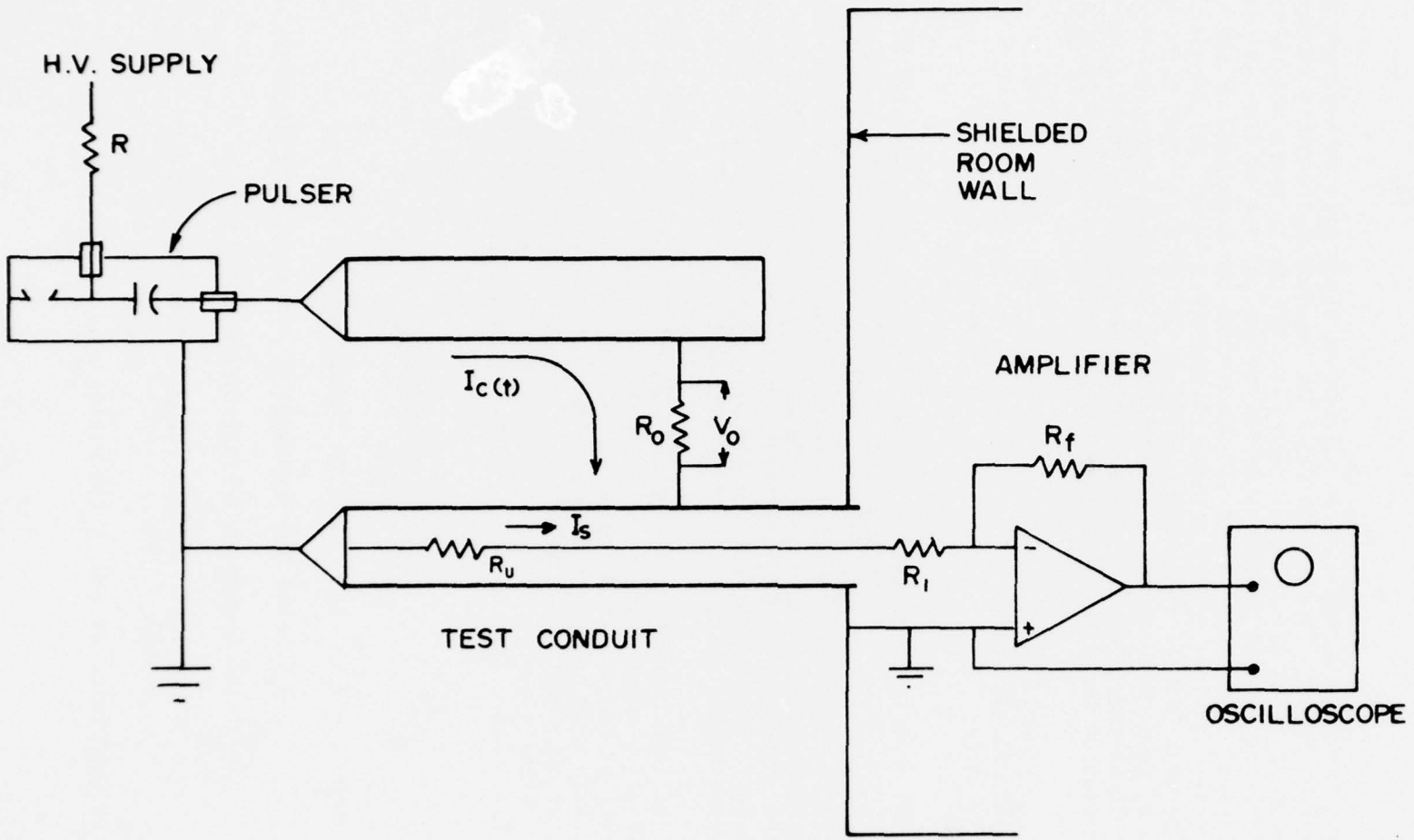

Figure C4. Conduit test configuration with matched sense wire.

Thus, with the proper selection of τ, the driving current produced in this experiment can be made to approximate an impulse function and provide a means of directly verifying the theoretical calculations.

To measure the signals induced on a wire inside the conduit, a sense wire was inserted into the test conduit as shown in Figure C4. The sense wire was connected to the pulser end of the conduit through a terminating resistor (R_2) with the end of the conduit capped to keep leakage signals from entering the system. The sense wire ran the entire length of the conduit and extended into the shielded room where it was terminated through the load resistor, R_1, to the grounded wall of the shielded room. The voltage developed across R_1 was measured using an operational amplifier (gain, G) whose output was displayed on an oscilloscope. The scope traces from which the experimental data were taken were photographed.

To obtain the driving voltage for the sense wire, the electric field was integrated over the length of the conduit. It was assumed that the conduit was electrically short compared to the dominant wavelengths of interest in the internal electric field so that the lumped circuit approximation in Figure C5 could be used. The experimental results show that the time scales of interest are tens of microseconds for the aluminum conduit, to milliseconds for the steel conduit, which makes this approximation valid except for very long cylinders.

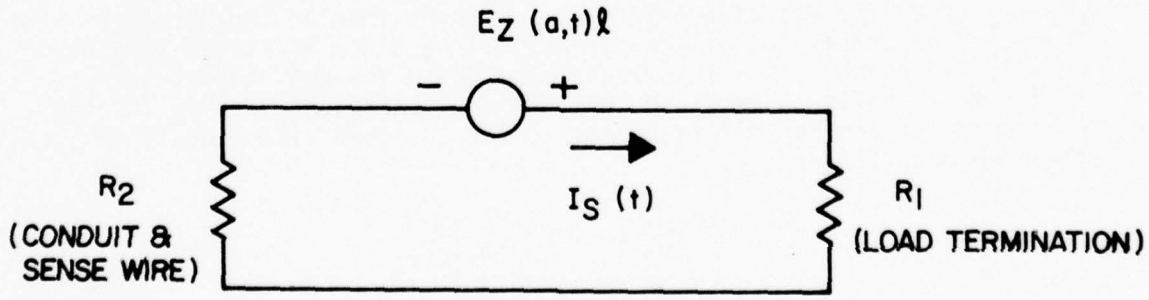

Figure C5. Equivalent circuit for calculation of conduit response.

When $R_2 = 0$ or is small, the voltage displayed on the oscilloscope will be

$$V_m(t) = GE(a,t)\ell = G\ QF\ S(\theta)\ell \qquad \text{[Eq C29]}$$

where G = the amplifier gain

ℓ = the conduit length

Thus this voltage becomes a direct measure of the internal electric field.

Since $S(\theta)$ has a peak value of 0.65604 which occurs at $\theta = 0.36701$, a direct measure of the shield parameters F and T can be obtained from the experiment. If the measured voltage has a peak value V_p which occurs at a time t_p from the time of impulse, then

$$F = \frac{V_p}{.65604\ Q\ell G} \qquad \text{[Eq C30]}$$

and

$$T = \frac{t_p}{.36701} \qquad \text{[Eq C31]}$$

(Since calculation of T requires only the determination of the time at which the peak occurs, which can be done quite accurately from scope traces, one can easily expect a 1 percent accuracy for T.

Thus, the two shield parameters needed to use Eq C17 can be directly found from experimental results without knowing the physical or material properties of the cylindrical shield. As stated earlier, this is important, since the values of σ and μ are not always known. Furthermore, having determined the shield parameters F_1 and T_1 for one size conduit, the parameters F_2 and T_2 for a second size conduit of the same material are:

$$\overline{F}_2 = \sqrt{\frac{a_1\ b_1}{a_2\ b_2}} \left(\frac{b_1 - a_1}{b_2 - a_2}\right)^3 F_1 \qquad \text{[Eq C32]}$$

$$T_2 = \left(\frac{b_2 - a_2}{b_1 - a_1}\right)^2 T_1 \qquad \text{[Eq C33]}$$

where a = interior radius

b = exterior radius.

The experiments were performed on standard aluminum and galvanized steel rigid wall conduits with nominal diameters of 1 and 2 in. (25 and 51 mm). Table C1 gives the values of interest for the experimental condition for each sample. Using the value of t_p from Table C1 and Eq C31, the value of T can be found for each sample so that the abscissa of Figure C6 can be scaled to provide the normalized impulse response function for each sample. Using the values given in Table C1, the value of the amplitude scaling factor M can be found:

$$M = .65604F \qquad \text{[Eq C34]}$$

Table C2 gives the experimental values of M and T obtained for the four test samples. The experimental data were normalized to a common peak of 1. Figures C7 and C8 show the comparisons for the four test samples and the excellent agreement which was obtained between theory and experiment.

Since the values for μ and σ for the aluminum and steel used in the test conduits are not known, directly comparing the experimentally determined values of M and T with the theoretical values is not possible. Assuming that the material properties are the same for each aluminum sample and the same for each steel sample, some comparisons can be made. From the definition of T, it is seen that:

$$\frac{T\ (1\text{-in. [25-mm] aluminum})}{T\ (2\text{-in. [51-mm] aluminum})} = \frac{T\ (1\text{-in. [25-mm] steel})}{T\ (2\text{-in. [51-mm] steel})} \qquad \text{[Eq C35]}$$

which is the case for the values presented in Table C2. Based on the conduits' dimensions, from Table C3 this ratio should be 1.32, which compares closely with the experimentally determined value of 1.43. This is well within the accuracy which can be expected due to variations in thickness and material properties.

In order to test Eq C22 for accuracy in predicting conduit response for a non-impulse driving function, a 1-in. (25-mm) aluminum test conduit was driven with an exponentially damped sinusoid current. The measured current on the conduit was of the form

$$I(t) = \exp(-t/\tau)\sin(2\pi ft) \qquad \text{[Eq C36]}$$

where $\tau = 4.62 \times 10^{-5}$ sec

$f = 31.5$ kHz

Table C1

Experimental Constants for the Calculation of T and M for the Four Test Conduits

Sample	τ	t_m (msec)	V_m (t_m) (mV)	G	l (m)	V (kV)	C (μf)	a (cm)	b (cm)
1-in. (25-mm) aluminum conduit	.0013	.031	24.	10	2.9	32.5	.01	1.33	1.67
2-in. (51-mm) aluminum conduit	.0013	.044	8.	10	2.9	33.5	.01	2.63	3.02
1-in. (25-mm) galvanized steel conduit	.0031	1.54	325.	1000	2.9	31.	.0211	1.3	1.67
2-in. (51-mm) galvanized steel conduit	.0031	2.20	170.	2000	2.9	30.	.0211	2.63	3.02

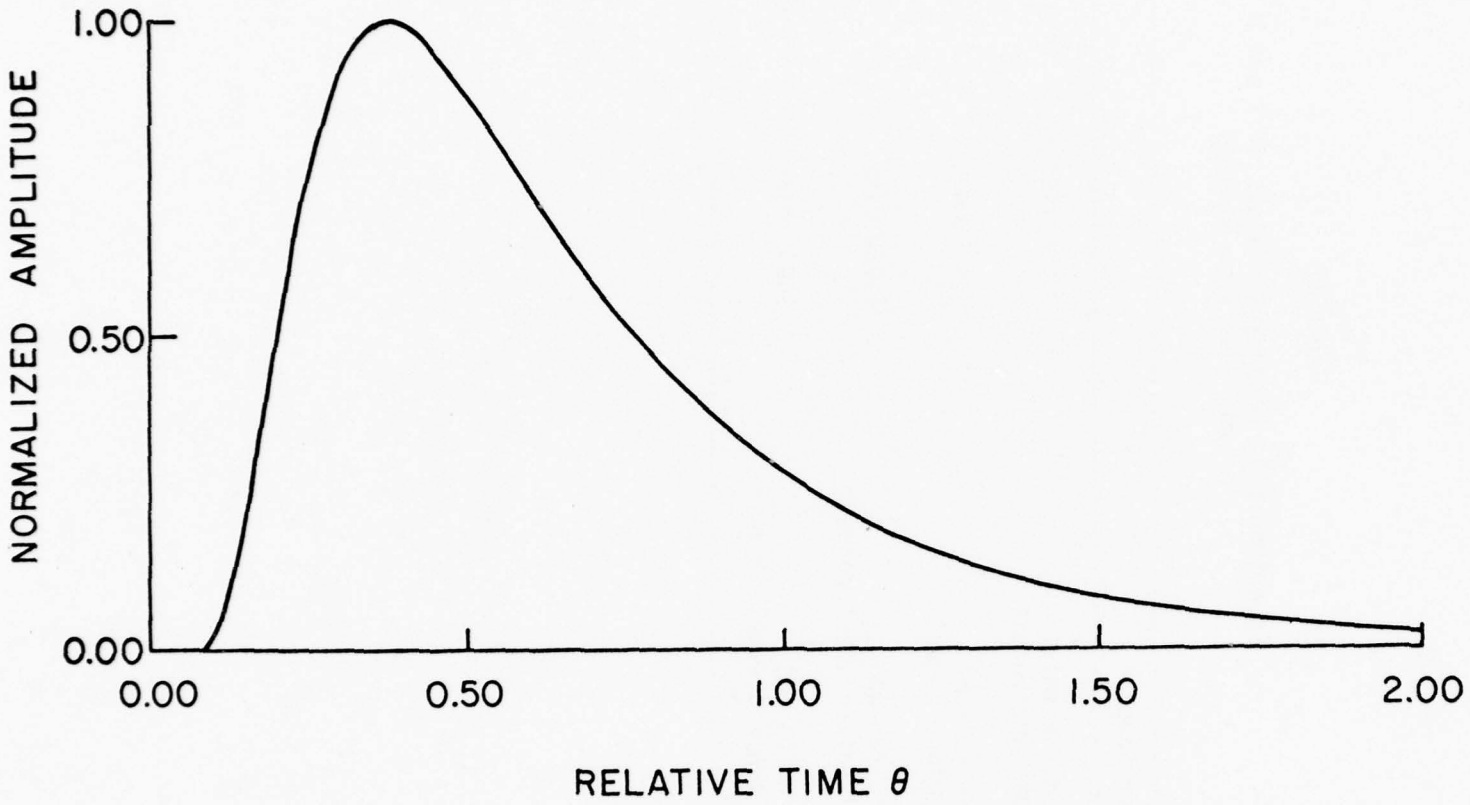

Figure C6. Normalized impulse response function for axial electric field.

Table C2

Experimentally Determined Values of T and M
for the Four Test Samples

Test Sample	T	M
1-in.(25-mm) aluminum conduit	0.084 msec	2.546
2-in.(51-mm) aluminum conduit	0.120 msec	0.824
1-in.(25-mm) galvanized steel conduit	4.200 msec	0.175
2-in.(51-mm) galvanized steel conduit	6.00 msec	0.0472

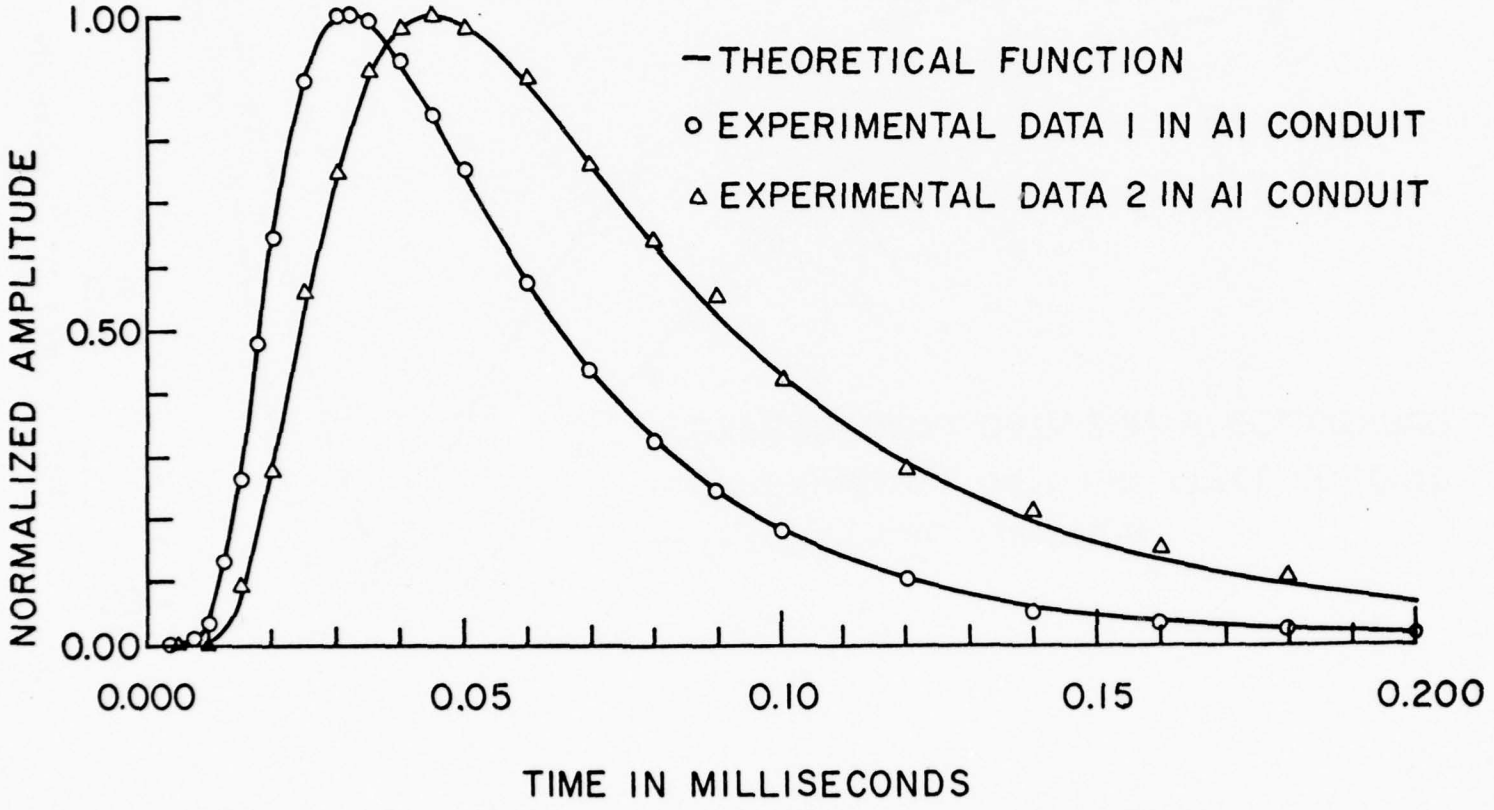

Figure C7. Normalized impulse response functions for 1- and 2-in. (25- and 51-mm) aluminum conduit.

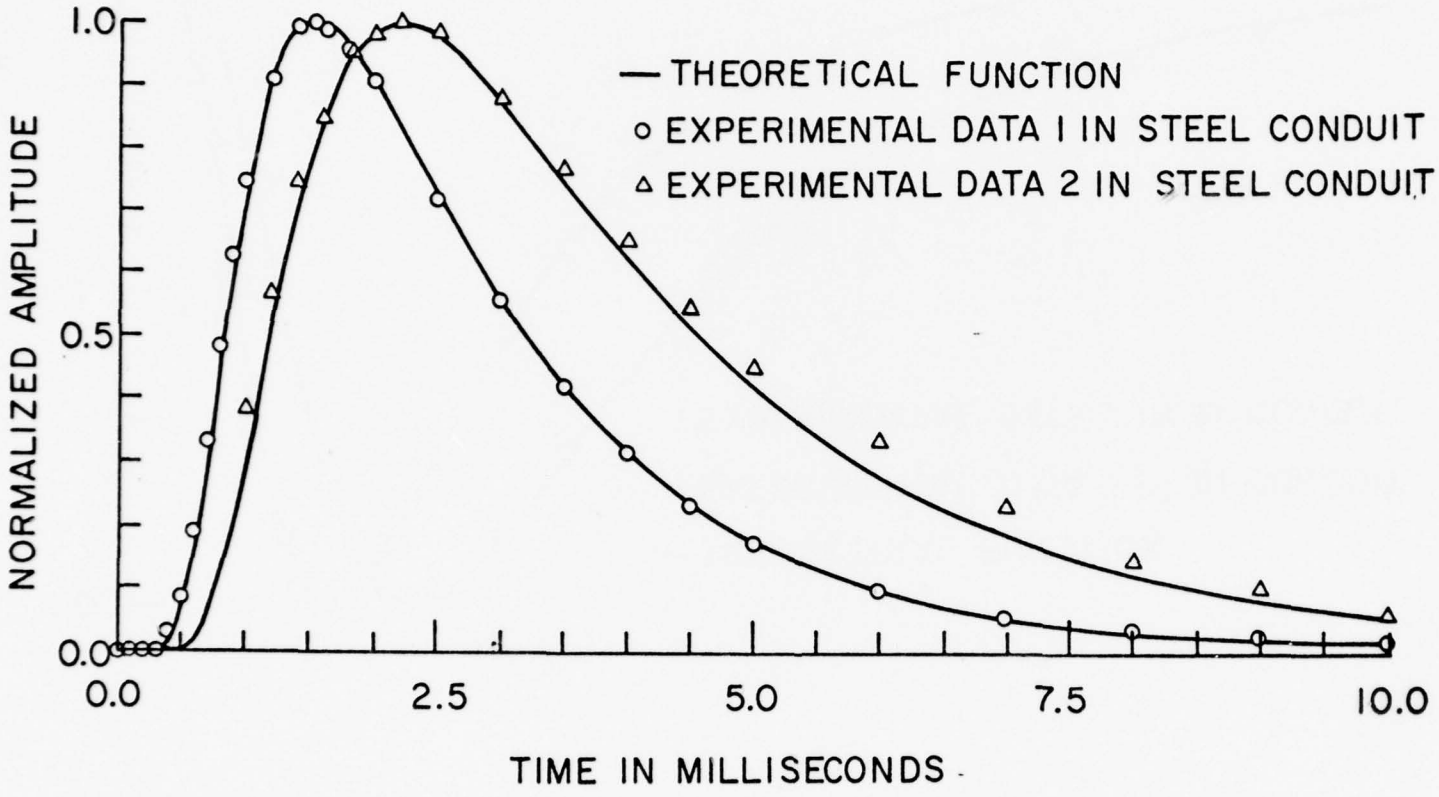

Figure C8. Normalized impulse response functions for 1- and 2-in. (25- and 51-mm) galvanized steel conduit.

Table C3

Design Dimensions of Rigid Conduit

Nominal Size of Conduit in. (mm)	Inner Radius a	Outer Radius b	Wall Thickness b-a	Cylindrical Compression Factor $\sqrt{\frac{b}{a}}$	Thickness to Radius Ratio $\frac{b-a}{a}$	Dimensional Shaping Factor $(b-a)^2$	Dimensional Magnitude Factor $\frac{1}{\sqrt{ab}(b-a)^3}$
	$m \times 10^{-2}$	$m \times 10^{-2}$	$m \times 10^{-2}$			$m^2 \times 10^{-5}$	$m \times 10^{8}$
1/4 (6)	.462	.686	.224	1.22	.484	.500	159.
3/8 (10)	.627	.859	.234	1.17	.368	.534	110.
1/2 (13)	.790	1.07	.277	1.16	.350	.767	51.3
3/4 (19)	1.05	1.33	.287	1.27	.274	.824	35.8
1 (25)	1.33	1.67	.338	1.12	.253	1.14	17.4
1-1/4 (32)	1.75	2.11	.356	1.10	.203	1.27	11.6
1-1/2 (38)	2.05	2.41	.368	1.09	.180	1.36	9.01
2 (51)	2.625	3.018	.391	1.072	.149	1.530	5.935
2-1/2 (64)	3.134	3.653	.518	1.079	.165	2.685	2.124
3 (76)	3.896	4.445	.549	1.068	.141	3.010	1.455
3-1/2 (89)	4.506	5.080	.574	1.062	.127	3.295	1.105
4 (102)	5.113	5.715	.602	1.057	.117	3.624	.848
5 (127)	6.411	7.066	.655	1.050	.102	4.294	.527
6 (152)	7.701	8.412	.711	1.045	.092	5.058	.345

Using Eq E22 and the experimental value of T from Table C2, the normalized voltage across R_1 can be predicted and compared with the measured signal. The comparison, shown in Figure C9, demonstrates the close agreement between the predicted and measured responses.

Frequency Domain

Flaw impedance or the transfer impedance of conduit is near the maximum dynamic range of measurement instrumentation. HDL did, however, make such a measurement on two sections of flexible conduit with wall thicknesses of 0.015 and 0.035 in. (0.381 and 0.889 mm). The length of the flexible section was approximately 20 in. (0.5 m). Figure C10 shows the results of this measurement. The theoretical limit for the maximum of the transfer function is the ratio of the DC resistances of the conduit and the conductor. The flaw impedance shows that only the low frequency components of a current exterior to the conduit will appear on a conductor inside the conduit.

Summary

It has been shown that calculation of the electric field on the inner surface of a hollow circular cylinder due to a current pulse on the outer surface can be greatly simplified with little loss in accuracy by replacing the modified Bessel functions appearing in the Laplace transform of the electric field by their asymptotic expansions for large arguments. The results are valid for those cylinders whose inner radius is large compared to the skin depth of the lowest frequency component in the surface current pulse.

The calculated electric field due to an impulse current has relatively simple series solutions which can be used in a convolution process for an arbitrary forcing function. It was shown that these electric field calculations can be uniquely specified by two parameters which depend only on the physical dimensions and material properties of the cylinder. It was demonstrated experimentally that these two parameters are easily measured and that experimental data can be put in the form of the theoretical calculations with excellent agreement for 1- and 2-in. (25- and 51-mm) diameter aluminum and steel cylinders. Finally, it was verified experimentally that the electric field could be predicted for a complicated current pulse through convolution with the impulse response.

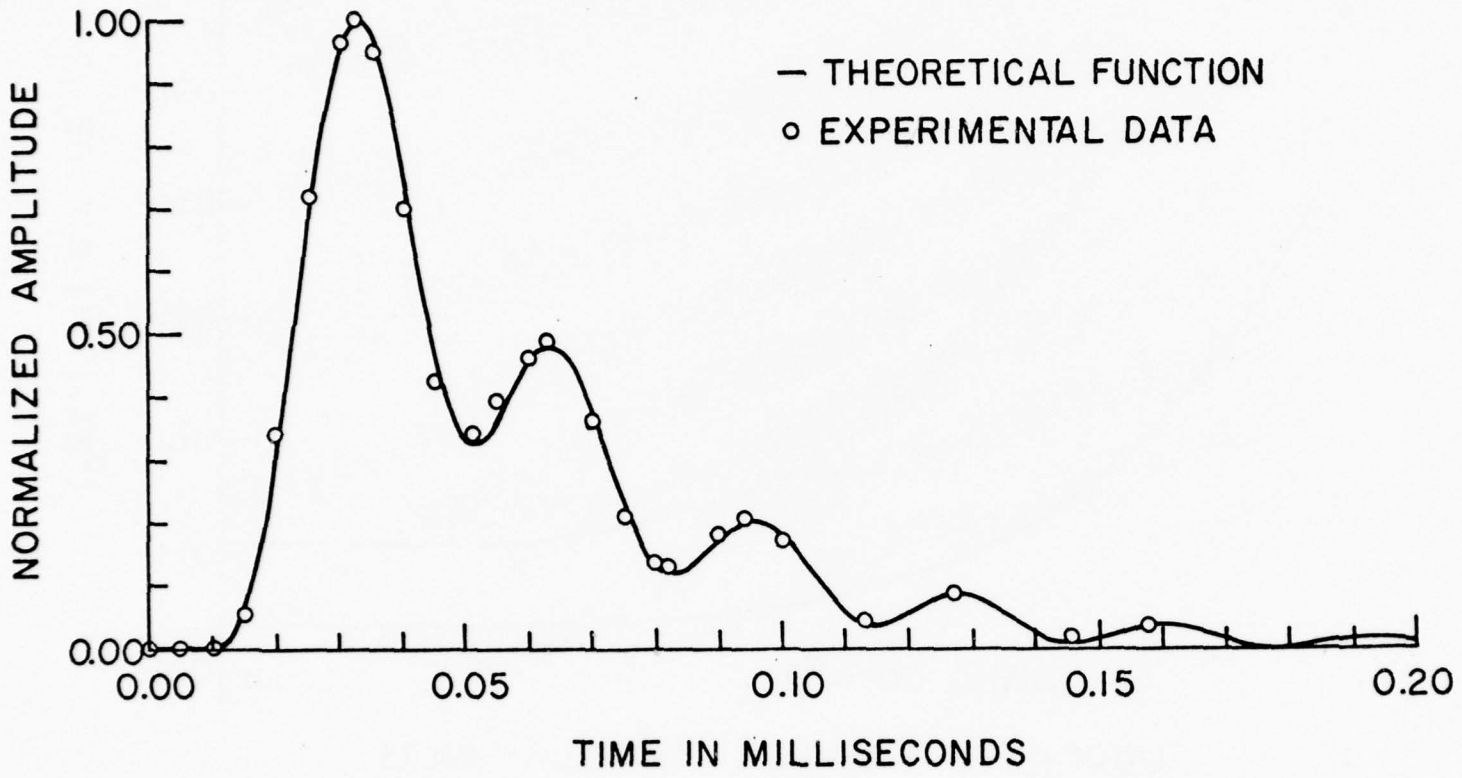

Figure C9. Normalized diffusion signal in 1-in. (25-mm) aluminum conduit for a damped sinusoid excitation current.

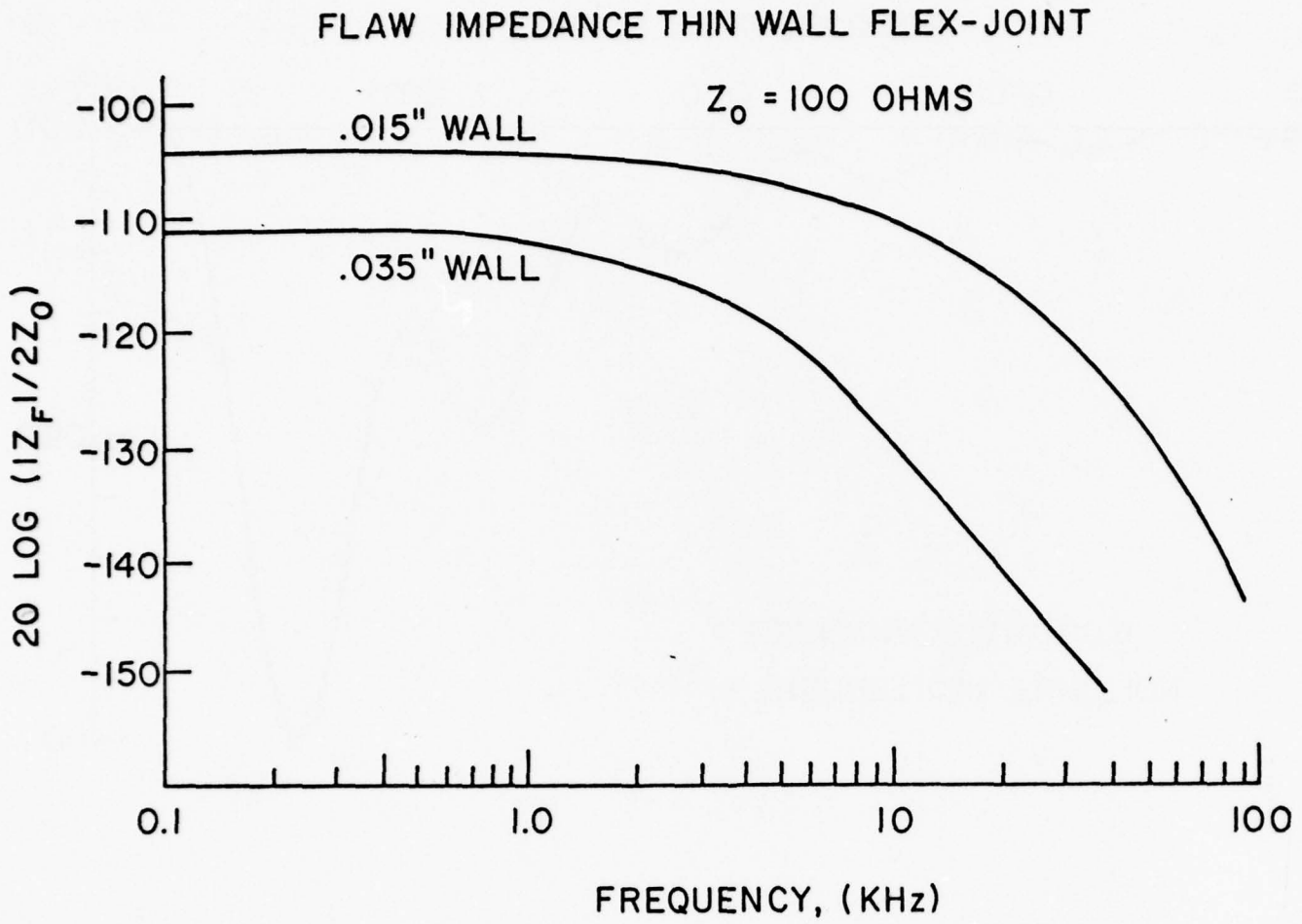

Figure C10. Flaw impedance of two flex-joints of different wall thickness without copper straps. (From H. A. Roberts, J. Capobianco, and F. Agee, *SAFEGU[illegible] Buried Conduit Studies* [HDL, undated]).

ANNEX TO APPENDIX C:

INVERSION OF THE LAPLACE TRANSFORMS

The Laplace transforms (Eqs C13 and C14) can be inverted by either of two techniques to obtain series representations of the electric field:

a. Expand the transform (Eq C13) in a Taylor series expansion and invert term by term to obtain the series expression of Eq C15.

b. Invert the transform (Eq C14) directly using the method of residues to obtain a second series solution given by Eq C16.

To apply the first method, Eq C13 is rewritten

$$\tilde{E}(a,s) = \left[\frac{Q}{\pi\sqrt{ab}}\sqrt{\frac{\mu}{\sigma}}\right]\frac{\sqrt{s}\,\exp[-(b-a)\sqrt{\mu\sigma s}]}{1-\exp[-2(b-a)\sqrt{\mu\sigma s}]} \qquad \text{[Eq C37]}$$

using the Taylor series expansion,

$$\frac{1}{1-x} = 1 + x + x^2 + \ldots = \sum_{n=0}^{\infty} x^n \qquad \text{[Eq C38]}$$

Then:

$$\tilde{E}(a,s) = \left[\frac{Q}{\pi\sqrt{ab}}\sqrt{\frac{\mu}{\sigma}}\right]\sum_{n=0}^{\infty}\sqrt{s}\,\exp[-(2n+1)(b-a)\sqrt{\mu\sigma s}] \qquad \text{[Eq C39]}$$

The inverse for each term is

$$L^{-1}\{\sqrt{s}\,e^{-k_n\sqrt{s}}\} = \frac{1}{\sqrt{\pi}}\,\frac{\exp[-k_n^2/4t]}{t^{3/2}}\left(\frac{k_n^2}{4t}-\frac{1}{2}\right) \qquad \text{[Eq C40]}$$

If a parameter, T, is defined as $\frac{\mu\sigma(b-a)^2}{4}$, depending only on material properties μ and σ and the wall thickness $(b-a)$, then a dimensionless variable, θ, may be defined as t/T so that the electric field at the inner surface of a hollow cylinder caused by an impulse current on its outer surface may be expressed as

$$E(a,\theta) = Q\left[\frac{8}{\pi^{3/2}\sqrt{ab}\,\mu\sigma^2(b-a)^3}\right]\left\{\sum_{n=0}^{\infty}\frac{\exp[-\frac{(2n+1)^2}{\theta}]}{\theta^{3/2}}\left[\frac{(2n+1)^2}{\theta}-\frac{1}{2}\right]\right\} \qquad \text{[Eq C41]}$$

Table C4 evaluates the term in braces in Eq C41.

To obtain the second series representation consider Eq C37 in the form

$$\tilde{E}(a,s) = \left[\frac{Q}{2\pi\sqrt{ab}}\sqrt{\frac{\mu}{\sigma}}\right]\frac{\sqrt{s}}{\sinh(2\sqrt{T}\sqrt{s})} \qquad \text{[Eq C42]}$$

then the inverse is

$$\tilde{E}(a,s) = \left[\frac{Q}{2\pi\sqrt{ab}}\sqrt{\frac{\mu}{\sigma}}\right]\frac{1}{2\pi j}\int_{\gamma-j\infty}^{\gamma+j\infty}\frac{\sqrt{s}\,\exp(st)}{\sinh(2\sqrt{T}\sqrt{s})}\,ds \qquad \text{[Eq C43]}$$

$$= \left[\frac{Q}{2\pi\sqrt{ab}}\sqrt{\frac{\mu}{\sigma}}\right]\sum_{n=0}^{\infty} R_n$$

where R_n = the residues at the poles (sn) of the integrand

The residues are given by

$$R_n = \frac{\sqrt{s}\,\exp(st)}{\frac{d}{ds}[\sinh(2\sqrt{T}\sqrt{s}]}\Bigg|_{s=s_n} = \frac{1}{\sqrt{T}}\frac{\sqrt{s}\,\exp(st)}{\cosh(2\sqrt{T}\sqrt{s})}\Bigg|_{s=s_n} \qquad \text{[Eq C44]}$$

where s_n is the nth zero of

$$\sinh(2\sqrt{T}\sqrt{s}) \qquad \text{[Eq C45]}$$

Since the roots of Eq C45 are

$$s_n = -\frac{n^2\pi^2}{4T} \qquad \text{[Eq C46]}$$

and

$$\cosh(jn\pi) = \cos(n\pi) = (-1)^n \qquad \text{[Eq C47]}$$

Table C4

Evaluation of $S(\theta) = \sum_{n=0}^{\infty} \frac{\exp[-\frac{(2n+1)^2}{\theta}]}{\theta^{3/2}} [\frac{(2n+1)^2}{\theta} - \frac{1}{2}]$

Θ/n	0	1	2	S(θ)
.0	.00000			.00000
.1	.01364			.01364
.2	.33900			.33900
.3	.61513			.61513
∴.36701	.65604			.65604
.4	.64894			.64894
.5	.57418	.00000		.57418
.6	.47413	.00001		.47414
.7	.37997	.00006		.38002
.8	.30030	.00020		.30050
.9	.23562	.00051		.23612
1.0	.18394	.00105		.18499
1.1	.14286	.00186		.14472
1.2	.11020	.00295		.11315
1.3	.08417	.00427		.08843
1.4	.06333	.00578		.06911
1.5	.04658	.00742		.05400
1.6	.03306	.00913		.04219
1.7	.02211	.01086	.00000	.03297
1.8	.01320	.01256	.00001	.02576
1.9	.00594	.01418	.00001	.02013
2.0	.00000	.01571	.00002	.01573

then

$$R_n = \frac{(-1)^{n+1}}{\sqrt{T}} \frac{n^2\pi^2}{4T} \exp[-\frac{n^2\pi^2}{4T} t] \qquad \text{[Eq C48]}$$

Thus, the second series representation of the electric field is

$$E(a,\theta) = Q[\frac{8}{\pi^{3/2}\sqrt{ab}\ \mu\sigma^2(b-a)^3}]$$

$$\{\frac{\sqrt{\pi}}{2}[\sum_{n=1}^{\infty}(-1)^{n+1} \frac{n^2\pi^2}{4} \exp[-\frac{n^2\pi^2}{4} \theta]\} \qquad \text{[Eq C49]}$$

Table C5 evaluates the quantity in braces in Eq C49.

Erskine[15] applied this technique directly to the expression in brackets in Eq C9. This latter expression is similar to that obtained by Erskine, but without the computational difficulties of evaluating the residues of the inversion integral of Eq C9. For thin wall cylinders (b/a≈1) Erskine's results reduce to an expression similar to Eq C16.

[15] J. L. Erskine, "Calculation of the Fields in a Closed Cylinder Resulting from an Electromagnetic Pulse," *IEEE Electromagnetic Compatibility Symposium Record* (1968), pp 291-297.

Table C5

Evaluation of $S(\theta) = \sum_{n=1}^{\infty} (-1)^{n+1} \frac{\sqrt{\pi}}{2} \frac{n^2\pi^2}{4} \exp(-\frac{n^2\pi^2}{4}\theta)$

θ \ n	1	2	3	4	5	6	7	8	9	S(θ)
.1	1.70855	-3.25997	2.13603	-0.67512	0.11449	-0.01092	.00060	-.0002	.00000	.01364
.2	1.33496	-1.21502	.23184	- .01303	.00024	.00000				.33900
.3	1.04306	- .45285	.02516	- .00025	.00000					.61513
.36701	.88411	- .23374	.00568	- .00002						.65604
.4	.81499	- .16878	.00273	- .00000						.64894
.5	.63679	- .06291	.00030							.57418
.6	.49755	- .02345	.00003							.47414
.7	.38876	- .00874	.00000							.38002
.8	.30375	- .00326								.30050
.9	.23734	- .00121								.23612
1.0	.18544	- .00045								.18499
1.1	.14457	- .00017								.14472
1.2	.11321	- .00006								.11315
1.3	.08846	- .00002								.08843
1.4	.06912	- .00001								.06911
1.5	.05400	- .00000								.05400
1.6	.04219									.04219
1.7	.03297									.03297
1.8	.02576									.02576
1.9	.02013									.02013
2.0	.01573									.01573

APPENDIX D:

DESIGN DIMENSIONS AND PARAMETERS OF ELECTRICAL CONDUIT

The EMP penetration of solid conduit has been shown to depend upon the physical dimensions of conduit (Appendix C). This appendix summarizes the design dimensions for electrical conduit. Table D1 gives the design dimensions for rigid metal conduit, Table D2 covers intermediate metal conduit, and Table D3 covers electrical metallic tubing (EMT). Table D4 summarizes the nominal dimensions and several derived parameters of ferrous metal and aluminum that enter into EMP calculations.*

*Note that since electric field is usually expressed in volts/meter, calculations use SI units.

Table D1

Dimensions of Rigid Metal Conduit*

Trade Size of Conduit, in. (mm)	Outside Diameter, in. (mm)	Inside Diamteter, in. (mm)		Wall Thickness, in. (mm)	
		Ferrous Metal and Aluminum	Silicon-Bronze Alloy	Ferrous Metal and Aluminum	Silicon-Bronze Alloy
1/4 (6)	0.540 (13.72)	0.364 (9.246)	0.382 (9.703)	0.088 (2.235)	0.079 (2.007)
3/8 (10)	0.675 (17.15)	0.493 (12.52)	0.503 (12.78)	0.091 (2.311)	0.086 (2.184)
1/2 (13)	0.840 (21.34)	0.622 (15.80)	0.636 (16.15)	0.109 (2.769)	0.102 (2.591)
3/4 (19)	1.050 (26.67)	0.824 (20.93)	0.834 (21.18)	0.113 (2.870)	0.108 (2.743)
1 (25)	1.315 (33.40)	1.049 (26.64)	1.075 (27.31)	0.133 (3.378)	0.120 (3.048)
1-1/4 (32)	1.660 (42.16)	1.380 (35.05)	1.382 (35.10)	0.140 (3.556)	0.139 (3.531)
1-1/2 (38)	1.900 (48.26)	1.610 (40.89)	1.614 (41.00)	0.145 (3.683)	0.143 (3.632)
2 (51)	2.375 (60.33)	2.067 (52.50)	2.077 (52.76)	0.154 (3.912)	0.149 (3.785)
2-1/2 (64)	2.875 (73.03)	2.469 (62.71)	2.519 (63.98)	0.203 (5.156)	0.176 (4.521)
3 (76)	3.500 (88.90)	3.068 (77.93)	3.084 (78.33)	0.216 (5.486)	0.208 (5.283)
3-1/2 (89)	4.000 (101.6)	3.548 (90.12)	3.548 (90.12)	0.226 (5.740)	0.226 (5.740)
4 (102)	4.500 (114.3)	4.026 (102.3)	4.026 (102.3)	0.237 (6.020)	0.237 (6.020)
4-1/2 (114)	5.000 (127.0)	4.506 (114.5)	-	0.247 (6.274)	-
5 (127)	5.563 (141.3)	5.047 (128.2)	-	0.258 (6.553)	-
6 (152)	6.625 (168.3)	6.065 (154.1)	-	0.280 (7.112)	-

*From UL, Inc., Standard 6 (1976), Table 5-2.

Table D2

Intermediate Metal Conduit (IMC) Dimensions*

Trade Size, in. (mm)	IMC Type I Outside Diameter, in. (mm) Min.	IMC Type I Outside Diameter, in. (mm) Max.	IMC Type I Wall Thickness, in. (mm)**	IMC Type II Outside Diameter, in. (mm) Min.	IMC Type II Outside Diameter, in. (mm) Max.	IMC Type II Wall Thickness, in. (mm)†	IMC Type II Length of Finished IMC ft	IMC Type II Length of Finished IMC in. (m)
1/2 (13)	0.810 (20.57)	0.820 (20.83)	0.070 (1.778)	0.825 (20.96)	0.840 (21.34)	0.085 (2.159)	9	11 1/4 (3.03)
3/4 (19)	1.024 (26.01)	1.034 (26.26)	0.075 (1.905)	1.035 (26.29)	1.050 (26.67)	0.085 (2.159)	9	11 1/4 (3/03)
1 (25)	1.285 (32.64)	1.295 (32.89)	0.085 (2.159)	1.300 (33.02)	1.315 (33.40)	0.108 (2.743)	9	11 (3.02)
1-1/4 (32)	1.630 (41.40)	1.645 (41.78)	0.085 (2.159)	1.645 (41.78)	1.660 (42.16)	0.108 (2.743)	9	11 (3.02)
1-1/2 (38)	1.875 (47.63)	1.890 (48.01)	0.090 (2.032)	1.885 (47.88)	1.900 (48.26)	0.108 (2.743)	9	11 (3.02)
2 (51)	2.352 (59.74)	2.367 (60.12)	0.095 (2.413)	2.360 (59.94)	2.375 (60.33)	0.108 (2.743)	9	11 (3.02)
2-1/2 (64)	2.847 (72.31)	2.867 (72.82)	0.130 (3.302)	2.850 (72.39)	2.875 (73.03)	0.155 (3.937)	9	10 1/2 (3.01)
3 (76)	3.466 (88.04)	3.486 (88.54)	0.130 (3.302)	3.475 (88.27)	3.500 (88.90)	0.155 (3.937)	9	10 1/2 (3.01)
3-1/2 (89)	3.961 (100.61)	3.981 (101.1)	0.130 (3.302)	3.975 (101.0)	4.000 (101.6)	0.160 (4.064)	9	10 1/4 (3.00)
4 (102)	4.476 (113.2)	4.476 (113.7)	0.130 (3.302)	4.475 (113.7)	4.500 (114.3)	0.160 (4.064)	9	10 1/4 (3.00)

*From UL, Inc., "Revised Outline of Proposed Investigation for Intermediate Metal Conduit" (1976), Table 8.1.

**Tolerance Type I: +0.015 in. (0.381 mm) for 1/2 through 2 in. (13 through 51 mm)
+0.020 in. (0.508 mm) for 2 1/2 through 4 in. (64 through 102 mm)
-0.000 in. (0.000 mm) for 1/2 through 4 in. (13 through 102 mm)

†Tolerance Type II: +0.020 in. (0.508 mm) for 1/2 through 2 in. (13 through 51 mm)
+0.025 in. (0.685 mm) for 2 1/2 through 4 in. (64 through 102 mm)
-0.000 in. (0.000 mm) for 1/2 through 4 in. (64 through 102 mm)

Table D3

Dimensions and Weight of Electrical Metallic Tubing (Thin Walled Conduit)*

Trade Size of Tubing, in. (mm)	External Diameter, in. (mm)	Internal Diameter,** in. (mm)	Wall Thickness,** in. (mm)	Minimum Acceptable Weight in Pounds per Foot of Length (kg/m)
3/8 (10)	0.577 ± 0.005 (14.66 ± 0.127)	0.493 (12.52)	0.042 (1.067)	0.230† (0.342
1/2 (13)	0.706 ± 0.005 (17.93 ± 0.127)	0.622 (15.80)	0.042 (1.067)	0.285† (0.372)
3/4 (19)	0.922 ± 0.005 (23.42 ± 0.127)	0.824 (20.93)	0.049 (1.245)	0.435† (0.647)
1 (25)	1.163 ± 0.005 (29.54 ± 0.127)	1.049 (26.64)	0.057 (1.448)	0.640† (0.952)
1-1/4 (32)	1.510 + 0.005 (38.35 ± 0.127)	1.380 (35.05)	0.065 (1.651)	0.950† (1.414)
1-1/2 (38)	1.740 ± 0.005 (44.20 ± 0.127)	1.610 (40.89)	0.065 (1.651)	1.10† (1.64)
2 (51)	2.197 ± 0.005 (55.80 ± 0.127)	2.067 (52.50)	0.065 (1.651)	1.40† (2.08)
2-1/2 (64)	2.875 ± 0.005 ††(73.03 ±)	2.731 ††(69.37)	0.072 ††(1.829)	2.05 + (3.05)
3 (76)	3.500 ± 0.005 ††(88.90 ±)	3.356 ††(85.24)	0.072 ††(1.829)	2.50 + (3.72)
3-1/2 (89)	4.000 ± 0.005 ††(101.6 ±)	3.834 ††(97.38)	0.083 ††(2.108)	3.25 + (4.84)
4 (102)	4.500 ± 0.005 ††(114.3 ±)	4.334 ††(110.1)	0.083 ††(2.108)	3.70 + (5.51)

*From UL, Inc., *Standard 797* (1974), Table 4.2

**Not a requirement; included for information only.

†The minimum acceptable weight of 3/8- to 2-in. (10-to 51-mm) nonferrous tubing is to be determined by multiplying the weight shown for steel tubing by the ratio of the density (in pounds per cubic inch) of the nonferrous alloy used to 0.283, which is the density of steel in pounds per cubic inch.

††The dimensions of the 2 1/2-, 3-, 3 1/2- and 4-in. (64-,76-,89-,and 102-mm) sizes of nonferrous tubing are to be established by appropriate investigation taking into account the characteristics of the particular alloy used.

†The minimum acceptable weight of the 2 1/2-, 3-, 3 1/2- and 4-in. (64-, 76-, 89-, and 102-mm) sizes of nonferrous tubing is to be established by investigation of the effect that the dimensions and the particular alloy used have on the strength and rigidity of the finished tubing.

Table D4

Nominal Dimensions and Parameters of Ferrous Metal and Aluminum Rigid Conduit

Nominal Size of Conduit in. (mm)	Inner Radius a	Outer Radius b	Wall Thickness b-a	Cylindrical Compression Factor $\sqrt{\frac{b}{a}}$	Thickness to Radius Ratio $\frac{b-a}{a}$	Dimensional Shaping Factor $(b-a)^2$	Dimensional Magnitude Factor $\frac{4}{\sqrt{ab}(b-a)}$
	$m \times 10^{-2}$	$m \times 10^{-2}$	$m \times 10^{-2}$			$m^2 \times 10^{-5}$	$m^{-4} \times 10$
1/4 (6)	.462	.686	.224	1.22	.484	.500	159.
3/8 (10)	.627	.859	.234	1.17	.368	.534	110.
1/2 (13)	.790	1.07	.277	1.16	.350	.767	51.3
3/4 (19)	1.05	1.33	.287	1.27	.274	.824	35.8
1 (25)	1.33	1.67	.338	1.12	.253	1.14	17.4
1-1/4 (32)	1.75	2.11	.356	1.10	.203	1.27	11.6
1-1/2 (38)	2.05	2.41	.368	1.09	.180	1.36	9.01
2 (51)	2.625	3.018	.391	1.072	.149	1.530	5.935
2-1/2 (64)	3.134	3.653	.518	1.079	.165	2.685	2.124
3 (76)	3.896	4.445	.549	1.068	.141	3.010	1.455
3-1/2 (89)	4.506	5.080	.574	1.062	.127	3.295	1.105
4 (102)	5.113	5.715	.602	1.057	.117	3.624	.848
5 (127)	6.411	7.066	.655	1.050	.102	4.294	.527
6 (152)	7.701	8.412	.711	1.045	.092	5.058	.34

APPENDIX E:

MATERIAL PROPERTIES OF ELECTRICAL CONDUIT

The material properties of electrical conduit significantly affect the EMP penetration of the conduit. To make accurate EMP penetration predictions, it is necessary to know the electrical conductivity, σ, and the magnetic permeability, μ.

Most electrical conduit standards (and thus most conduit manufacturers) are concerned primarily with mechanical properties (e.g., strength, cutting properties, and bending properties) and corrosion resistance, so that in many cases it is difficult to find values or to deduce a range of values of the electrical properties for electrical conduit.

Since electrical conduit is not usually manufacturered from conductor grade materials, the electrical conductivity is rarely measured or specified. Similarly, the permeability is not available for electrical conduit because the materials used in conduit are not generally regarded as electromagnetic shielding materials. However, although the physical properties of electrical conduit are not tabulated in the general literature, the values of the physical properties for closely related materials may in some cases permit an estimate of the conduit values. This approach is hampered somewhat by variations in chemical composition, heat treatment, and mechanical working--all of which affect the electrical properties.

Guidance for installation of electrical metallic tubing, rigid metal conduit, and intermediate metal conduit is provided by the National Electrical Code (NEC);[16] however, no specification is given for conduit material. Specifications for conduit manufacture have been set by other agencies such as American National Standards Institute (ANSI) and Underwriters' Laboratories (UL).

To be approved by UL, individual conduit product lines (i.e., conduit fittings, and junction boxes) must be manufactured in accordance with UL standards. The requirements for electrical metallic tubing stated in UL 797[17] are:

> 2.1 Each tube used in the manufacture of electrical metallic tubing shall be of mild steel, a silicon-bronze alloy containing at least 1.25 percent silicon, an aluminum-base alloy containing no more than 0.40 percent copper, or other metal which, upon

[16] National Electrical Code, 1975 Edition, NFPA No. 70-1975, National Fire Protection Association (1974). This has been approved by the American National Standards Institute and is also know as ANSI C1-1975.

[17] *Standard for Electrical Metallic Tubing*, UL797 (UL, Inc., June 20, 1973). Approved as ANSI 33.98-1973, June 20, 1973.

investigation, is found to be suitable for the purpose. The tube shall be uniformly thick throughout the length of the tube. The welding of all seams shall be thoroughly well done.

The requirements for rigid metal conduit stated in UL 6[18] are:

2.1 Each tube used in the manufacture of rigid metal conduit shall be of steel, wrought iron, silicon-bronze alloy C65100 (low-silicon bronze B) or C65500 (high-silicon bronze A) as detailed in the American Society for Testing and Materials "Standard Specification for Copper-Silicon Alloy Seamless Pipe and Tube" (ASTM B315-1976), and aluminum alloy containing no more than 0.40 percent copper, or another metal that upon investigation, is found suitable for the purpose.

The requirements for rigid aluminum conduit specified in WW-C-00540c[19] are:

3.2 Detail. Conduit, couplings, elbows, and nipples furnished under this specification shall conform to the United States of America Standards Institute (USASI) Standard C80.5.

However, concerning the composition of rigid aluminum conduit, USAS C80.5-1966 states:[20]

3.4 Alloy. The conduit shall be made of an aluminum alloy containing not more than 0.40 percent copper.

Except for the 0.40 percent copper, the alloy is not specified; however, the Aluminum Association states:[21]

Composition and Manufacture. Rigid aluminum conduit is extruded from the magnesium-silicide, 6063-T1 alloy. Special precautions are taken to obtain a lower copper content than industry standards permit. In this way the corrosion resistance of the alloy is greatly increased.

Typical composition limits for aluminum conduit metal are given in Table E1.

Nominal values for the electrical resistivity are shown in Table E2 for various tempers. This suggests that even with the same nominal chemical composition, the electrical resistivity may vary up to 13 percent depending upon the temper.

---

[18] *Standard for Rigid Metal Conduit*, UL6, 8th Ed. (UL, 1976), p 5.

[19] *Interim Federal Specification Conduit, Metal, Rigid; and Coupling, Elbow, and Nipples, Electrical Conduit: Aluminum*, WW-C-00540c(GSA-FSS) (Federal Supply Service, General Services Administration, 1967), p 2.

[20] *USA Standard Specification for Rigid Aluminum Conduit*, USAS C80.5-1966 (ANSIO).

[21] *Aluminum Electrical Conductor Handbook* (The Aluminum Association), p 17-2.

Table E1

Composition Limits of Aluminum Conduit Alloy

	Percentage Limits per Industry Standards	Aluminum Conduit, Typical Percentages
Copper	0.10 max.*	0.02
Silicon	0.20 to 0.6	0.40
Iron	0.35 max.	0.20
Magnesium	0.45 to 0.9	0.7
Manganese	0.10 max.	0.01
Chromium	0.10 max.	0.01
Titanium	0.10 max.	0.01
Zinc	0.10 max.	0.02
Others	0.15 max.	Trace
Aluminum	Remainder	Remainder

*Maximum limit set by the Aluminum Association. Alloys with up to 0.40 percent copper are acceptable to UL for use in rigid aluminum conduit; typical conduit uses only 0.02, or 95 percent less. (From *Aluminum Electrical Conductors Handbook*, p 17-6.)

Table E2

Variation of Typical Values of Electrical Resistivity of Alloy 6063 with Temper*

Temper	Electrical Resistivity (Ω-m)	Electrical Conductivity (mho/m)
O	3.0×10^{-8}	3.3×10^{7}
T1	3.4×10^{-8}	2.9×10^{7}
T5	3.1×10^{-8}	3.2×10^{7}
T6, T83	3.3×10^{-8}	3.0×10^{7}

*From *Aluminum Standards and Data*, 5th Ed. (Aluminum Association, 1976), p 39.

Table E3 shows nominal values of resistivity for pure aluminum cited in the literature. Values of resistivity for aluminum are occasionally suggested as suitable for use in shielding studies; however, it is apparent that the typical values cited for pure aluminum differ from those given for aluminum conduit alloy.

As part of this study, the resistivity of one specimen of nominal 1-in. (25-mm) rigid aluminum conduit was measured. It was found that

$$\rho = 3.8 \times 10^{-8} \ \Omega\text{-m} \qquad \text{[Eq E1]}$$

or

$$\sigma = 2.6 \times 10^{7} \ \text{mho/m} \qquad \text{[Eq E2]}$$

Since the alloy in aluminum conduit is primarily aluminum, one would expect that the permeability should be near that of pure aluminum, i.e., a relative permeability which is essentially constant and nearly equal to 1. Aluminum is actually paramagnetic with a maximum relative permeability[22] of 1.00000065. The actual permeability of aluminum conduit alloy does not appear to be available in the literature or in any of the standards.

However, it is easier to establish parameters for aluminum conduit than for ferrous conduit because the material composition is primarily aluminum with only small quantities of alloying elements and impurities. The specifications for rigid steel conduit, zinc coated, are given in UL6, WW-C-581d,[23] and ANSI C80.1-1971;[24] however, the composition of the steel is not specified. The requirements for electrical metallic tubing (EMT) are given in UL 797, WW-C-563A,[25] and USAS C80.3-1966;[26]

[22] *Reference Data for Radio Engineers*, 6th Ed. (H. W. Sams & Co., 1975), p 4-32.

[23] *Federal Specification Conduit, Metal, Rigid; and Coupling, Elbow, and Nipple, Electrical Conduit: Zinc Coated*, WW-C-81d (Federal Supply Service, General Services Administration, 5 June 1962).

[24] *American National Standard Specification for Rigid Steel Conduit, Zinc Coated*, ANSI C80.1-1971 (R-1966) (ANSI).

[25] *Federal Specification Conduit, Metal, Rigid: Electrical, Thin-Wall Steel Type (Electrical Metallic Tubing); Straight Lengths, Elbows, and Bends*, WW-C-563A (General Services Administration, December 1973).

[26] *USA Standard Specification for Electrical Metallic Tubing, Zinc Coated*, USAS C80.3-1966 (ANSI).

Table E3

Typical Values of Electrical Resistivity
and Conductivity of Aluminum

ρ(ohm-meter)	σ(mho/meter)	Reference
2.50×10^{-8} (0°C)	4.00×10^{7}	*
2.74×10^{-8} (22°C)	3.65×10^{7}	*
2.7809×10^{-8} (20°C)	3.5960×10^{7}	**
2.62×10^{-8} (20°C)	3.82×10^{7}	†
2.65×10^{-8}	3.77×10^{7}	††

*D. E. Gray, *American Institute of Physics Handbook*, 3rd Ed. (McGraw Hill, 1972), p 9-39.

**E. G. Fink, Editor-in-Chief, and J. M. Carroll, Associate Editor, *Standard Handbook for Electrical Engineers*, 10th Ed. (McGraw Hill, 1968), p 4-8.

†*Standard Handbook for Electrical Engineers, Reference Data for Radio Engineers*, 6th Ed. (H. W. Sams & Co., 1975), p 4-21.

††T. Lyman, Ed., *Metals Handbook*, Vol 1, 8th Ed. (American Society for Metals, 1961).

however, again the composition of the steel is not specified. In both cases, requirements are made for mechanical properties, but the heat treatment or mechanical working of the materials is not specified. It would be expected that there will be some variation in the chemical composition, mechanical working, and heat treatment of different conduit.

Conduit conductivity and permeability are rarely measured. However, conduit and line pipe steels are generally similar, and the conductivity of line pipe steel has been determined.[27] The resistivities (in micro-ohm-centimeters) of 24 line pipe steels representative of the range of composition used in manufacturing API 5L, API 5LX (through X60), ASTM A 53, and ASTM A 106 grades were determined. The resistivities range from 14.97 to 22.83 μohm-cm.

Table E4 shows the chemical compositions of the line pipe steel specimens. The range (in percent by weight) of each constituent was:

Carbon	0.13-0.29
Manganese	0.39-1.28
Phosphorus	0.007-0.073
Sulfur	0.018-0.034
Silicon	0.026-0.250
Vanadium	0.0-0.08

A multiple regression analysis indicated that 97.2 percent of the variation in resistivity could be accounted for by the elements manganese, silicon, and phosphorus, whereas the effect of carbon, vanadium, and sulfur (within the range of the steels considered) was not significant. The resistivity (in micro-ohm centimeters) can be calculated from the chemical composition by Eq E3 using the percents of manganese, silicon, and phosphorus:

$$\rho = 11.59 + 5.43\ (\%Mn) + 16.1\ (\%Si) + 15.4\ (\%P)$$

Calculated and actual resistivities are compared in Table E5.

The permeability of steel is complicated by the ferromagnetic nature of the steel. Ferromagnetic materials are characterized by

a. Relatively large values of permeability

b. Variation of permeability with field strength

c. Saturation at high magnetic field intensities

[27] S. S. Brown and F. W. Anney, *Electrical Resistivity of Line Pipe Steels*, Paper No. 69, 20th Annual Conference of National Association of Corrosion Engineers (1964).

Table E4

Chemical Composition of Line Pipe Steel Specimens*

Specimen Number	Major Constituents, Except Iron (Weight %)					
	Carbon	Manganese	Phosphorus	Sulfur	Silicon	Vanadium
1	.23	.45	.011	.024	.051	-
2	.27	.45	.009	.018	.050	-
3	.19	.51	.007	.020	.160	-
4	.24	.98	.011	.027	.160	-
5	.26	.89	.009	.026	.180	-
6*	.24	.94	.013	.026	.040	-
7	.18	.48	.008	.030	.150	-
8	.21	.46	.008	.034	.150	-
9	.19	.52	.007	.022	.160	-
10	.28	.88	.010	.021	.160	-
11	.27	.94	.012	.020	.170	-
12	.21	.89	.013	.028	.170	-
13	.25	.82	.009	.025	.033	-
14	.29	.80	.007	.025	.048	-
15	.26	.80	.010	.026	.051	-
16	.22	1.28	.010	.027	.054	.06
17	.18	1.19	.011	.026	.050	.06
18	.21	1.22	.010	.026	.066	.07
19	.23	1.28	.015	.029	.250	.08
20	.19	.97	.009	.020	.250	.06
21	.18	1.20	.012	.020	.200	.07
22	.15	.45	.070	.026	.029	-
23	.13	.49	.073	.023	.026	-
24	.14	.39	.067	.021	.033	-

*Five samples of this composition, designated by 6A, 6B, 6C, 6D, and 6E, were made for the electrical resistivity determinations. (From S. S. Brown and F. W. Anney, *Electrical Resistivity of Line Pipe Steels*, Paper No. 69, 20th Annual Conference of National Association of Corrosion Engineers [1964].)

Table E5

Comparison of Measured and Calculated Resistivity*
(Using the Percentage of Mn, Si, and P and the Equation
$\rho = 11.59 + 5.43\ [\%Mn] + 16.1\ [\%Si] + 15.4\ [\%P]$)

Specimen No.	Measured Resistivity micro-ohm-cm	Calculated Resistivity micro-ohm-cm	Deviation Measured Minus Calculated
1	15.51	15.02	.49
2	14.97	14.98	-.01
3	17.00	17.04	-.04
4	19.69	19.66	.03
5	20.05	19.46	.59
6	16.87	17.54	-.67
7	15.98	16.73	-.75
8	16.38	16.63	-.25
9	17.19	17.10	.09
10	19.77	19.10	.67
11	19.35	19.62	-.27
12	19.13	19.36	-.23
13	16.80	16.71	.09
14	17.24	16.81	.43
15	16.70	16.91	-.21
16	19.30	19.56	-.26
17	19.33	19.03	.30
18	19.56	19.43	.13
19	22.83	22.80	.03
20	21.39	21.02	.37
21	21.02	21.51	-.49
22	15.79	15.58	.21
23	15.66	15.79	-.13
24	15.26	15.27	-.01

*From S. S. Brown and F. W. Anney, *Electrical Resistivity of Line Pipe Steels*, Paper No. 69, 20th Annual Conference of National Association of Corrosion Engineers (1964).

d. Hysteresis (a nonlinear dependence of the magnetization on the previous magnetic history of the material).

The magnetic properties of steel are often strongly dependent on chemical composition, mechanical working and heat treatment. Table E6 shows nominal values of the relative permeability

$$\mu_r = \frac{\mu}{\mu_o} = 1 + \frac{M}{\mu_o H}$$

for several iron alloys where

μ_o = permeability of free space

M = magnetization

H = magnetic field intensity.

It is apparent that magnetic properties are greatly influenced by chemical composition.

Based on DC resistance measurements and RFI attenuation measurements, the conductivity and the single value of relative permeability μ shown in Table E7 have been suggested for the purpose of calculating theoretical shielding effectiveness. The product $\mu\sigma$ based on these suggested values is also shown in Table E7.

Unfortunately, the permeability of conduit steel does not appear to be tabulated in the literature.

Table E6

Relative Permeability of Various Ferromagnetic Materials

Material	Initial	Maximum	Reference
Very pure iron	4,000	8,000	*
Silicon iron	3,500	7,000	
Transformer iron	3,000	5,500	
Machine steel	300	450	
Cast iron	60	90	
Low carbon iron	200	2,200-5,500	**
1010 steel	200	3,800	
1% Si silicon steel	400-650	1,700-6,000	

*_Reference Data for Radio Engineers_, 6th Ed. (H. W. Sams & Co., 1975), p 4-32.

**T. Lyman, Editor, _Metals Handbook_, 8th Ed., Vol 1 (American Society for Metals, 1966).

Table E7

Properties of Shielding Materials Based on DC Resistance Measurements and RFI Attenuation Measurements*

Material Type	Conductivity, σ (mho/m)	Relative Permeability μ_r	$\mu\sigma$
Galvanized steel	1.056×10^7	270	3580
Hot rolled steel	0.958×10^7	160	1930
Cold rolled steel	0.942×10^7	127	1500
Terne steel	0.907×10^7	157	1790

*From R. B. Cowdell, R. A. Hupp, and J. N. O'Leary, *RFI Attenuating Materials and Structures*, Technical Report AFAPL-TR-69-89 (Air Force Aero Propulsion Laboratory, Air Force Systems Command, 1969), p 125.

APPENDIX F:

EMP PENETRATION OF DEFECTS, CONDUIT FITTINGS, AND RELATED HARDWARE

Approach

As previously indicated, the solid conduit provides the basic shielding in a conduit system. Defects arising in the conduit such as cracks and breaks may seriously compromise the shielding. Certain hardware items may also compromise the EMP shielding of the system. Completed conduit systems may include numerous fittings and related hardware such as couplings, unions, case access fittings (condulets), pull boxes, junction boxes, and flexible sections. The fittings and hardware used are usually standard conduit accessories, since very few fittings and hardware items have been designed specifically for EMP-hardened structures. Thus, these items may compromise the EMP shielding. In order to assess the EMP penetration of the conduit system, it is therefore necessary to evaluate the leakage contribution as a result of various defects and hardware items for the current waveshape of interest.

The problem of determining the electromagnetic field leakage through conduit fittings or defects is less amenable to direct analytical solutions than is the problem of determining the electromagnetic field penetration of solid conduit. The analysis is complicated by the complex, varied, and often irregular geometries associated with fittings and defects.

Since the exact mathematical analysis of even relatively simple defects, conduit fittings, and hardware items is a very difficult (and in some cases, nearly impossible) task, some reliance must necessarily be placed on empirical results. On the other hand, the signals resulting from defects quite often depend on the magnitude and waveshape of the applied current as well as the characteristics of the defect itself. Thus, complete reliance on empirical data would necessitate acquisition of enormous amounts of data to account for the potential variations in waveshape and characteristics of defects which might occur in actual conduit systems. The resultant volume of data would be difficult (if not impossible) to use, and extrapolation to situations for which data were not taken would not be easy.

Obviously, some compromise between a purely theoretical approach and a purely empirical approach is required to arrive at a useful result for the designer of conduit systems. This study therefore based its approach on relatively simple mathematical models supplemented with experimental evaluation of certain parameters.

The signals induced on an internal wire within a defective conduit can be considered to arise as a result of the wire coupling with the electric and magnetic fields associated with the current in the vicinity of the defect. In some cases, the induced signal might be interpreted as a result of direct electric field and magnetic flux leakage. Alternatively, the signal might be considered to result from the impedance of a defect changing as the current distribution changes during a pulse. Or, the signals might be interpreted as arising from the change in electric and magnetic fields at the outer surface of a conduit, since the electromagnetic fields would be expected to change as the current--which initially flows almost exclusively on the surface--penetrates into the conduit material. Regardless of the exact nature of their origin, the observed phenomena can be described to a first approximation by a general model in which the driving voltage induced by a defect has a waveshape that is proportional to the applied conduit current plus its time derivative. This appendix considers some details of this general model for EMP penetrations of defects.

Electrical Discontinuities

Time Domain

To a first approximation, the electric field in the vicinity of a defect may be considered to be related to the potential across a resistive component of the defect while the current is being applied. In other words, the voltage on the sense wire might be modeled as

$$V_L(t) = R_1 I(t) \qquad \text{[Eq F1]}$$

where R_1 = a coefficient representing the linkage between the conduit current and the sense wire.

In the proposed model for defects for a particular position of the sense wire, the coefficient R_1 (in units of ohms) would be characteristic of a given defect and should be constant for that defect. Qualitatively, one would expect this coefficient to vary from defect to defect depending on resistance across the defect and proximity of the sense wire to the defect.

A contribution to the leakage signal due to this effect should have the same waveshape as the applied current. In other words,

$$\frac{I_o(t)}{I_c(t)} = \text{a constant} \qquad \text{[Eq F2]}$$

Frequency Domain

In the frequency domain, the Fourier transform of the induced voltage

$$V(t) = R_1 I(t) \qquad \text{[Eq F3]}$$

is

$$V(\omega) = R_1 I(\omega) \qquad \text{[Eq F4]}$$

The flaw impedance for resistive flaws will be essentially independent of frequency. Thus, the conduit current and the conductor current will have identical waveforms:

$$\frac{I_o(\omega)}{I_c(\omega)} = \text{a constant} \qquad \text{[Eq F5]}$$

Rusty couplings are an example of electrical discontinuities which are almost entirely resistive.

Apertures

Theoretical Analysis

Time Domain. In the presence of an aperture, a second source of a leakage signal could be linkage of magnetic flux with the sense wire. Qualitatively, one would expect the induced voltage on the sense wire to be proportional to the time rate of change of the flux, i.e.,

$$V_L \propto -\frac{d\Phi}{dt} \qquad \text{[Eq F6]}$$

The flux is proportional to the magnetic flux density B

$$\Phi \propto B \qquad \text{[Eq F7]}$$

In nonmagnetic materials

$$B = \mu_o H(t) \qquad \text{[Eq F8]}$$

and

$$H(t) \propto I(t) \qquad \text{[Eq F9]}$$

It follows that a contribution from this source would be expected to be of the form

$$V_L = M_2 \frac{dI(t)}{dt} \qquad \text{[Eq F10]}$$

where M_2 = a coefficient representing the linkage between the magnetic flux and the sense wire

In the proposed model for defects, the coefficient M_2 (in units of henrys) would be constant for a given sense wire and defect configuration. However, one would expect the coefficient to vary with defect dimensions as well as the proximity of the sense wire to the defect. A contribution to the leakage signal from this mechanism would be expected to be proportional to the time derivative of the applied current.

The general model for the direct field penetration of a defect is therefore proposed to be:

$$V_L = R_1 I + M_2 \frac{dI}{dt} \qquad \text{[Eq F11]}$$

where R_1 and M_2 = constants indicating the coupling coefficients between the sense wire and the electric and magnetic fields, respectively.

Frequency Domain. The Fourier transform of

$$V_L(t) = M_2 \frac{dI(t)}{dt} \qquad \text{[Eq F12]}$$

is

$$\hat{V}_L(\omega) = M_2 \, j\omega \, \hat{I}(\omega) \qquad \text{[Eq F13]}$$

Thus,

$$\frac{\hat{V}_L(\omega)}{\hat{I}(\omega)} = j\omega M_2 \qquad \text{[Eq F14]}$$

Hence, one would expect the transfer impedance to be frequency-dependent.

HDL-measured values for flaw impedance of apertures show an approximate 20 dB per decade increase in Z_F. This implies that

$$Z_F = cj\omega \qquad \text{[Eq F15]}$$

where c = a constant

$j = \sqrt{-1}$

$\omega = 2\pi f$

f = frequency

Thus, from Figure F1 and since $Z_f << Z_o$ in most cases

I_o is: $$I_o(\omega) = \frac{Z_F}{2Z_o} I_c(\omega) = \frac{c}{2Z_o} j\omega\, I_c(\omega) \qquad \text{[Eq F16]}$$

and

$$I_o(t) = \frac{c}{2Z_o} \frac{1}{2\pi} \int_{-\infty}^{\infty} j\omega I_c(\omega)\, e^{j\omega t}\, d\omega = \frac{c}{2Z_o} \frac{d}{dt} I_c(t) \qquad \text{[Eq F17]}$$

The constant

$$\frac{c}{2Z_o} = \frac{Z_F(\omega)}{2Z_o} \frac{1}{\omega} \qquad \text{[Eq F18]}$$

can be evaluated from the measured flaw impedance curve.

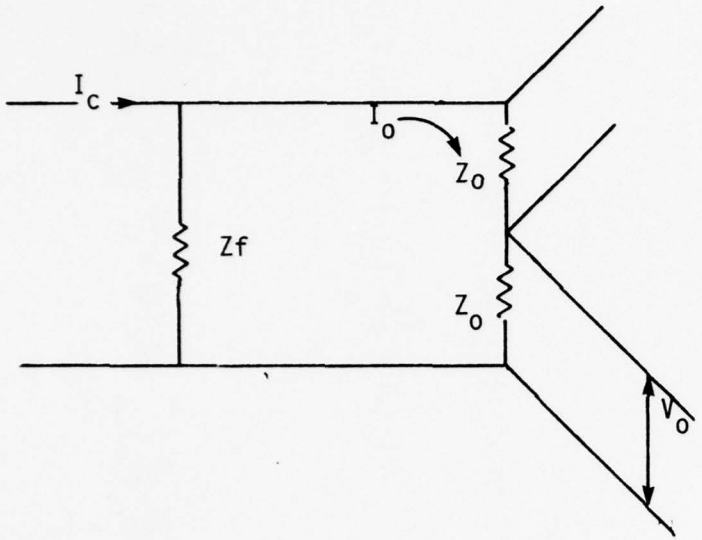

Z_f = flaw impedance

I_c = conduit current

I_o = current induced on transmission line

Z_f = transmission line impedance

V_o = induced voltage

$$I_o = \frac{I_c Z_f}{2Z_o + Z_f}$$

Figure F1. Conduit flaw impedance concept.

It should be noted that in general the flaw impedance will not be an easily recognizable function, and calculation of the Fourier transform of the function will be more complicated than this example.

Empirical Results

Time Domain. As stated previously, the matched sense wire signal for a conduit having an aperture has been hypothesized to include three basic components: (a) a small contribution due to diffusion, (b) a resistive component proportional to the current applied to the conduit, and (c) the component due to induced signals resulting from leakage of the electromagnetic fields through the aperture. The third --or leakage--component is further hypothesized to be proportional to the time derivative of the applied conduit current. To test the hypothetical model for the matched sense wire for a conduit with an aperture, a series of measurements was made on aluminum conduit samples. A solid conduit was tested to show the diffusion and resistive components of the signal. Six other samples containing accurately machined slots 1/2, 1, 2, 4, 8, and 16 cm long were tested to show the leakage signal contribution. The slots were machined to the lengths stated with a depth of exactly one-half of the conduit diameter. Thus, for the slot length, one-half of the wall was machined out. Figure F2 shows the conduit samples.

The sense wire signal was measured with the wire held exactly centered in the conduit. Centering was accomplished by means of two plastic (Lucite) washers placed inside the conduit with a center hole in each washer for passage of the sense wire.

The current source for these experiments was the battery discharge configuration described in Appendix B. The current was injected into the conduit samples by means of 12 AWG copper wires attached to the conduit using stainless steel radiator hose clamps (Figure F3). To minimize the resistive and diffusion components of the signal, the current was injected 1 cm from the slot ends. The injection wires were placed on the side away from the slot opening to minimize field distortion due to the wires.

Verification of the mathematical model was accomplished using the following steps:

a. Measurement and recording of the injected current and matched sense wire signals for the six conduit slot samples

b. Determination of the constants and coefficients of the equation from the ERDAC III data

c. Plotting of the ERDAC III data using a PDP-11 minicomputer, tape data transfer system, and a Calcomp 565 plotter

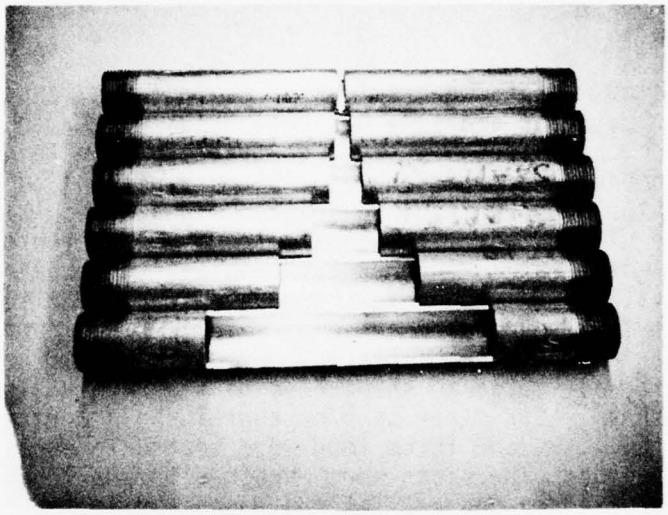

Figure F2. Conduit slot samples.

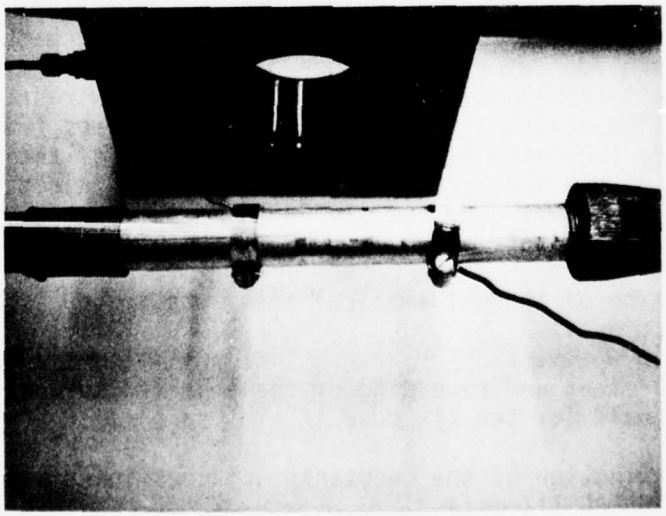

Figure F3. Current injection connections for slot tests.

d. Superimposing plots of the mathematical model expression (with constants as determined in step b) on the ERDAC III data plots.

Step a. A conduit sample having an 8-cm-long slot with injection 1 cm from each slot end (or 10-cm distance between injection points) was compared with a solid conduit with current injection over a 10-cm distance. Figure F4 shows the ERDAC III signals for the solid conduit and Figure F5 shows the ERDAC III signals for the conduit sample with an 8-cm slot. For both conduit samples, the measured current peak was 369 ERDAC III units, which converts to 227.4 A. The measured sense wire signal for the solid conduit had a peak value of 19 ERDAC III units, which converts to 1.86 mV. For the 8-cm slot, the sense wire signal tail was asymptotic to a value of 42.4 ERDAC III units, which converts to 4.14 mV.

From purely resistive considerations, the expected sense wire voltage would be defined by

$$V_R = [I_c \; R_L] \times \frac{1}{2} L \qquad \text{[Eq F19]}$$

where V_R = the voltage across the sense wire terminating resistor

I_c = the injected conduit current

R_L = the resistance per unit of length

L = the conduit length over which current is injected

The factor of 1/2 is used because of the voltage division by the two sense wire matching resistors.

Through measurement of resistivity, the aluminum conduit was found to have a resistance of 2.4×10^{-4} ohms/m. Using this value and the 227.4-A conduit current, the anticipated voltage across the sense wire terminating resistor for a 10-cm solid conduit is 2.73 mV. With a sample of the same length containing an 8-cm slot the same wire voltage should be 4.91 mV. The difference between the expected and measured values may be partially attributable to the accuracy of the ERDAC III (0.5 percent of full scale, and partially to the method of injecting current, wherein current density within the 10-cm length is not uniform within the conduit. At any rate, the values presented do show that the contribution due to diffusion current in the time frame of interest and for the test method used is small.

Step b. In the present case, the applied current has the form shown in Eq F20 and Figure F6:

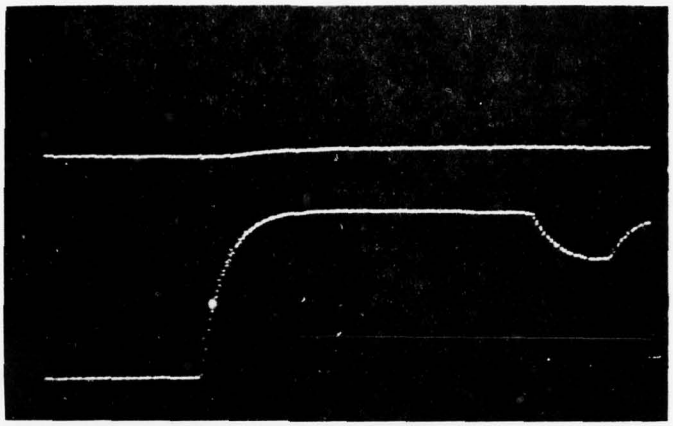

Channel 1 (upper) 0.1 V full scale
Channel 2 (lower) 1.0 V full scale
(Time displayed: 720 μsec)

Figure F4. Solid conduit, ERDAC III recording of injected current (lower trace) and sense wire signal (upper trace).

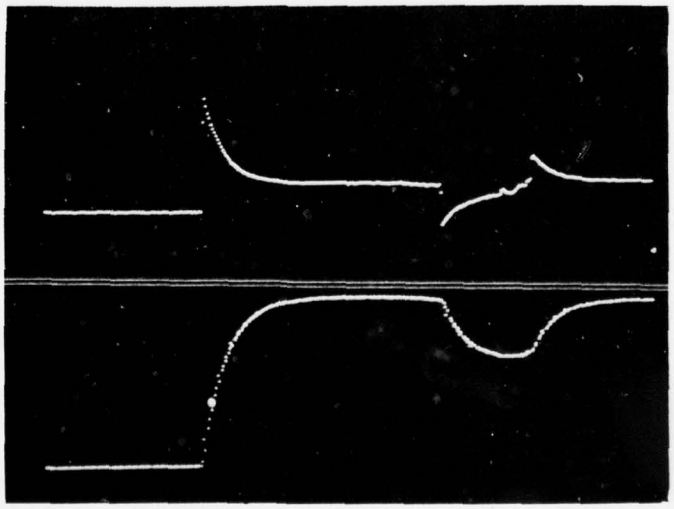

Channel 1 (upper) 0.1 V full scale
Channel 2 (lower) 1.0 V full scale
(Time displayed: 720 μsec)

Figure F5. Conduit with 8-cm slot, ERDAC III recording of injected current (lower trace) and sense wire signal (upper trace).

$$I(t) = I_o\,[1-e^{-t/\tau_o}] \qquad \text{[Eq F20]}$$

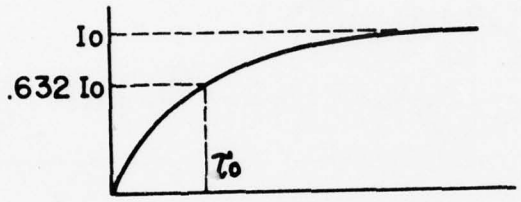

Figure F6. Form of applied current.

The derivative of the applied current has the form shown in Eq F21 and Figure F7.

$$\frac{dI}{dt} = \frac{I_o}{\tau_o}\, e^{-t/\tau_o} \qquad \text{[Eq F21]}$$

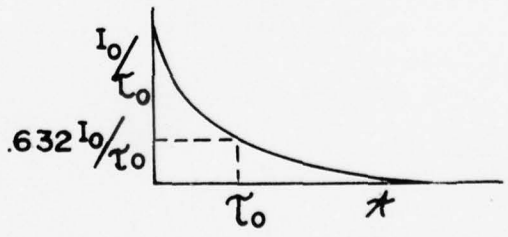

Figure F7. Form of the derivative of the applied current.

According to this general model, the total leakage signal measured will be

$$V_L = R_L[I_o(1-e^{-t/\tau_o})] + M[\frac{I_o}{\tau_o}\, e^{-t/\tau_o}] \qquad \text{[Eq F22]}$$

AD-A056 218 CONSTRUCTION ENGINEERING RESEARCH LAB (ARMY) CHchampai--ETC F/G 9/5
DEVELOPMENT OF CONDUIT DESIGN ANALYTICAL PROCEDURE.(U)
JUN 78 W CROISANT, P NIELSEN, D SIEBER

UNCLASSIFIED CERL-IR-M-234 NL

2 OF 2
AD A056218

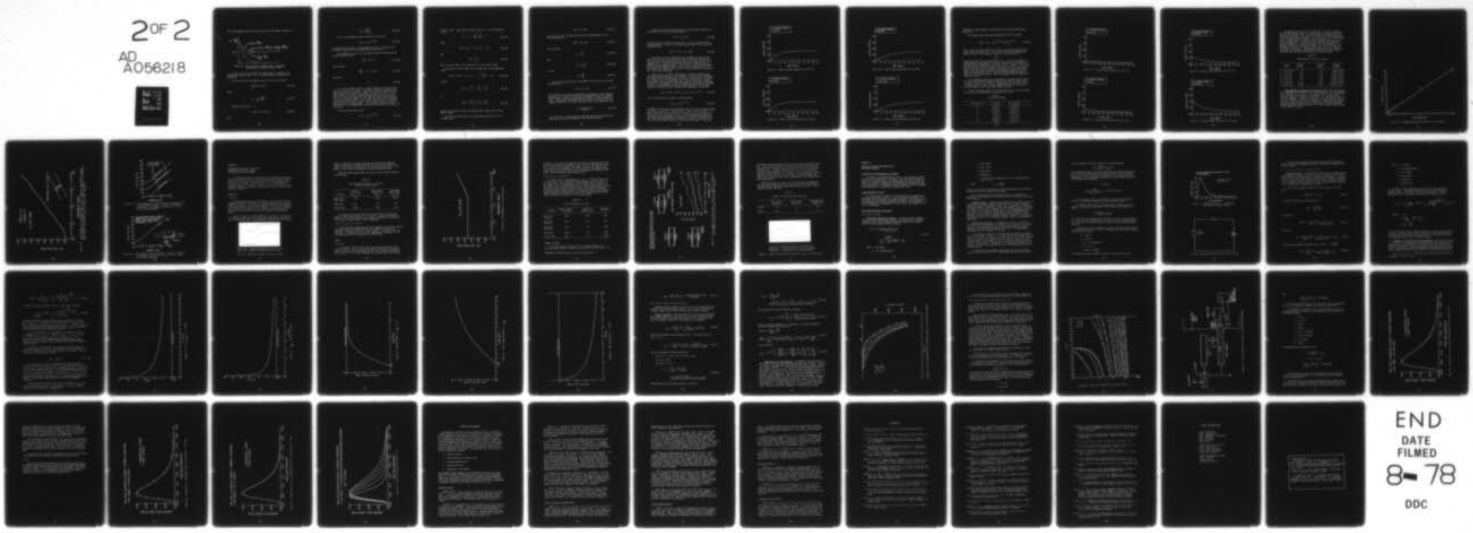

END
DATE FILMED
8-78
DDC

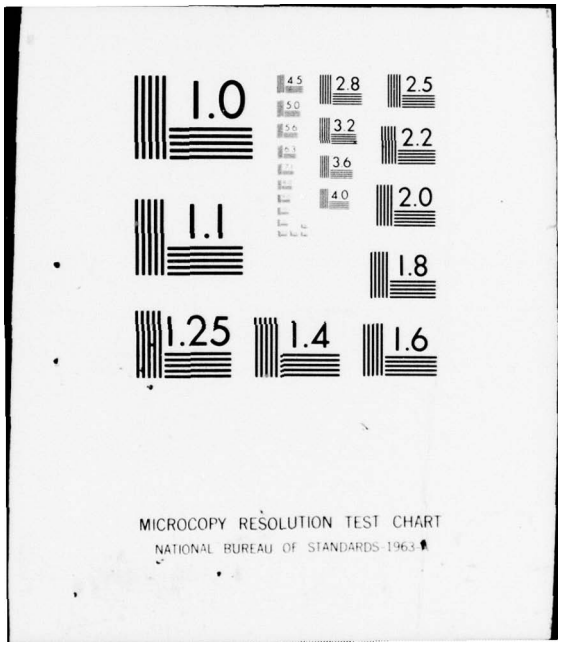
1.0
1.1
1.25
1.4
1.6
1.8
2.0
2.2
2.5
2.8
3.2
3.6
4.0
4.5
5.0
5.6
MICROCOPY RESOLUTION TEST CHART
NATIONAL BUREAU OF STANDARDS-1963-A

Thus, the leakage signal will have the typical form shown in Figure F8.

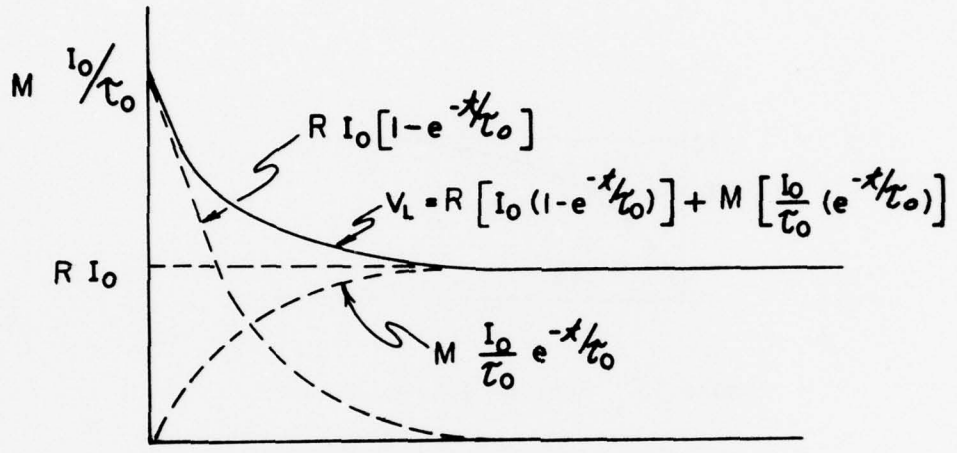

Figure F8. Typical form of leakage signal. Individual contributions are shown by broken lines.

The next task is to evaluate the coefficients R_1 and M_2 for the defect under consideration. This is accomplished by a combination of procedures.

First, notice that the applied current for very late times is

$$\lim_{t\to\infty} V_L(t) = R_1 I_o \qquad \text{[Eq F23]}$$

Hence

$$R_1 = \lim_{t\to\infty} \frac{V_L(t)}{I(t)} \qquad \text{[Eq F24]}$$

Second, note that at $\tau = 0$

$$V_L(o) = 0 + M_2\, I_o/\tau_o \qquad \text{[Eq F25]}$$

Hence

$$M_2 = \frac{V_L(o)}{(I_o/\tau_o)} \qquad \text{[Eq F26]}$$

Thus, if the measured current can be fit to the form

$$I(t) = I_o\,[1-e^{-t/\tau_o}] \qquad \text{[Eq F27]}$$

by appropriate selection of the parameters I_o and τ_o, then the coefficients R_1 and M_2 can be evaluated with relative ease.

The parameters I_o and τ_o can be readily deduced from the applied current by noting that

$$\lim_{t\to\infty} I(t) = I_o \qquad \text{[Eq F28]}$$

and that when

$$\frac{I(t)}{I_o} = 1-e^{-1} = 0.632 \qquad \text{[Eq F29]}$$

the time is

$$t = \tau_o \qquad \text{[Eq F30]}$$

In practice, however, there is some variability in the digitized data for a variety of reasons. For example, when monitoring both the applied current and the leakage signal, the transient digitizer alternately samples the signals at a sampling interval of 1 μsec. Hence, data points for a specific signal are spaced at intervals of 2 μsec, which is significant compared to the time constants of the excitation current and leakage signals. This causes some difficulty in determining exactly the time of the start of the current pulse as well as the peak value of the leakage signal. This situation requires a slight modification in the fundamental technique of evaluating the coefficients R_1 and M_2.

Consider the applied current

$$I(t) = I_o\,[1-e^{-t/\tau_o}] \qquad \text{[Eq F27]}$$

for early times. Note that for small values of x, a series expansion yields

$$e^{-x} = 1 - x + \frac{x^2}{2!} + \frac{x^3}{3!} + \ldots. \qquad \text{[Eq F31]}$$

Hence

$$I(t) = I_o\,[1 - (1 - t/\tau_o + \ldots.)] \qquad \text{[Eq F32]}$$

and

$$I(t) \simeq \frac{I_o}{\tau_o}\,t \qquad \text{[Eq F33]}$$

Thus, for early times, the current pulse is very nearly linear.

Similarly, for small times, series expansion of the exponentials yields

$$V_L(t) = R_1 I_o[1 - (1-t/\tau_o+. \;.\;.)] + \frac{M_2 I_o}{\tau_o}[1 - t/\tau_o+. \;.\;.] \qquad \text{[Eq F34]}$$

so that

$$V_L(t) \simeq \frac{R_1 I_o}{\tau_o}\,t + \frac{M_2 I_o}{\tau_o} - \frac{M_2 I_o}{\tau_o} \qquad \text{[Eq F35]}$$

or

$$V_L(t) \simeq \frac{M_2 I_o}{\tau_o} + \frac{I_o}{\tau_o}\left[R_1 + \frac{M_2}{\tau_o}\right] t \qquad \text{[Eq F36]}$$

Hence, for very early times, the leakage signal should also be very nearly linear.

The first few data points for the applied current are fit to a straight line:

$$I(t) = A_1 + B_1 t \qquad \text{[Eq F37]}$$

Similarly, the first few data points for the leakage signal are fit to a straight line:

$$V_L(t) = A_2 + B_2 t \qquad \text{[Eq F38]}$$

Then note that

$$B_1 = \frac{I_o}{\tau_o} \qquad \text{[Eq F39]}$$

and

$$A_2 = M_2 \frac{I_o}{\tau_o} \qquad \text{[Eq F40]}$$

so that

$$M_2 = \frac{A_2}{B_1} \qquad \text{[Eq F41]}$$

The first few data points of the ERDAC III were fit to a straight line defined by

$$I(t) = A_1 + B_1 t \qquad \text{[Eq F37]}$$

This straight-line fit was accomplished by performing a least squares regression to a straight line using a programmable desk top calculator (HP-65) which yielded the coefficients A_1 and B_1 in terms of ERDAC III units. Using these coefficients and the value of the baseline of the conduit current I(t), a value of the start time T_o was determined from

$$T_o = \frac{Y_{baseline} - A_1}{B_1} \qquad \text{[Eq F42]}$$

This value for T_o is more accurate than that which could have been obtained by using the first ERDAC III point above baseline.

Similarly, the first few data points of the measured leakage signal were fit to a straight line defined by

$$V_L(t) = A_2 + B_2 t \qquad \text{[Eq F38]}$$

with A_2 and B_2 calculated using the HP-65. Using T_o (obtained above) in this equation, a value for the peak leakage signal (I_o/τ_o) was then determined from

$$V_L(o) = I_o/\tau_o = A_2 + B_2 T_o \qquad \text{[Eq F43]}$$

The value for I_o was determined from the ERDAC III data by averaging the baseline of the injected-current waveform and subtracting this value from the averaged value to which the injected current rises asymptotically. The value thus obtained was then converted back to amperes from the ERDAC III units. The value for τ_o was then determined by interpolation between ERDAC III data points to determine the time when 0.632 (1/e) times the final value is reached relative to the value of T_o previously determined.

Steps c and d. A PDP-11 minicomputer, tape data transfer unit, and Calcomp 565 plotter were used to assist in verifying the mathematical model for the leakage signal through the conduit slots. The ERDAC III records which were recorded on tape were transferred to the tape data transfer unit, and from there were input into the PDP-11 computer. The PDP-11 was programmed to plot the waveforms as recorded by the ERDAC. In addition, a program was written to enable the PDP-11 and Calcomp plotter to compute and plot a summation of exponentials of the form

$$f(t) = ae^{-\alpha t} + be^{-\beta t} + ce^{-\gamma t} + de^{-\delta t} + ge^{-\theta t} \qquad \text{[Eq F44]}$$

Thus, after plotting the conduit current waveform

$$I(t) = I_o\,(1-e^{-t/\tau_o}) \qquad \text{[Eq F27]}$$

the ERDAC III data were used to derive values for I_o (the current maximum value) and τ_o (the 1/2 or e-fold value). In f(t) above (Eq F44), c, d, and g were set to zero, a and b were set equal to I_o, α was set to infinity, and β was set equal to $1/\tau_o$. This curve was then plotted as a continuous line superimposed onto the plot of the ERDAC recorded waveform, which was represented by a sequence of squares. Figures F9, F10, F11, and F12 show these curves for the noted slot lengths. Excellent

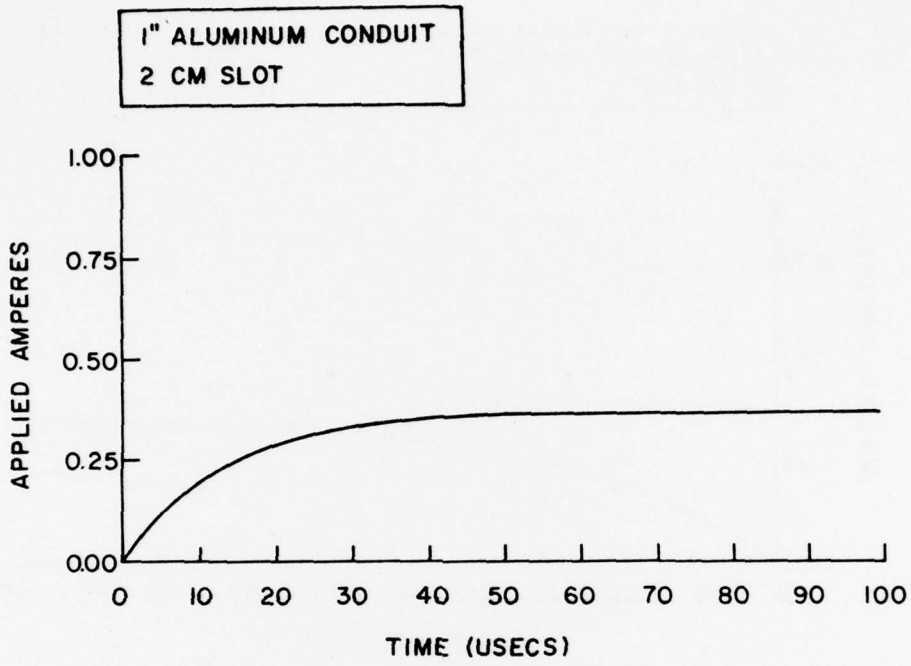

Figure F9. Conduit current waveform for 2-cm slot.

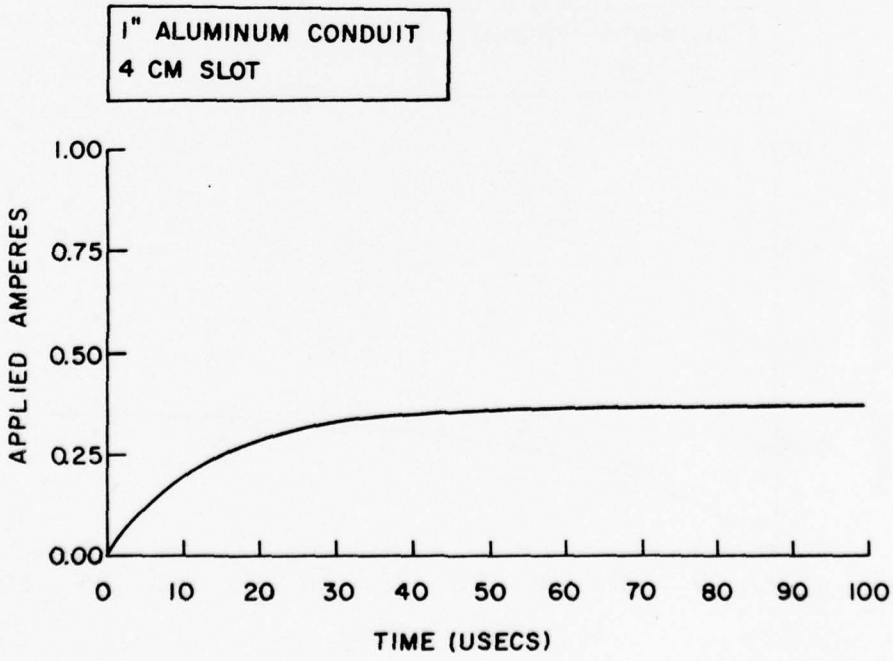

Figure F10. Conduit current waveform for 4-cm slot.

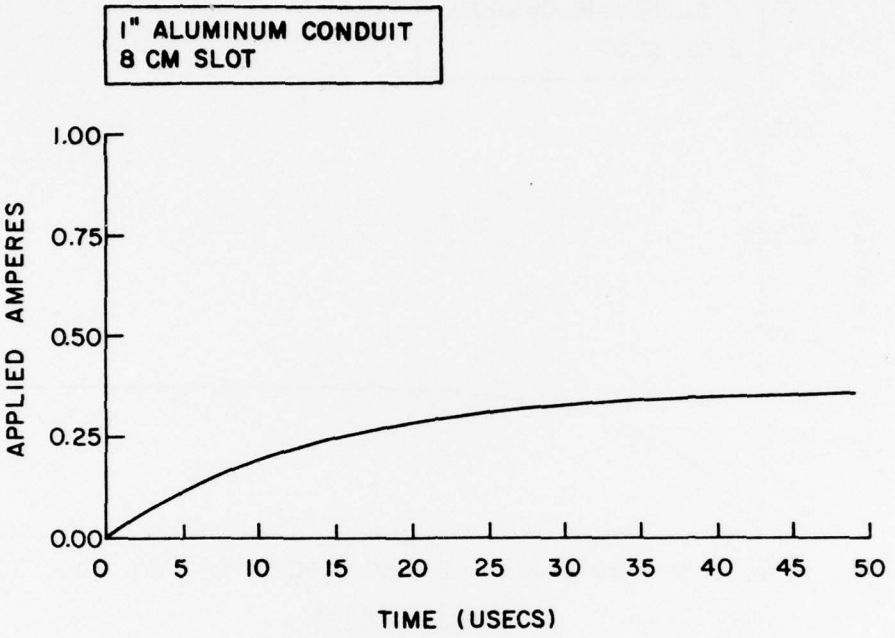

Figure F11. Conduit current waveform for 8-cm slot.

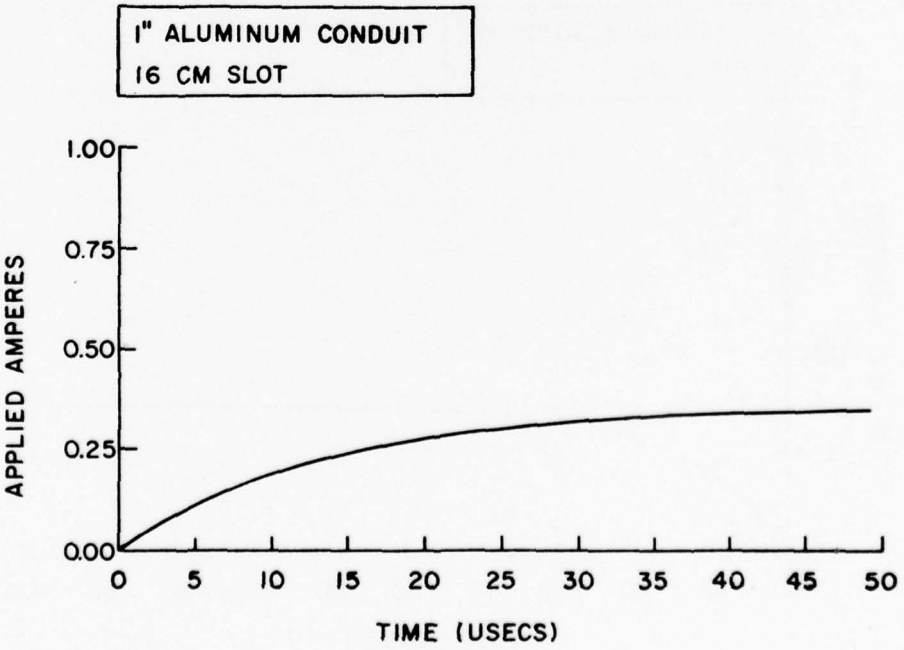

Figure F12. Conduit current waveform for 16-cm slot.

agreement is shown between the calculated curve and the experimental data curve.

The leakage signal has been hypothesized to be of the form

$$V_L(t) = R_1 I_o - R_1 I_o e^{-t/\tau_o} + M_2 \frac{I_o}{\tau_o} e^{-t/\tau_o} \qquad \text{[Eq F45]}$$

Thus, in Eq F44, d and g were set to zero, α was set to infinity, and β and γ were set equal to τ_o. A value for $R_1 I_o$ was derived from the ERDAC III data as the asymptotic value of V_L and the value for

$$M_2 \frac{I_o}{\tau_o}$$

was derived from $V_L(o)$, the peak value of V_L. Plots of the ERDAC recorded waveforms were made by a series of squares, and the calculated waveforms were superimposed as continuous lines. Figures F13, F14, F15 and F16 show the results for the 2, 4, 8, and 16-cm slots. Plots were not made for the 1/2- and 1-cm slots because of the low signal magnitudes. Each plot shows reasonably close agreement between the calculated and experimental curves. The conclusion can thus be drawn, at least to a first approximation, that the proposed model does define the sense wire signal.

It is therefore seen that the mathematical expression and a table of values for the coefficients R_1 and M_2 can be used to define every slot type of defect in a conduit. An hypothesis at this point is that a similar model will apply to more complex apertures, such as loose coupling threads, unions, and other conduit fittings.

Table F1 provides values for R_1 and M_2 for the six slots evaluated. Each value listed represents an average of two trials.

Table F1
Values of R_1 and M_2

Slot Size, cm	R_1, ohms	M_2, henries
1/2	5.8×10^{-6}	3.04×10^{-10}
1	6.36×10^{-6}	5.90×10^{-10}
2	7.44×10^{-6}	8.96×10^{-10}
4	1.21×10^{-5}	17.1×10^{-10}
8	1.80×10^{-5}	37.6×10^{-10}
16	2.99×10^{-5}	63.8×10^{-10}

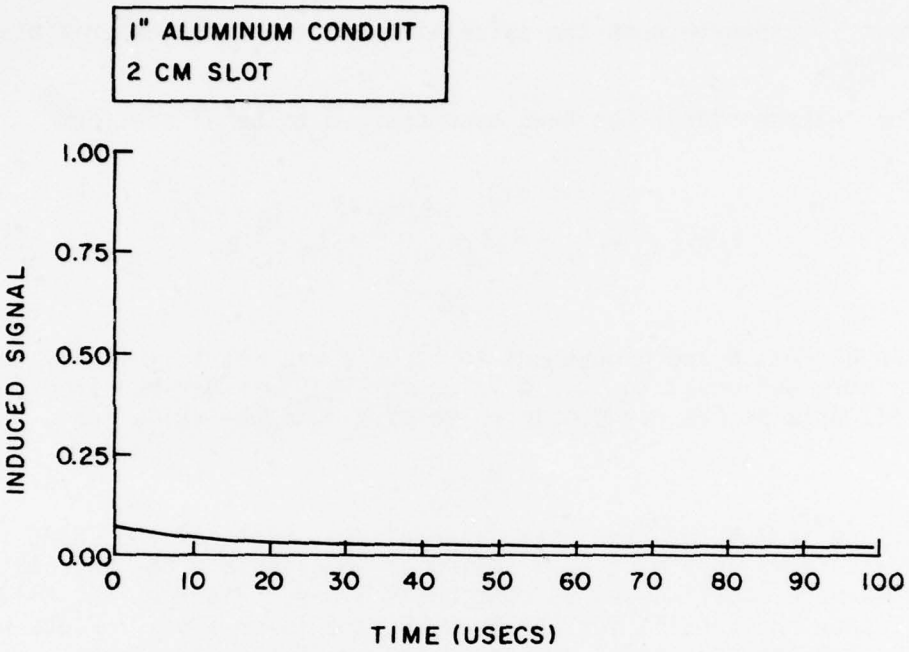

Figure F13. Leakage signal waveform for 2-cm slot.

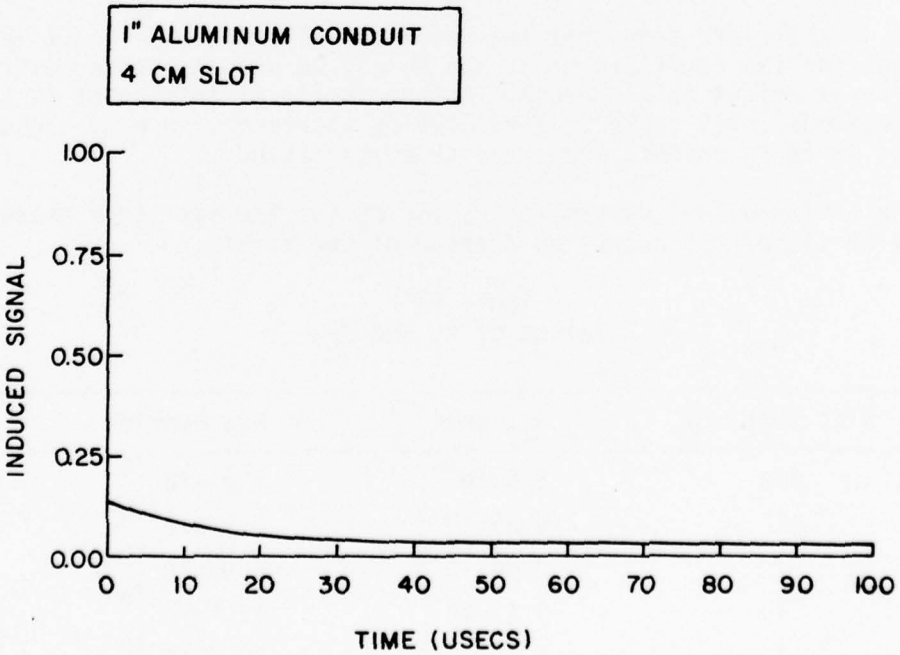

Figure F14. Leakage signal waveform for 4-cm slot.

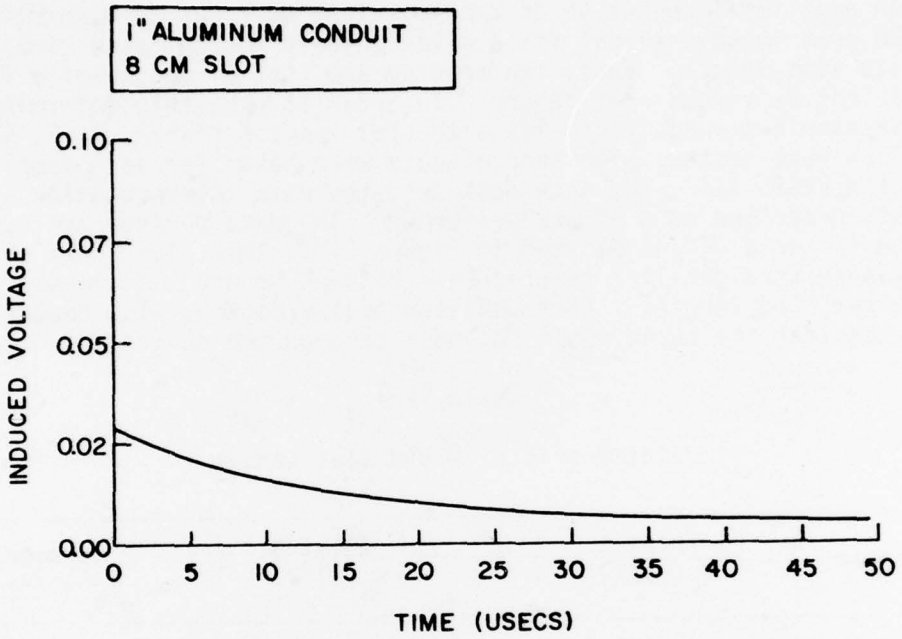

Figure F15. Leakage signal waveform for 8-cm slot.

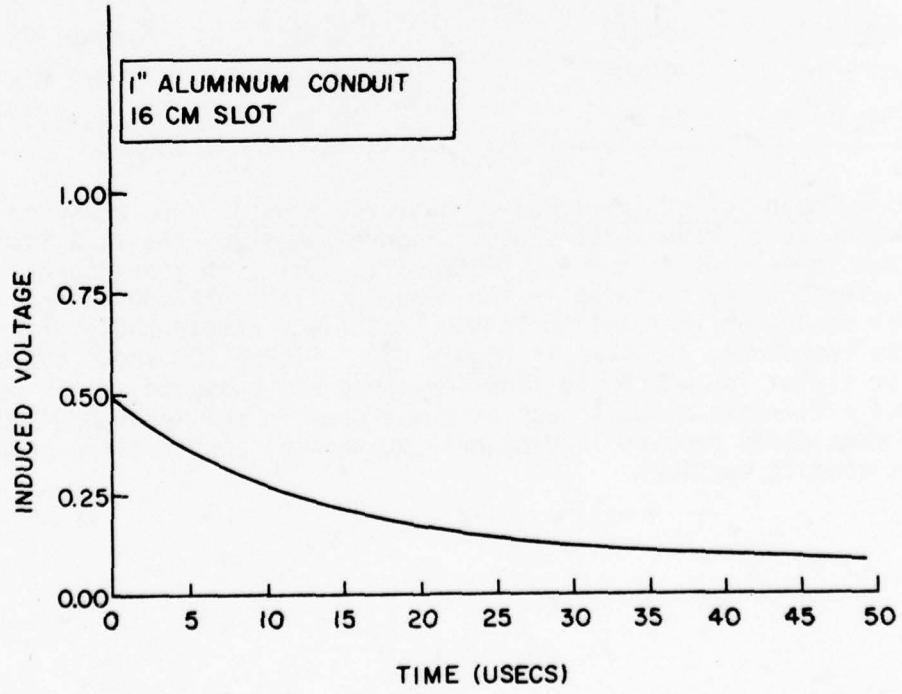

Figure F16. Leakage signal waveform for 16-cm slot.

An additional objective of the empirical work was to determine how the peak leakage signal for a given conduit current rise time varies with slot length. Thus, the problem was that of determining the coefficient M_2 versus slot length. In order to make this determination, the six aluminum conduit samples with slot lengths of 1/2, 1, 2, 4, 8, and 16 cm were tested. Two sets of data were taken for each sample, using the ERDAC III. For each data set, the data interpretation analysis described on p 99 was performed. The data derived are summarized in Table F2 and plotted in Figure F17. This plot shows an approximate straight-line relationship between M_2 and slot length for the larger slot lengths. Extrapolation of the data points, however, indicates that the curve would not pass through the origin.

Table F2

Relationship of M and Slot Length

Sample	Trial 1 $V_L(0)/B_1$	Trial 2 $V_L(0)/B_1$	Average $V_L(0)/B_1$
2-, 1/2-cm slot	.91	1.01	$.96 \times 9.77 \times 10^{-5}$
3-, 1-cm slot	1.95	1.78	$1.87 \times 9.77 \times 10^{-5}$
4-, 2-cm slot	3.01	2.66	$2.84 \times 9.77 \times 10^{-5}$
5-, 4-cm slot	5.16	5.64	$5.40 \times 9.77 \times 10^{-5}$
6-, 8-cm slot	11.49	12.31	$11.90 \times 9.77 \times 10^{-5}$
7-, 16-cm slot	20.00	20.30	$20.15 \times 9.77 \times 10^{-5}$

Flaw Impedance of Apertures (Transverse Slots). HDL measured the flaw impedance of transverse slots. Figure F18 shows the flaw impedance of a transverse slot in a 4-in. (102-mm) conduit with the internal conductor (sense wire) centered in the conduit. The location of the internal conductor in relation to the slot has a considerable effect on the flaw impedance, as shown in Figure F19. Figure F20 shows the worst case for a slot for which the flaw impedance was measured. This worst case was a flexible conduit such as those used in the SAFEGUARD BMD system completely removed leaving only a parallel copper strap connecting the conduit sections.

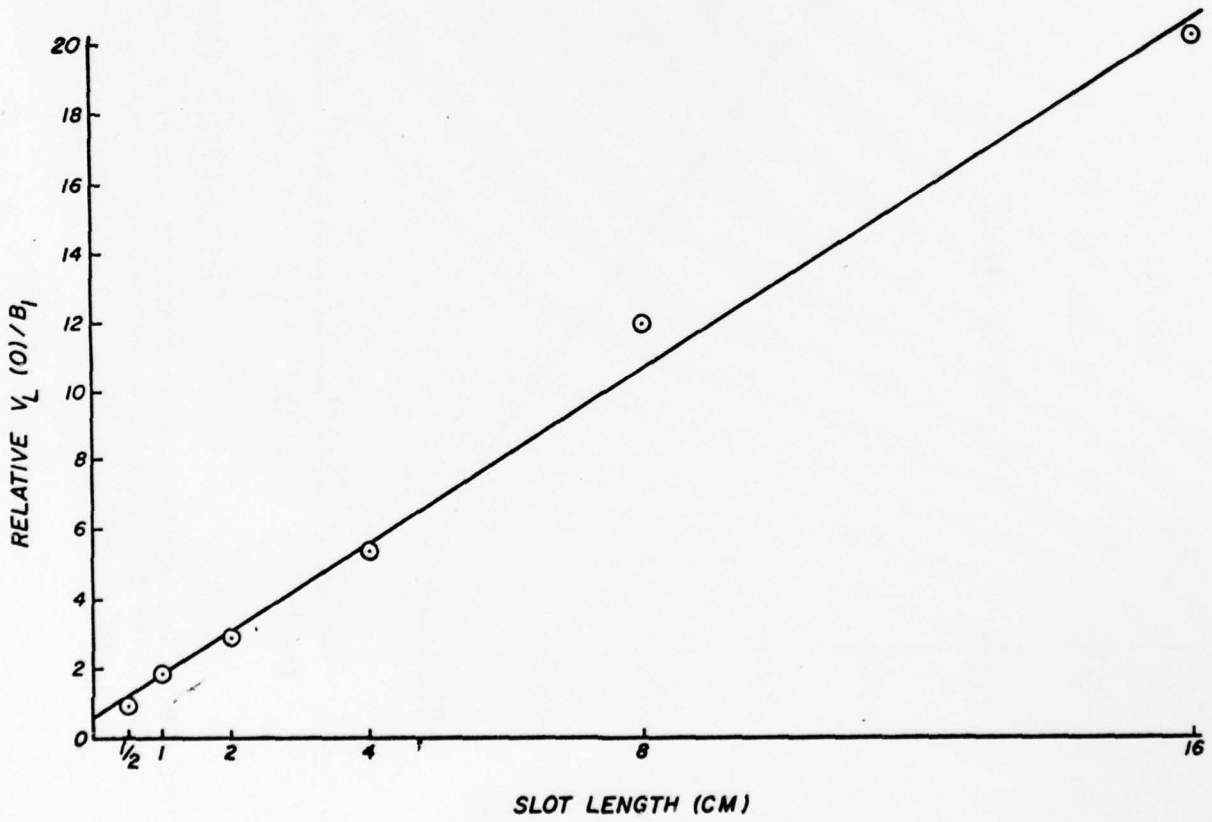

Figure F17. Leakage signal/applied current vs. slot length.

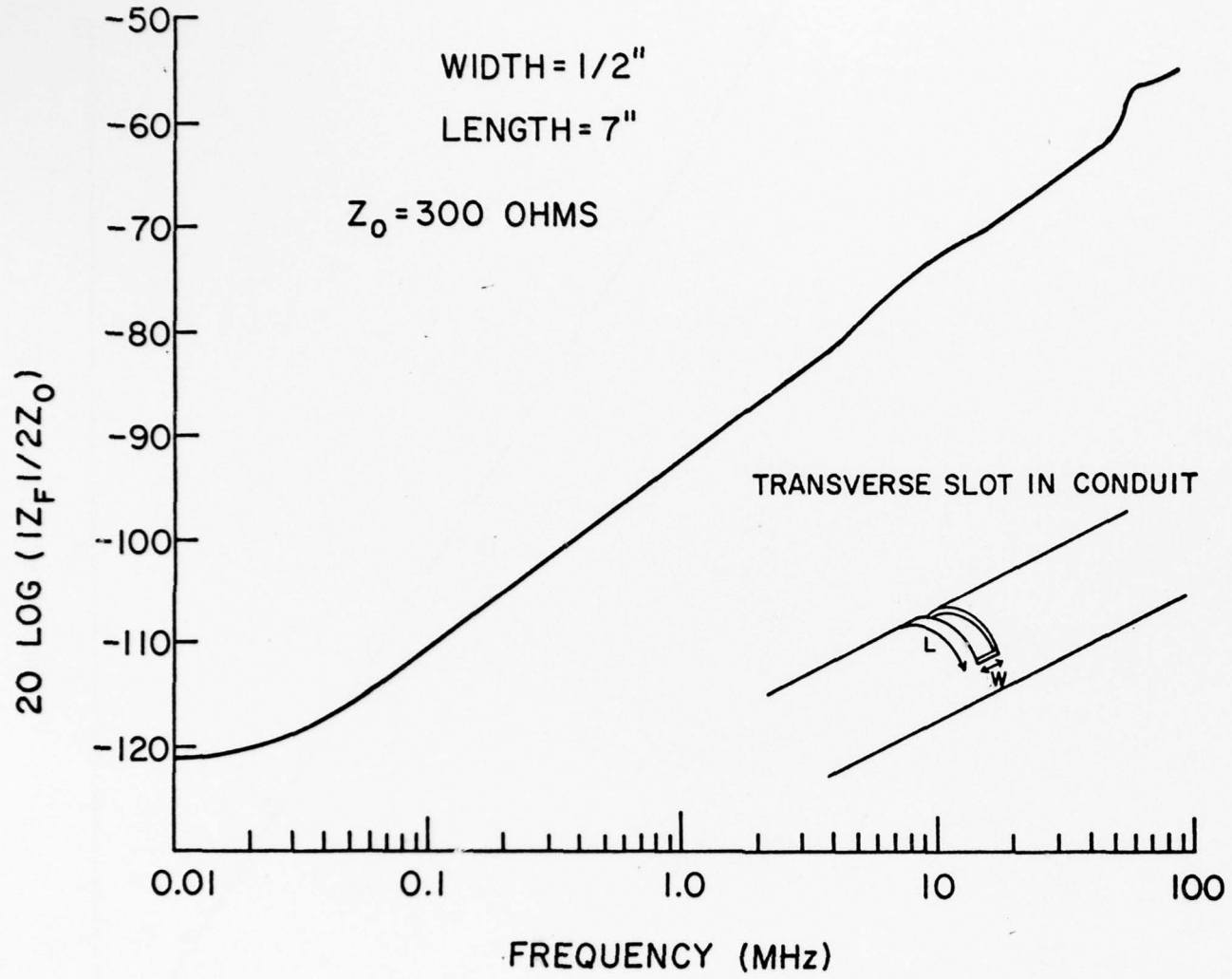

Figure F18. Flaw impedance of a transverse slot in a 4-in. (102-mm) inner diameter conduit with the sense wire centered in the conduit. (From H. A. Roberts, J. Capobianco, and F. Agee, *SAFEGUARD Buried Conduit Studies* [HDL, undated]).

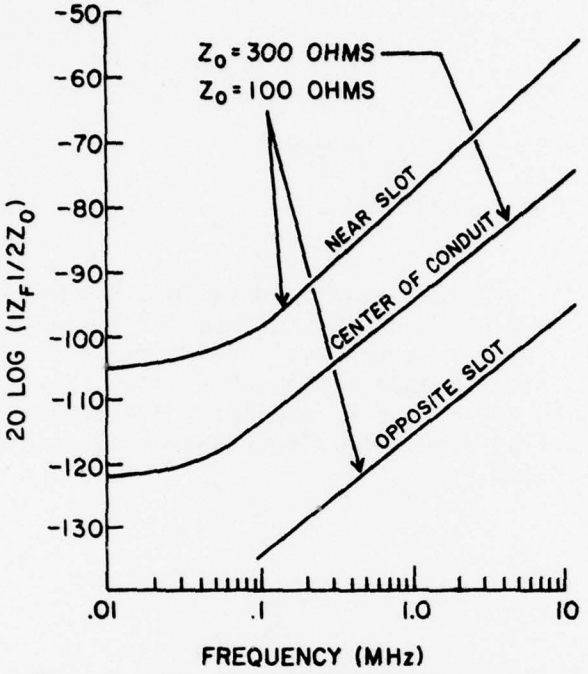

Figure F19. Flaw impedance of transverse slot with sense wire at three different positions. (From H. A. Roberts, J. Capobianco, and F. Agee, *SAFEGUARD Buried Conduit Studies* [HDL, undated]).

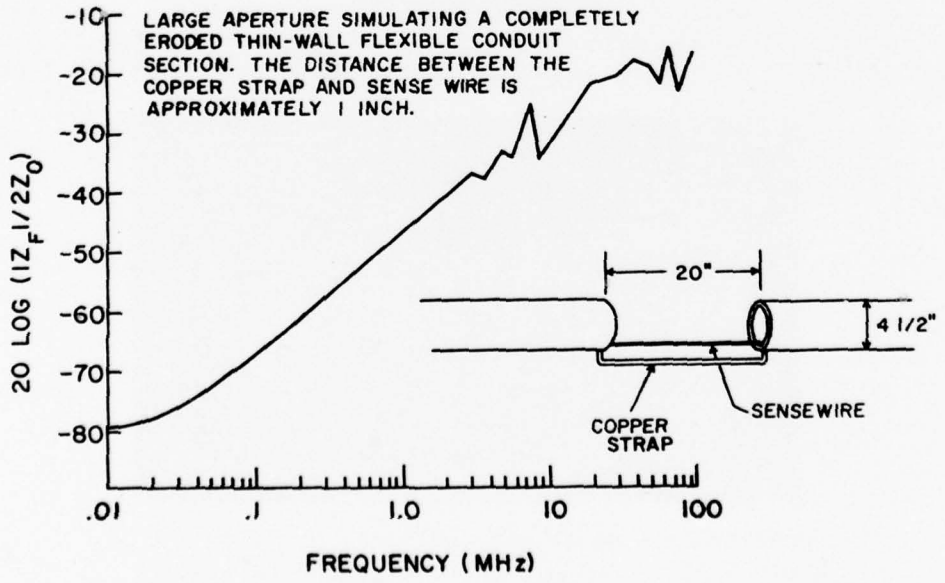

Figure F20. Flaw impedance of large aperture. (From H. A. Roberts, J. Capobianco, and F. Agee, *SAFEGUARD Buried Conduit Studies* [HDL, undated]).

APPENDIX G:

COEFFICIENTS FOR CALCULATION OF EMP PENETRATION OF DEFECTS, CONDUIT FITTINGS, AND RELATED HARDWARE

This appendix supplies coefficients for the mathematical model to enable a simple prediction of the anticipated EMP-induced disturbance for a number of types of conduit-related fittings or hardware items. Results of a time domain investigation of 1-in. (25-mm) aluminum couplings, unions, and a type C condulet (case access fitting), and a frequency domain flaw impedance investigation of rusted couplings and unions are summarized.

Couplings

Time Domain

An aluminum coupling (clean threads) was tested to determine the leakage and resistive components on a matched sense wire for varying degrees of tightness. The current injection method used was identical to the method used in testing slots (Appendix F). For each tightness level tested, the resistance of the coupling and thread matings was measured by the DC current injection and voltage drop measurement method.

Figure G1 shows the recorded ERDAC III waveform for injected current and the matched sense wire signal for a very loose coupling (1/2 turns mated on each end). This photograph indicates that the leakage

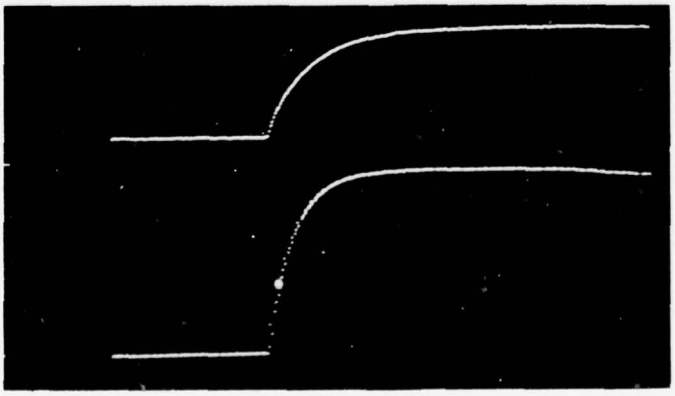

Upper trace - sense wire voltage, 0.1 V full scale
Lower trace - conduit current, 632 A full scale

Figure G1. ERDAC III waveforms for loose coupling.

signal is too small to measure relative to the resistive component. Careful examination also shows that the rise time for the sense wire signal is also longer than the rise time of the injected current. This delay in rise time is attributable to the diffusion delay time.

Table G1 presents peak sense wire signal versus coupling tightness and resistance.

Table G1

Peak Sense Wire Signals vs. Coupling Tightness and Resistance

Tightness	DC Resistance, ohms X 10^{-3}	Peak Conduit Current (I_C) amps	Peak Sense Wire Signals (V_L), mV
Hand tight less 1 turn	.307	123.5	109.0
Hand tight	0.011	121.0	19.5
Wrench tight	0.008	120.4	18.6

It should be noted that the data in Table G1 were derived with current injection over about 18 in. (0.46 m) of conduit, including the coupling. The signal measured thus includes a substantial contribution due to diffusion and resistive signal components.

Conduit Coupling Flaw Impedance

Figure G2 shows the HDL-measured flaw impedance for a rusted coupling. The shape of the flaw impedance curve will probably be similar for different thicknesses of the rust layer; however, its magnitude will be different. The impedance is virtually independent of frequency for the rusty coupling joint at frequencies less than 10 MHz.

Unions

Time Domain

An aluminum explosion-proof union was tested as described in the previous section. The union ends were wrench-tightened onto the mating conduit sections, but the coupling ring was set at varying tightnesses for the tests. In all tests performed, the leakage signal was too small

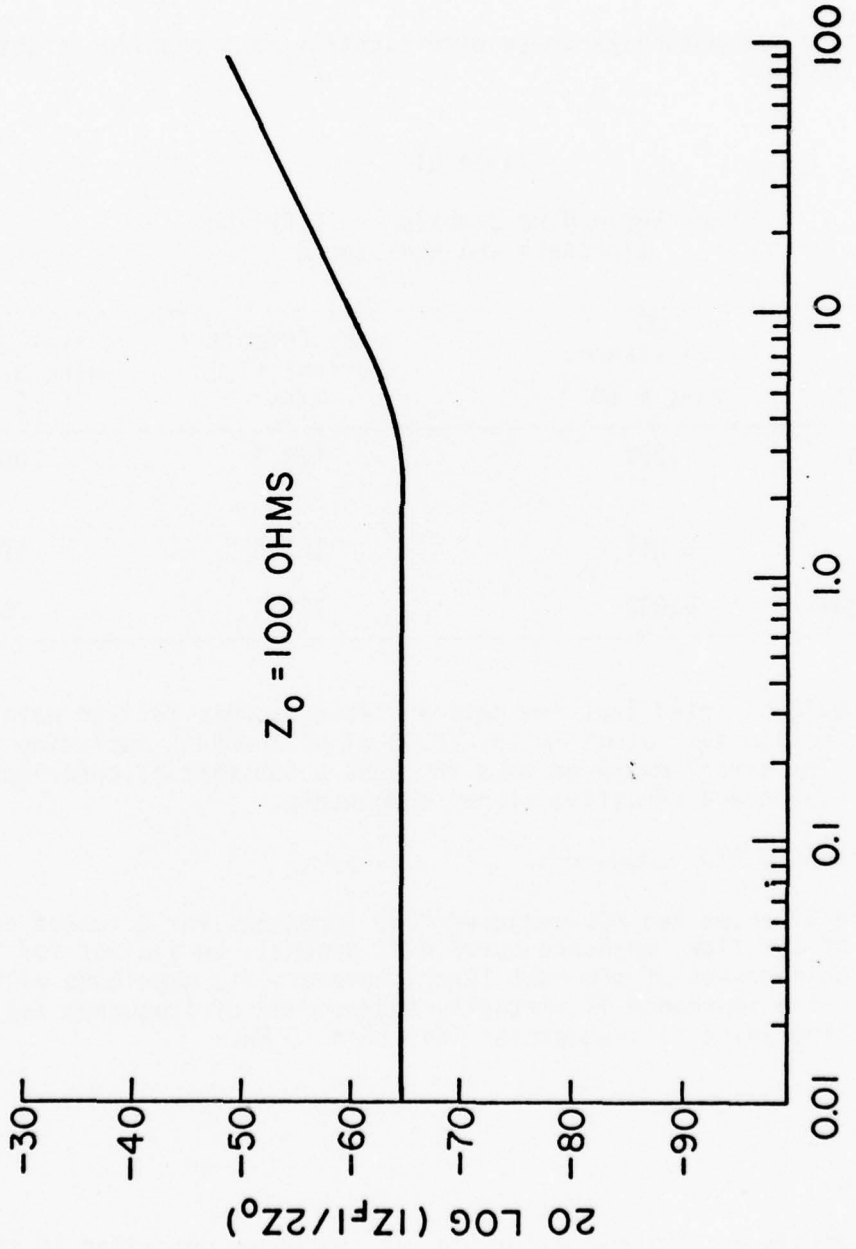

Figure G2. Flaw impedance of a rusted coupling.

to measure. The resistive component and diffusion components were thus the only signal portions measured. Since injection was made over about 18 in. (0.46 m) of the conduit including the union, the constant diffusion and resistive components for that portion of the sample prevent a correlation of sense wire signal versus the measured resistance of the union. Table G2 presents data from the tests.

Conduit Union Flaw Impedance

HDL measured the flaw impedance for a 4-in. (102-mm) conduit union for five cases: (a) a relatively loose assembly at 50 ft-lb (68 N-m) of torque, (b) a tight assembly at 300 ft-lb (407 N-m) of torque, (c) an assembly having a teflon washer placed between the mating faces of the union pieces, thus preventing contact, (d) an assembly having teflon insulation placed between concentric parts of the union, preventing adequate electrical contact, and (e) an assembly having a Lucite wedge placed between the mating faces of the union, preventing even contact. Figure G3 presents the results of these measurements.

Table G2

Union Time Domain Test Data

Tightness	Conduit Current, (I_C) amps	Sense Wire Signal, V_L mV	Resistance, mΩ
Hand tight 2 turns	227.3	37.9	0.26
Hand tight 1/2 turn	225.4	10.6	0.071
Hand tight 1/8 turn	231.6	6.2	0.036
Hand tight	231.6	3.7	0.022
Wrench tight	242.1	3.2	0.018

Conduit Fittings

An aluminum conduit fitting (Type C, straight-through, 1-in. [25.4-mm] Electrolet*) was tested as described for the couplings. The

*Electrolet is a brand name of the Killark Corporation.

Five cases investigated using a clean union. Case I was torqued to 50 ft-lbs and all other cases were torqued to 300 ft-lbs.

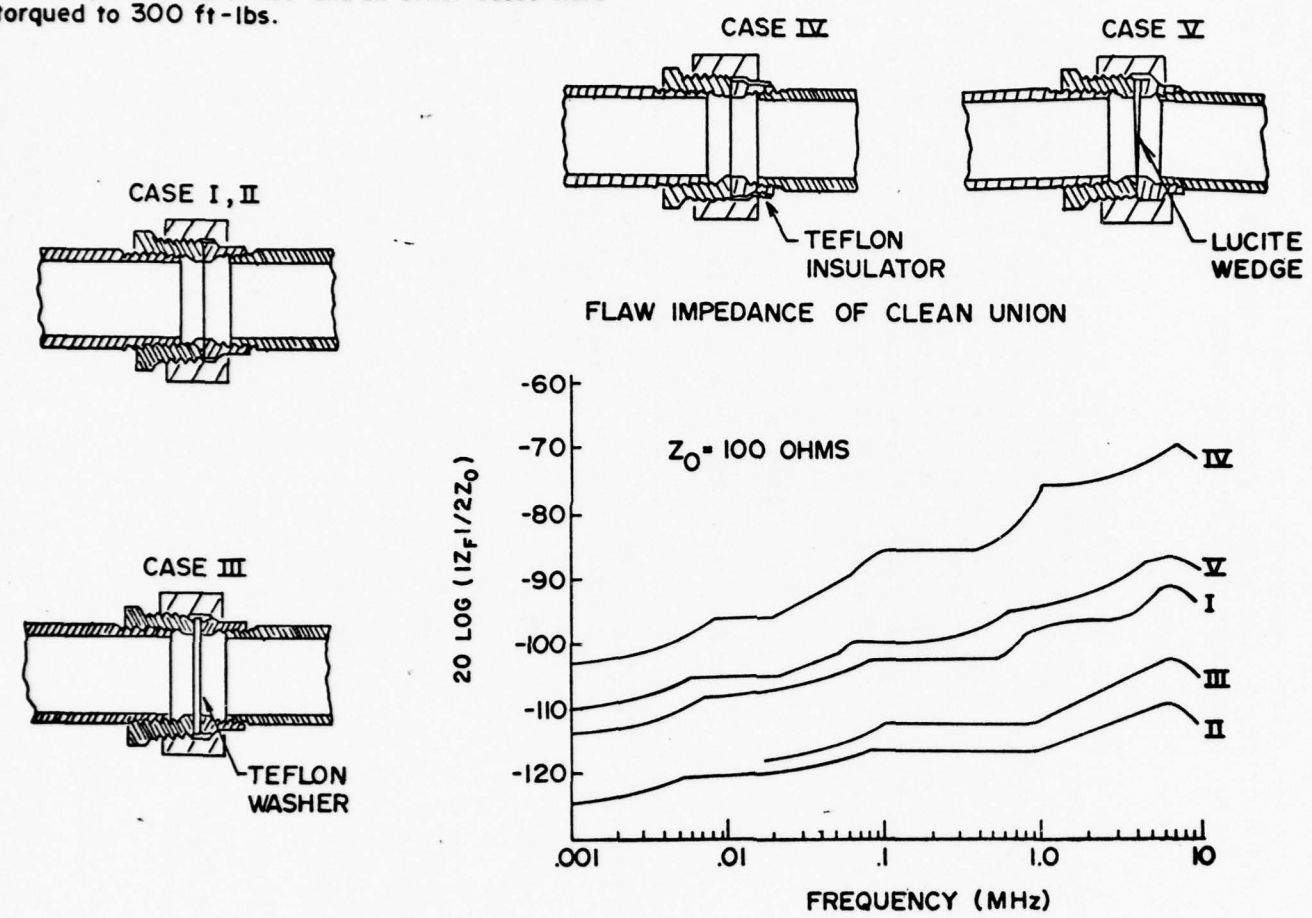

Figure G3. Flaw impedance of conduit union. (From H. A. Roberts, J. Capobianco, and F. Agee, *SAFEGUARD Buried Conduit Studies* [HDL, undated]).

fitting was wrench-tightened onto the mating conduit sections at each end. Tests were made with and without the aluminum cover plate on. Figure G4 shows the ERDAC III recorded signals for the fitting with the cover off. A leakage component exists, but it is much smaller than the leakage component for a conduit with slot length and size comparable to the opening in the fitting. This difference is attributable to the fact that the fitting flange extends well beyond the sense wire and thus the fields must penetrate much more deeply than in the slotted sample.

When tested with the cover on, the leakage signal component on the sense wire became too small to measure, but the diffusion and resistive signal components remained essentially the same. Table G3 presents data for the tests.

Table G3

Conduit Fitting Time Domain Test Data

	Peak Conduit Current, A	Peak Leakage Signal, mV	Peak Resistive Signal, mV
Lid off	221.7	3.3	3.8
Lid on	227.3	0	4.1

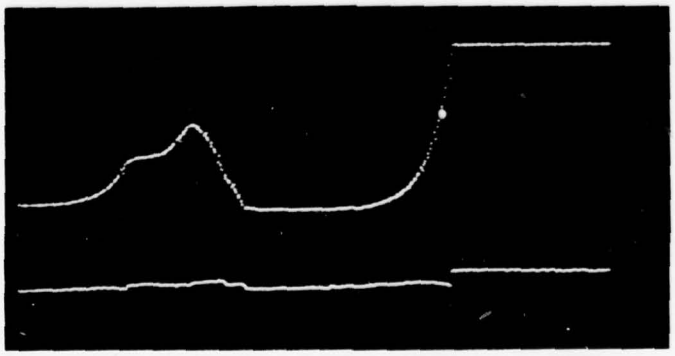

Top trace = sense wire signal, 0.1 V full scale
Bottom trace = conduit current, 632.4 A full scale
(time base: 1 μsec/sample, 725 μsec displayed)

Figure G4. ERDAC III waveforms for Electrolet, Type C with cover off.

APPENDIX H:

EFFECTS OF CIRCUIT CONFIGURATION ON
EMP-INDUCED SIGNALS

Transmission Line Propagation of Signals

For rapidly varying EMP-induced signals, the propagation must be analyzed using transmission line theory. The onset of the signal at the end of a conduit system will be delayed by the time it takes the signal to travel the distance from the location of the defect to the end of the conduit. Furthermore, possible reflections due to mismatch in termination of a transmission line may also arise.

Lumped Parameter Circuits

For slowly varying signals, the transmission line properties become less significant, and in the limit such problems approach the equivalent circuit problem with lumped parameters. The time delay due to propagation time becomes negligible for slowly varying signals, since the velocity of propagation is nearly that of the speed of light ($c = 3 \times 10^8$ m/sec).

EMP-Induced Voltages and Currents

Open Circuit Voltage

Time Domain Theoretical Analysis. The open circuit voltage induced on a sense wire within a conduit can be expressed as the EMP-induced electric field integrated along the length of the conduit. Eq H1 gives the relation for this voltage:

$$E(a,\theta) = \ell Q\left[\frac{8}{\pi^{3/2}\sqrt{ab}\,\mu\sigma^2(b-a)^3}\right] \left\{\sum_{n=0}^{\infty} \frac{e^{-\frac{(2n+1)^2}{\theta}}}{\theta^{3/2}}\left[\frac{(2n+1)^2}{\theta} - \frac{1}{2}\right]\right\} \qquad \text{[Eq H1]}$$

where ℓ = the length

Q = the injected charge

a = inner radius

b = outer radius

σ = conductivity

μ = permeability

θ = a relative time expressed in units of a characteristic time $\theta = t/T$

where $$T = \mu\sigma \frac{(b-a)^2}{4}$$

Eq H1 is the product of the electric field expression (Eq C15) derived in Appendix C and the length of the conduit.

Eq H1 converges well for short times, which is convenient for generation of the response to an impulse current injected on the surface of the conduit.

Frequency Domain. To derive an expression for the open circuit voltage (Eq H1), the EMP-induced internal electric field was integrated along the length of the conduit. After this integration, all that was introduced to modify the expression for the internal electric field was the length of the conduit. Because of this time-independent modification, the Fourier transform of the open-circuit voltage expression is equivalent to the Fourier transform of the internal electric field; therefore, the open circuit voltage frequency response is equivalent to the induced electric field frequency response, which is investigated in Appendix C.

Experimental Evaluation. To determine if Eq H1 is accurate in describing the amplitude and time response of the open-circuit voltage induced by an injected-current pulse which approximates an impulse function, the experimental procedure described in the Experimental Evaluation section of Appendix C was used.

A 3-m length of nominal 1-in (25-mm) aluminum conduit was placed in the setup shown in Figure C4. A current pulse with an amplitude of 350 A, a rise time of 10 nsec, and a fall time of 1.5 μsec was injected onto the surface of the conduit. The rise and fall times of the injected current pulse are much shorter in duration than any of the time scales of the response. The open-circuit voltage was measured with a digital recording oscilloscope which gave a high degree of accuracy for the data points.

To determine the experimental agreement of Eq H1 and the data points, a plot of Eq H1 was fit to the experimental data for the open

circuit voltage by selecting values for T and the quantity

$$\left[\frac{\ell Q\, 8}{\pi^{3/2}\sqrt{ab}\,\mu\sigma^2\,(b-a)^3}\right].$$

The experimental data points were normalized and plotted on the theoretical curve calculated using the selected values for the parameters. Empirically, it was found that the theoretical curve was in excellent agreement with the experimental data points if the following values for the parameters were selected:

$$T = 85\ \mu\text{sec}$$

$$\left\{\frac{\ell Q 8}{\pi^{3/2}\sqrt{ab}\,\mu\sigma^2(b-a)^3}\right\} = 3.38 \times 10^{-3}\ \text{volts}$$

As can be seen from its plot (Figure H1), the time response of Eq H1 is in excellent agreement with the experimental data.

To evaluate the accuracy of the theoretical relation used to determine the amplitude of the open circuit voltage, the constant in Eq H1,

$$\ell Q\left\{\frac{8}{\pi^{3/2}\sqrt{ab}\,\mu\sigma^2(b-a)^3}\right\}$$

was calculated using parameters of the conduit and the injected charge. This value was then compared with the value required in the theoretical calculation of the peak amplitude to be equal to the experimental peak amplitude.

As previously noted, the empirical value of the amplitude parameter was determined to be 3.38×10^{-3} V. The theoretical value was calculated to be 3.36×10^{-3} using:

$a = .0133$ m

$b = 0.0167$ m

$\mu = 4\pi \times 10^{-7}$ henrys/m

$Q = 4 \times 10^{-4}$ c

$\sigma = 2.64 \times 10^{7}$ mhos/m

The theoretical value is within 1 percent of the empirical value.

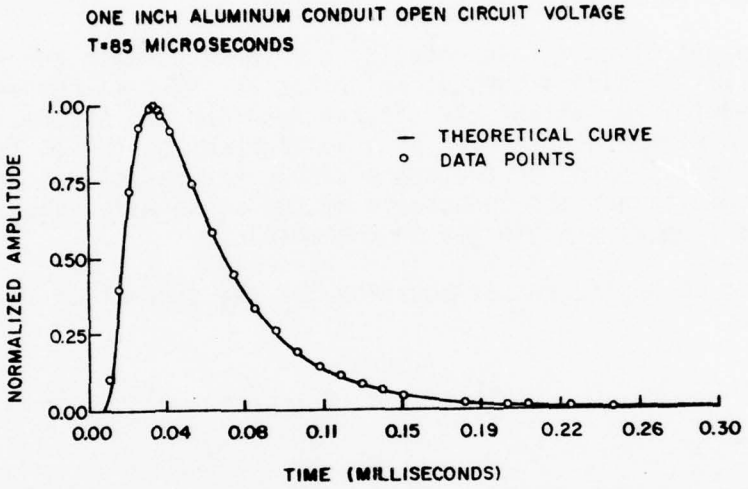

Figure H1. Theoretical curve vs. experimental data points for open circuit.

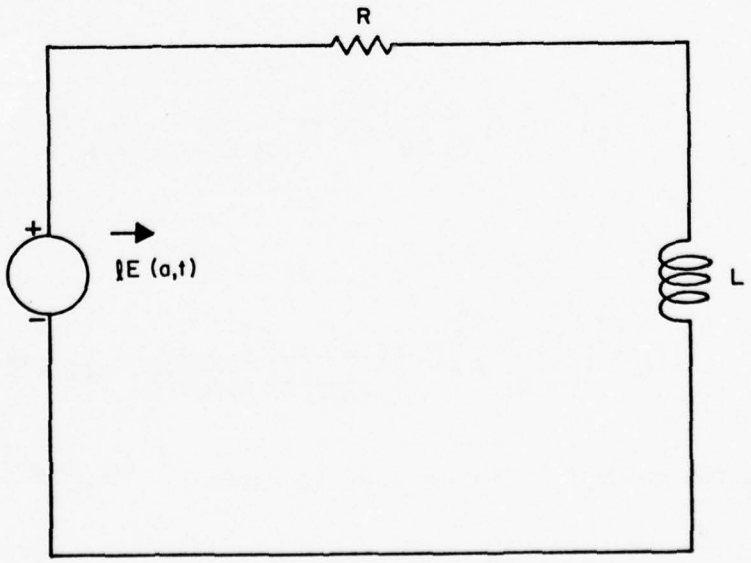

Figure H2. Equivalent circuit--short circuit current.

In summary, the theoretical expression for the open circuit voltage is in excellent agreement with the experimentally determined open circuit voltage.

Short Circuit Current--Theoretical Analysis

Equivalent Circuit. In modeling the short circuit current induced on a sense wire inside a conduit which has an injected current pulse, a lumped parameter equivalent circuit can describe the system. Figure H2 shows such a circuit consisting of a voltage source (which is the open circuit voltage induced on the sense wire), the resistance of the sense wire and conduit, and the inductance of the sense wire-conduit combination. Capacitance is neglected in the model.

Writing the differential equation for the current in the loop gives

$$L \frac{dI}{dt} + RI = \ell \bar{E}_z (a,t) \qquad \text{[Eq H2]}$$

The Laplace transform of this equation is

$$I(s) = \frac{\bar{E}_z (a,s)}{(Ls + R)} \qquad \text{[Eq H3]}$$

From Eq C14,

$$\bar{E}_z (a,s) = \frac{Q}{2\pi\sqrt{ab}} \sqrt{\frac{\mu}{\sigma}} \left[\frac{\sqrt{s}}{\sinh[(b-a)\sqrt{\mu\sigma a}]}\right] \qquad \text{[Eq H4]}$$

Therefore,

$$I(s) = \left[\frac{\ell Q}{2\pi\sqrt{ab}} \sqrt{\frac{\mu}{\sigma}}\right] \cdot \left[\frac{\sqrt{s}}{\sinh[(b-a)\sqrt{\mu\sigma a}]}\right] \cdot \frac{1}{Ls + R} \qquad \text{[Eq H5]}$$

Introducing the conduit diffusion time T, where $T = \frac{\mu\sigma (b-a)^2}{4}$

$$I(s) = \frac{\ell Q}{2\pi\sqrt{ab}} \sqrt{\frac{\mu}{\sigma}} \frac{\sqrt{s}}{[\sinh[2\sqrt{T}\sqrt{s}]][Ls + R]} \qquad \text{[Eq H6]}$$

where ℓ = the length

Q = the charge injected

b = outer radius

a = inner radius

μ = permeability

σ = conductivity

To return to the time domain, the inverse Laplace transform of Eq H6 was taken. The method used here to invert is the method of residues, which is described in the annex to Appendix C. The time domain solution for the short circuit current is given by Eq H7

$$I(t) = A \left\{ \frac{\sqrt{\alpha}}{\sin 2\sqrt{\alpha}} e^{-\alpha\theta} + \sum_{n=1}^{\infty} \frac{(-1)^n n^2 e^{\frac{-n^2\pi^2}{4}\theta}}{n^2 - \frac{4\alpha}{\pi^2}} \right\} \quad \text{[Eq H7]}$$

where: $\theta = t/T$

$$A = \left[\frac{\ell Q}{2\pi\sqrt{ab}} \sqrt{\frac{M}{\sigma}} \frac{1}{L} \frac{1}{\sqrt{T}}\right]$$

$$\alpha = \frac{TR}{L} \neq \frac{n^2\pi^2}{4}$$

Eq H7 is the short circuit current response to an impulse current pulse, in terms of relative time θ (which is the ratio of the diffusion time and time) and a dimensionless parameter which is the ratio of the conduit diffusion time T and the L/R time constant.

Properties of Short Circuit Current Response. Starting with Eq H7, it is possible to investigate such properties as where in time the peak current occurs, the amplitude of the peak current, the relationship between the parameter α and the peak amplitude and the time of the peak, and the relationship between the amplitude of the peak and time of the peak. These properties are investigated in the following two sections.

Time of Peak Current. The maximum current occurs at the time for which $\frac{dI}{dt} = 0$. That is, when

$$\frac{dI}{dt} = TA \left\{ \frac{-\alpha^{3/2} e^{-\alpha\theta}}{\sin(2\sqrt{\alpha})} + \sum_{n=1}^{\infty} \frac{(-1)^n (-\frac{n^2\pi^2}{4}) n^2 e^{-\frac{n^2\pi^2}{4}\theta}}{[n^2 - \frac{4\alpha}{\pi^2}]} \right\} = 0 \quad \text{[Eq H8]}$$

Therefore, the time of the peak occurs at some θ peak such that

$$\frac{\alpha^{3/2}}{\sin(2\sqrt{\alpha})} e^{-\alpha\theta_{peak}} + \sum_{n=1}^{\infty} \frac{(-1)^n \frac{n^4\pi^2}{4} e^{-\frac{n^2\pi^2}{4}\theta_{peak}}}{[n^2 - \frac{4\alpha}{\pi^2}]} = 0 \quad \text{[Eq H9]}$$

The above relation involves finding the zero of an infinite series, but if θ_{peak} is ~1 or larger, a first approximation of θ_{peak} can be found using the first term of the infinite series. The first approximation could then be used to determine the value of θ_{peak} by iteration which gives a maximum for a specified value of α.

θ_{peak} was determined on a programmable calculator by iteration. The minimum value of θ_{peak} is .36701 for large α. This is also the value of the open circuit voltage peak (see Appendix C). As α approaches zero, the time at which the peak occurs becomes longer. Figures H3 and H4 are plots of the time that the peak occurs (relative time θ) versus α.

The time at which the short circuit peak will occur can be calculated from Figures H3 and H4 if the diffusion time of the conduit (Table C2) and the value of the time constant L/R are known. The time of the peak is given by the relation:

$$t_{peak} = \theta_{peak} T \quad \text{[Eq. H10]}$$

Peak Amplitude of Current. The expression in the brackets in Eq H7 was evaluated at various values of θ_{peak} determined in the previous section. Figures H5 and H6 plot the peak amplitude of the expression in the brackets versus θ_{peak}. As can be seen from the plots, the quantity in the brackets reaches a limiting value of .5 as θ_{peak} gets larger, which implies α approaches zero. The peak amplitude of the expression in the brackets was also plotted versus the parameter α (Figure H7).

The amplitude of the peak current can be determined if θ_{peak} is known (Figures H5 and H6) or if the parameter α is known (Figure H7). The peak current amplitude is then given by:

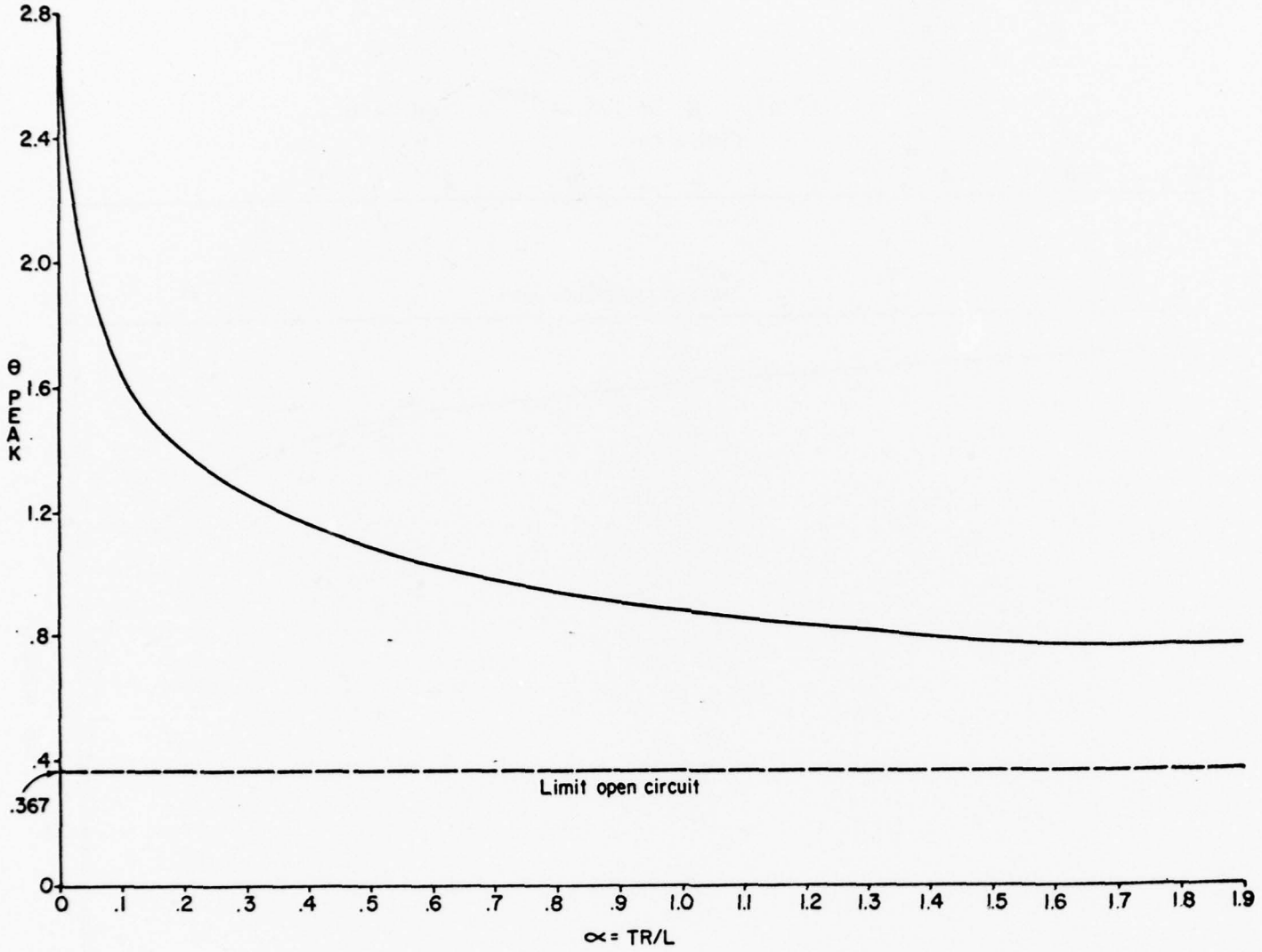

Figure H3. Plot of θ_{peak} vs. $\alpha = T(R/L)$.

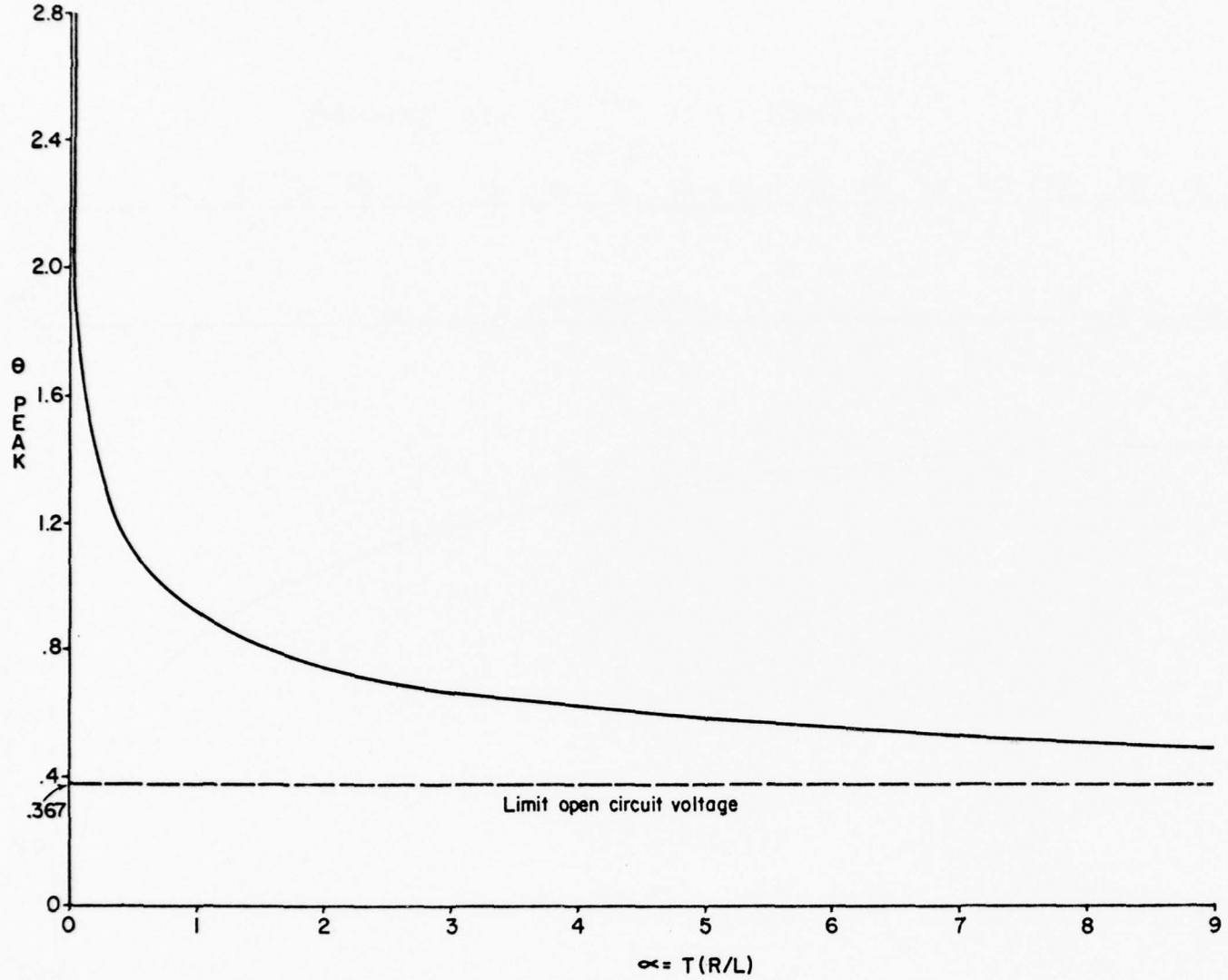

Figure H4. $\theta_{peak} = t/T$ vs. $\alpha = T(R/L)$.

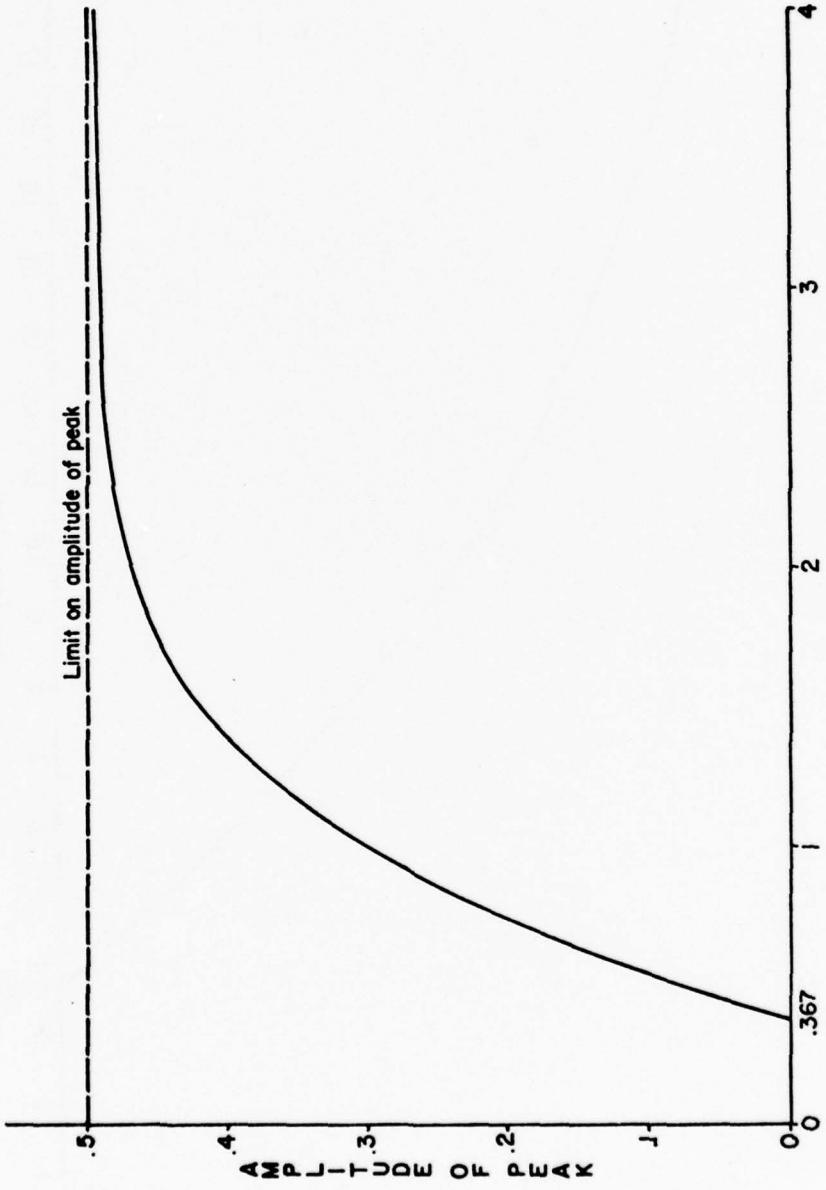

Figure H5. Peak amplitude vs. $\theta_{peak} = t/T$.

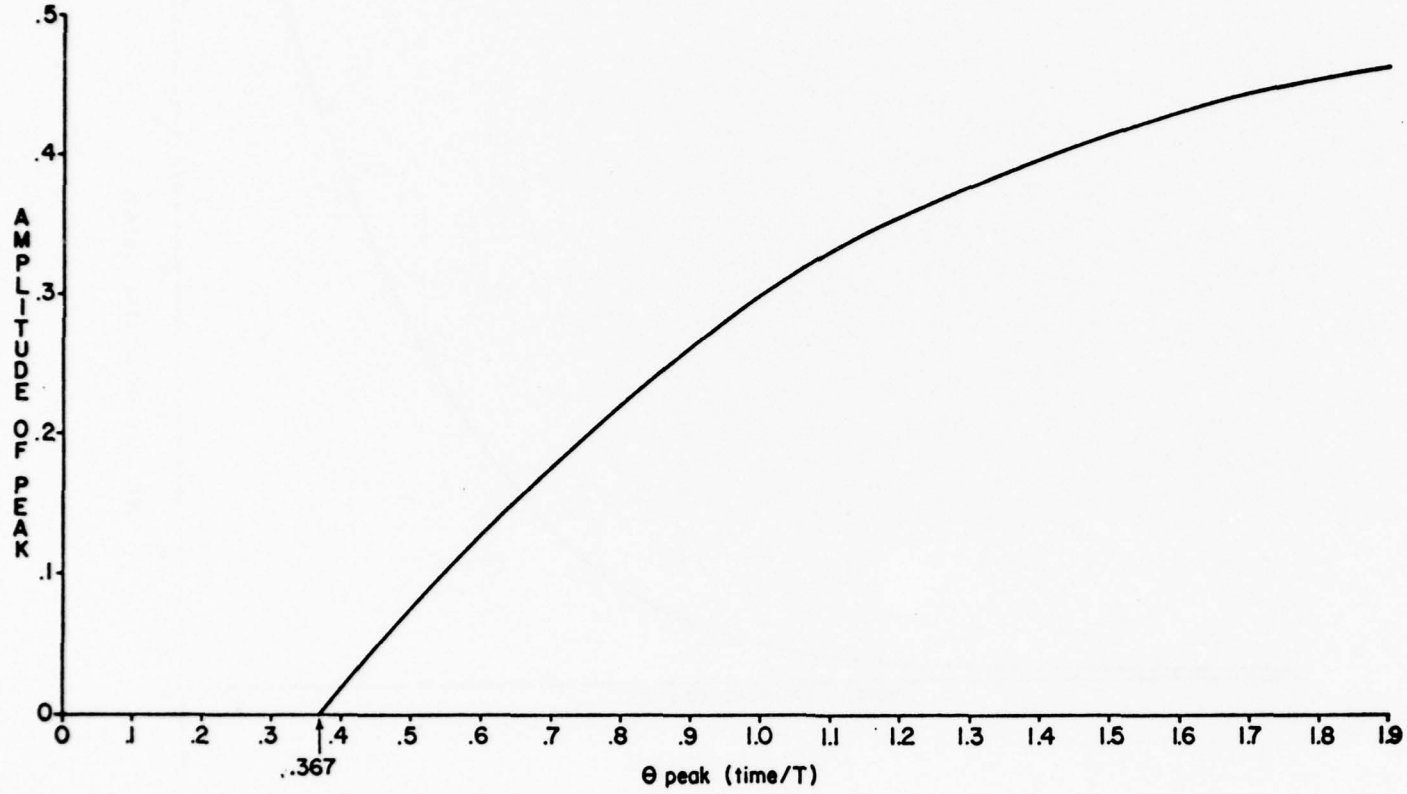

Figure H6. Plot of magnitude peak vs. θ_{peak}.

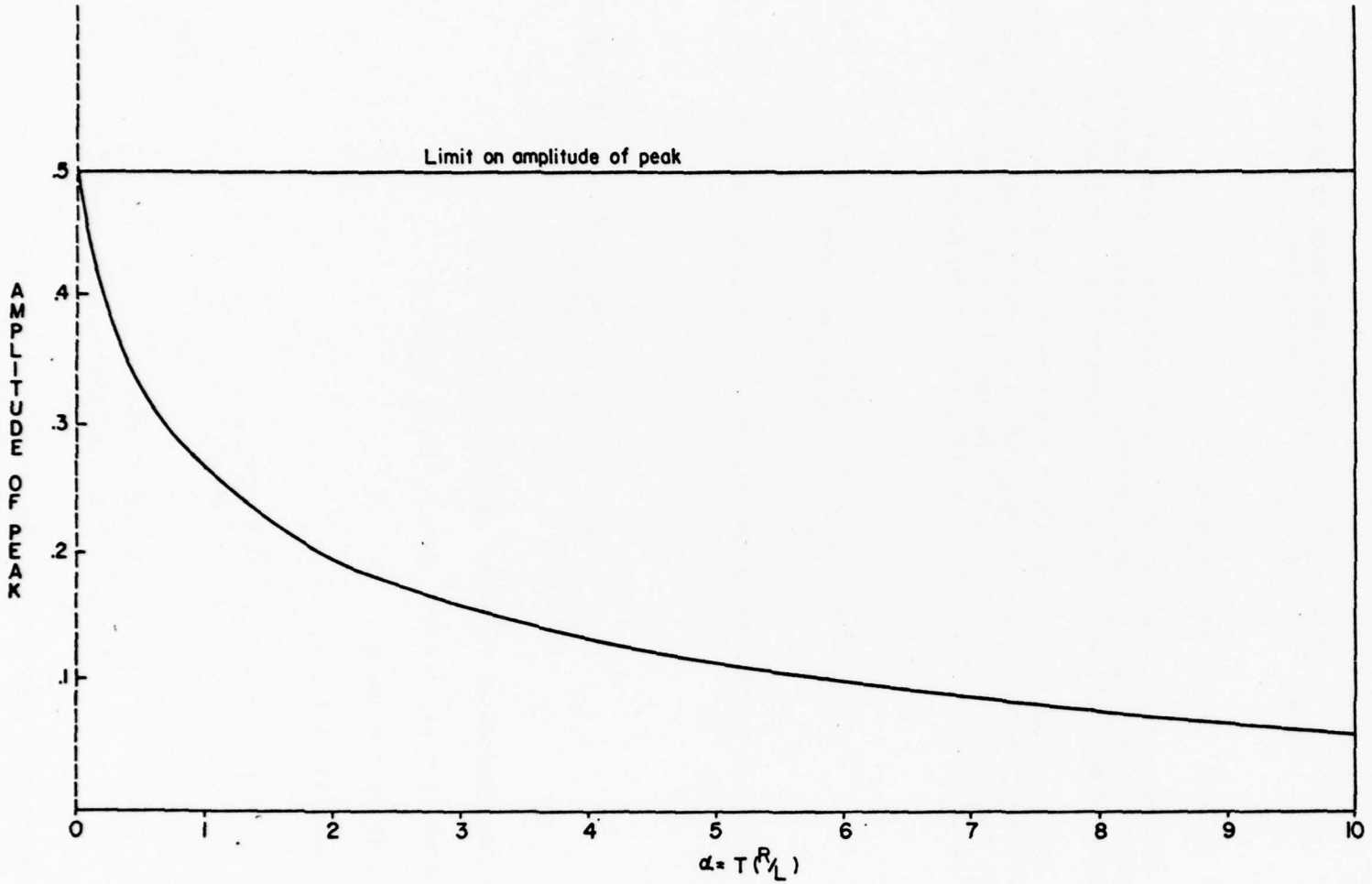

Figure H7. Peak amplitude vs. $\alpha = T(R/L)$.

$$I_{peak} = \left[\frac{\ell Q}{2\pi}\sqrt{\frac{\mu}{\sigma}}\frac{1}{L}\frac{1}{\sqrt{T}}\right] \cdot \begin{matrix}\text{peak amplitude of term} \\ \text{in brackets}\end{matrix} \qquad \text{[Eq H11]}$$

Short Circuit Current Frequency--Domain

Although the main objective of this study is to examine the time variation in the short circuit current, it is useful to consider the frequency domain of the short circuit current transfer function.

Fourier Transform. From the definition of the Fourier transform, the transfer function for the short circuit current equation (Eq H6) can be modified by the simple substitution of $s = j\omega$ to obtain the Fourier transform. After this substitution, Eq H6 becomes

$$I_{(j\omega)} = \left[\frac{\ell Q}{2\pi\sqrt{ab}}\sqrt{\frac{\mu}{\sigma}}\right] \frac{\sqrt{j\omega}}{\sinh(2\sqrt{j\omega}T)} \cdot \frac{1}{[j\omega L + R]} \qquad \text{[Eq H12]}$$

Multiplying numerator and denominator by $(R - j\omega L)$ and letting $\sqrt{j} = \sqrt{2}/2\ (1 + j)$,

$$I_{(j\omega)} = \left[\frac{\ell Q}{2\pi\sqrt{ab}}\sqrt{\frac{\mu}{\sigma}}\right] \frac{\sqrt{\omega}}{R^2+\omega^2L^2}\left[\frac{\sqrt{j}\ (R-j\omega L)}{\sinh(\sqrt{2\omega T} + j\sqrt{2\omega T})}\right] \qquad \text{[Eq H13]}$$

Using transcendental function identities:

$$\sinh (x + y) = \sinh x \cosh y + \cosh x \sinh y$$

$$\cosh (jB) = \cos B$$

$$\sinh (jB) = j \sin B$$

$$I_{(j\omega)} = \left[\frac{\ell\ Q}{2\pi\sqrt{ab}}\sqrt{\frac{\mu}{\sigma}}\right] \frac{\sqrt{\omega}}{R^2+\omega^2L^2} \qquad \text{[Eq H14]}$$

$$\left[-\frac{\sqrt{j}\ (R - j\omega L)}{\sinh(\sqrt{2\omega T})\cos(\sqrt{2\omega T})+j\sin(\sqrt{2\omega T})\cosh\sqrt{2\omega T}}\right]$$

The magnitude of the transfer function is given by:

$$|I_{(j\omega)}| = \left[\frac{\ell Q}{2\pi\sqrt{ab}}\sqrt{\frac{\mu}{\sigma}}\right] \frac{\sqrt{\omega}}{\sqrt{R^2+\omega^2L^2}\left(\sinh^2\sqrt{2\omega T}\cos^2\sqrt{2\omega T}+\sin^2\sqrt{2\omega T}\cosh^2\sqrt{2\omega T}\right)^{1/2}} \quad \text{[Eq H15]}$$

The phase of the transfer function is given by:

$$\phi_{(j\omega)} = \tan^{-1}\left[\frac{(1-\frac{\omega R}{L}) - (1+\frac{\omega R}{L})(\coth\sqrt{2\omega T}\tan\sqrt{2\omega T})}{(1+\frac{\omega R}{L} + (1-\frac{\omega R}{L})(\coth\sqrt{2\omega T}\tan\sqrt{2\omega T})}\right] \quad \text{[Eq H16]}$$

When the relative frequency ξ is defined as $8\ \omega T$ and the parameter α as TR/L, the magnitude is given by

$$|G(j\omega)| = \left[\frac{\ell Q}{2\pi\sqrt{ab}}\sqrt{\frac{\mu}{\sigma}}\right] \frac{1}{2R\sqrt{2T}} \frac{\sqrt{\xi}}{\left(1+\frac{\xi^2}{8^2\alpha^2}\right)^{1/2}\left(\sinh^2(\frac{\sqrt{\xi}}{2})\cos^2(\frac{\sqrt{\xi}}{2}) + \sin^2(\frac{\sqrt{\xi}}{2})\cosh^2(\frac{\sqrt{\xi}}{2})\right)^{1/2}} \quad \text{[Eq H17]}$$

and the phase by:

$$\phi(j\omega) = \tan^{-1}\left\{\frac{[1-(\frac{\xi\alpha}{8T^2})] - [1+(\frac{\xi\alpha}{8T^2})]\coth(\frac{\sqrt{\xi}}{2})\tan(\frac{\sqrt{\xi}}{2})}{[1+(\frac{\xi\alpha}{8T^2})] + [1-(\frac{\xi\alpha}{8T^2})]\coth(\frac{\sqrt{\xi}}{2})\tan(\frac{\sqrt{\xi}}{2})}\right\} \quad \text{[Eq H18]}$$

Properties of Transfer Function. To determine the properties of the transfer function, both magnitude and phase were plotted. Figure H8 is a plot of the magnitude of the transfer function in decibels versus the relative frequency ξ. The transfer function magnitude was plotted for a range of 0.1 to ∞ for α. As can be seen from the plot, the magnitude is reduced by 150 dB within a relative frequency range of 800 to 1100 for the range of α. To convert the relative frequency ξ to frequency, the relationship $f(Hz) = \xi/8T2\pi$ can be employed. For 1 - in. (25-mm) aluminum conduit, T = 85 μsec, the relative frequency range of 800 to 1100 converts to 190 kHz and 260 kHz. Thus, for 1-in. (25-mm) aluminum conduit the attenuation is 150 dB at 200 kHz, and at 1 MHz the attenuation is greater than 250 dB. For 1-in. (25-mm) galvanized steel conduit, T = 4.2 msec (Table C2), the attenuation is 150 dB at about 4 kHz, and at MHz the attenuation is greater than 1200 dB.

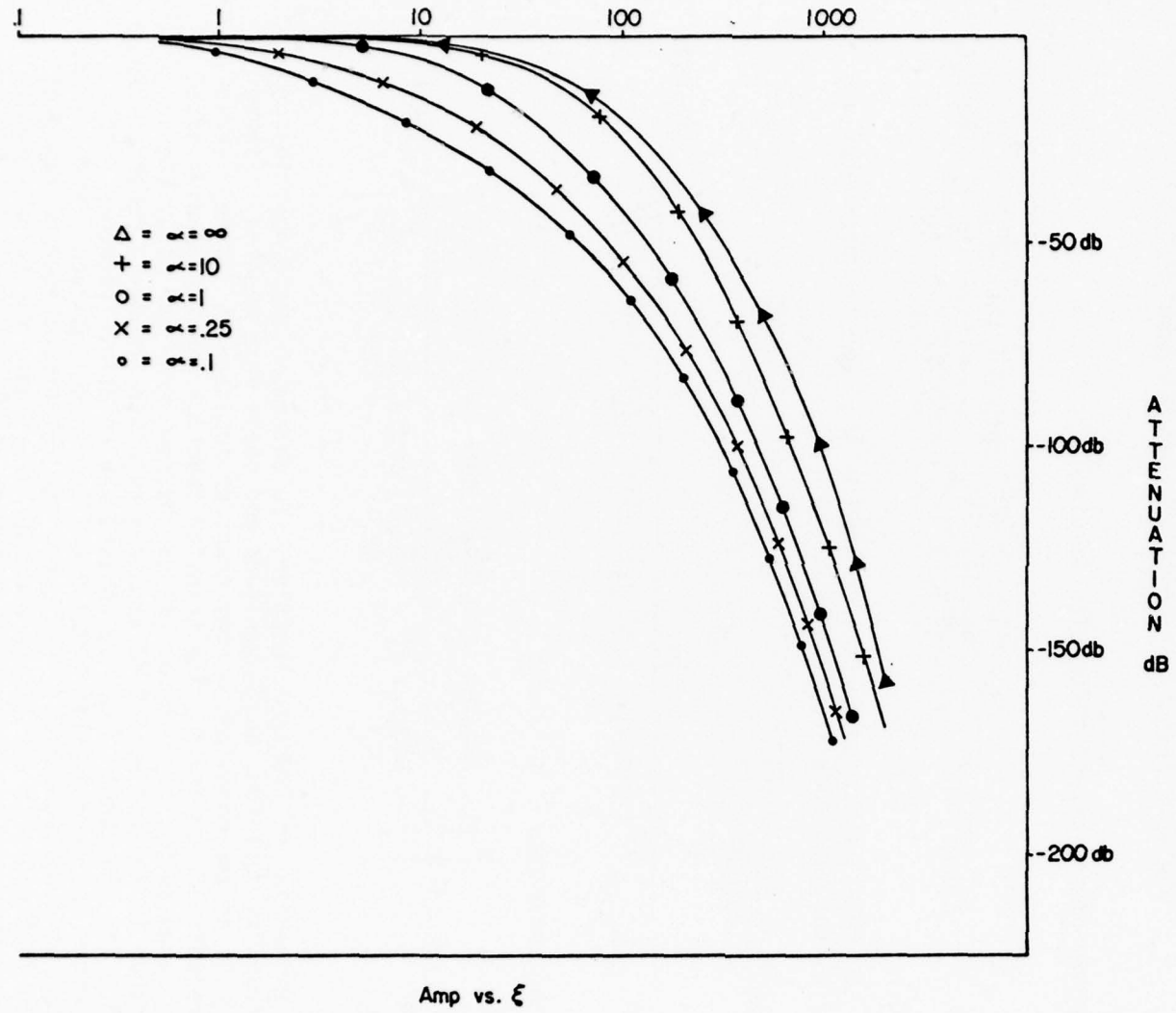

Figure H8. Plot of magnitude of the transfer function vs. the relative frequency.

The phase of the transfer function was plotted for a range of α of 0.1 to ∞, and a relative frequency range of 1 to 1000 (Figure H9).

Short Circuit Current - Experimental Evaluation

The theoretical expression Eq H7 was verified experimentally by measuring the short circuit current induced on the sense wire with a high current pulse injected on the surface of the conduit. The conduit used in this test was a 3-m length of nominal 1-in. (25-mm) aluminum conduit.

Figure H10 shows the experimental setup. A current pulse with an amplitude of 400 A, a rise time of 10 nsec, and a fall time of 1 μsec was injected on the surface of the conduit. The current pulse was such that it was a good approximation of an impulse function, and thus provided a means of directly verifying the theoretical expression.

To measure the current induced on a wire inside the conduit, a sense wire was inserted into the test conduit as shown in Figure H10. The sense wire was connected to the pulser end of the conduit through a resistor with the end of the conduit capped to keep leakage signals from entering the system. The sense wire ran the entire length of the conduit and extended into the shielded room where it was shorted to the grounded wall of the shielded room. A Pearson No. 411 inductive current probe was placed around the sense wire. Output of the current probe was then amplified by a high-speed operational amplifier and measured by a digital recording oscilloscope. Data points were then accurately read from the trace displayed by the scope.

Tests were also conducted with additional resistance in series with the sense wire inside a shielded room.

The resistance of the entire system was determined by injecting a DC current and measuring the voltage drop. The inductance of the system was measured using a Tektronix Model No. 130 L-C meter.

To determine the agreement of Eq H7 to the data points measured, the theoretical curve was fit to the experimental data for the short-circuit current by selecting values for T, L/R, and the quantity:

$$\left[-\frac{\ell Q}{2\pi\sqrt{ab}}\sqrt{\frac{\mu}{\sigma}}\right]\frac{1}{L}\frac{1}{\sqrt{T}}$$

The experimental data points were normalized and plotted on the theoretical curve calculated using the selected values for the parameters. Empirically, it was found that the theoretical curve was in excellent agreement with the experimental data points if the following values for the parameters were selected:

$$T = 85\ \mu\text{sec}$$

$$L/R = 80\ \mu\text{sec}$$

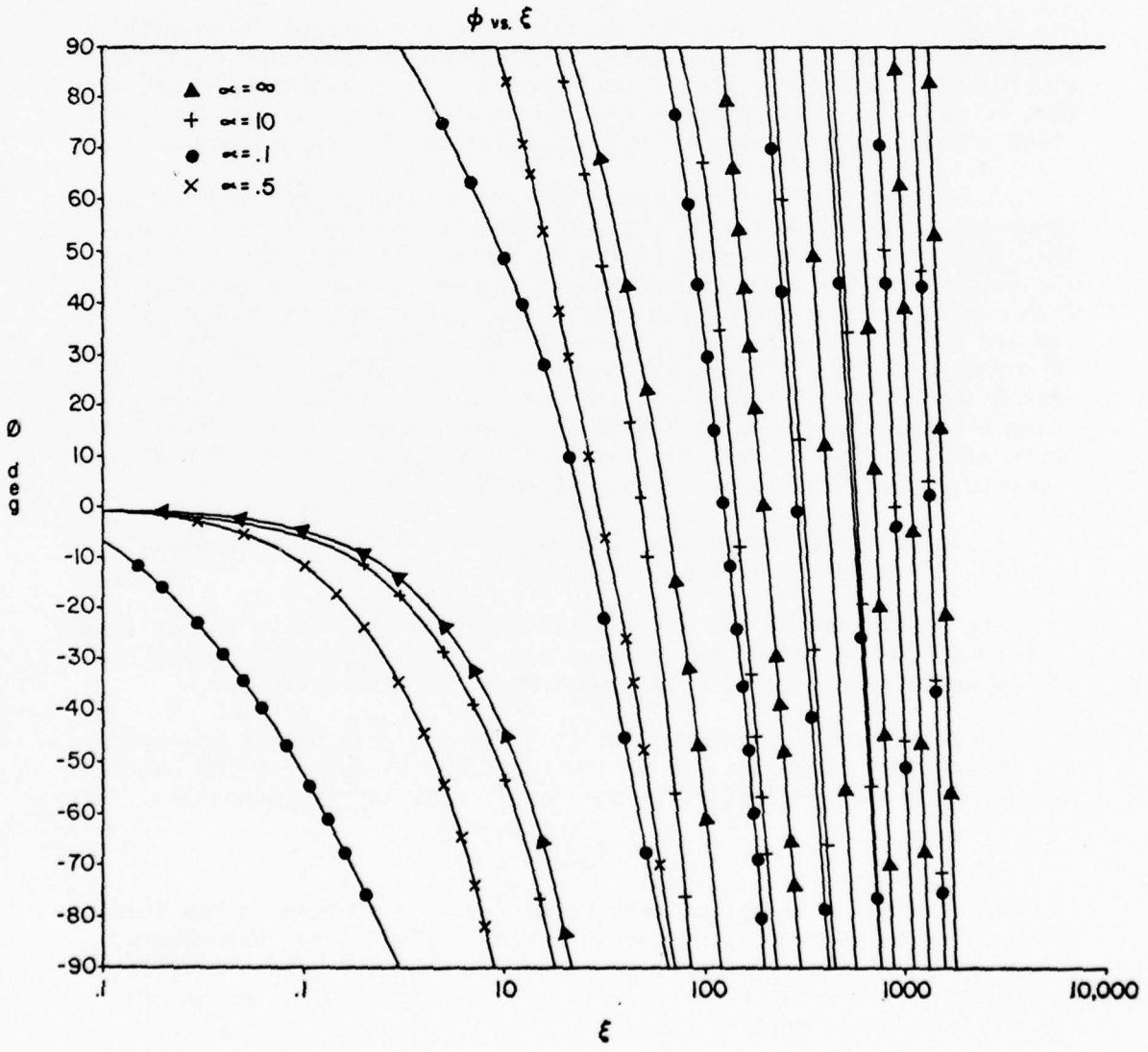

Figure H9. Plot of the phase of the transfer function.

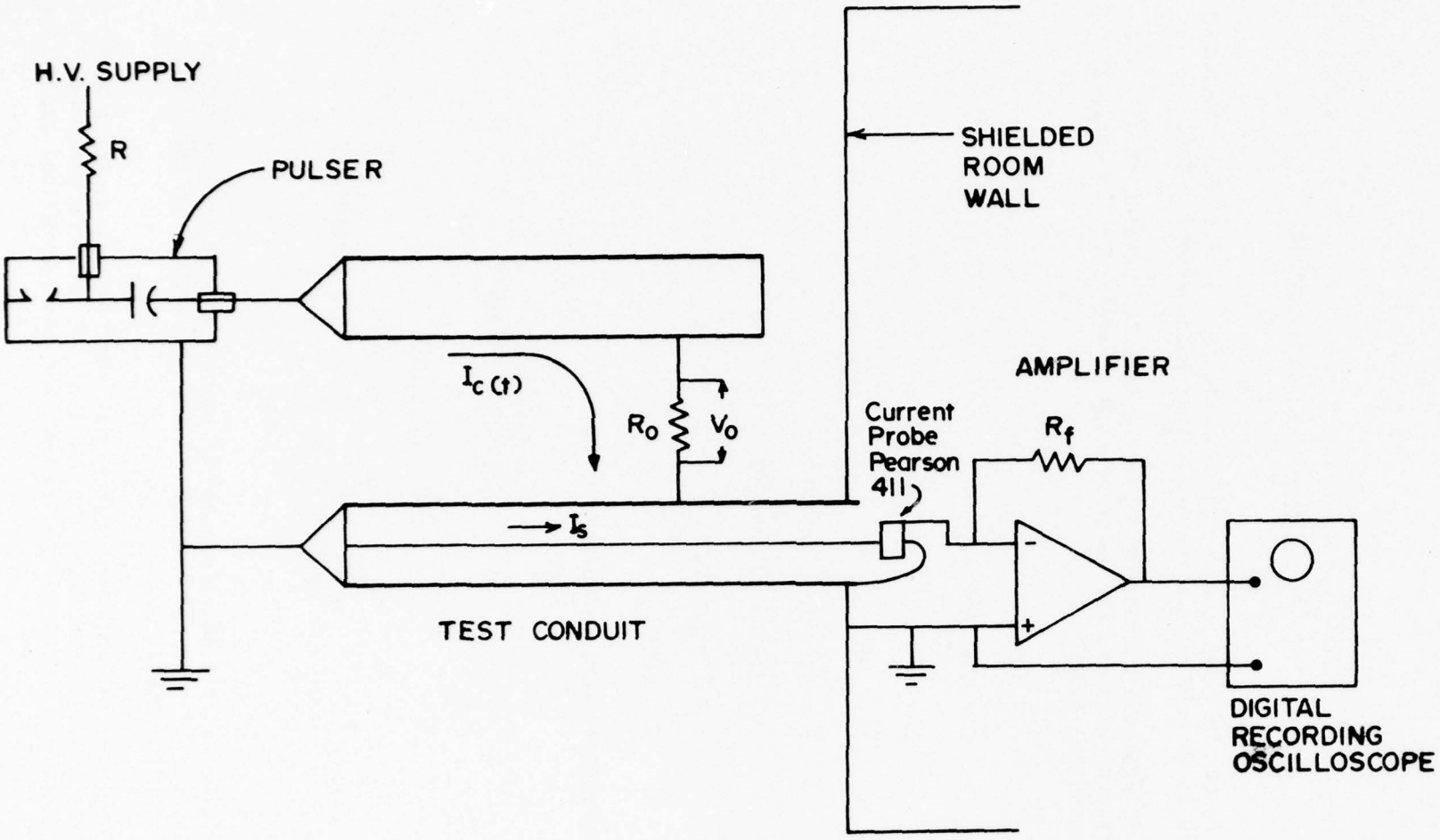

Figure H10. Test configuration for short circuit current measurement.

and

$$\left[\frac{\ell Q}{2\pi\sqrt{ab}}\sqrt{\frac{\mu}{\sigma}}\right]\frac{1}{L}\frac{1}{\sqrt{T}} = .1653 \text{ amperes}$$

As can be seen from the plot in Figure H11, the time response of Eq H20 is in excellent agreement with the experimental data.

To evaluate the agreement of the selected parameters with the measured parameters, the value of each parameter was calculated from the measured values:

$\ell = 2.99$ m

$Q = 4 \times 10^{-4}$ C

$a = .0133$ m

$b = .0167$ m

$\mu = 4\pi \times 10^{-7}$ henrys/m

$\sigma = 2.53 \times 10^{7}$ mhos/m

$L = 1.5$ μhenrys

$R = .0182$ Ω

The parameters were calculated to be:

$$T = \frac{\mu\sigma(b-a)^2}{4} = 93 \text{ μsec}$$

$$L/R = 82.5 \text{ μsec}$$

$$\left[\frac{\ell Q}{2\pi\sqrt{ab}}\sqrt{\frac{\mu}{\sigma}}\right]\frac{1}{L}\frac{1}{\sqrt{T}} = .1973 \text{ amperes}$$

These calculated values are in agreement with the theoretical values, considering the accuracy of the measurement of the values used in the calculation.

Experimental data were taken with additional resistance added to the system, thus decreasing the value of the L/R time constant. The resistance was increased to .029 ohms and the theoretical expression

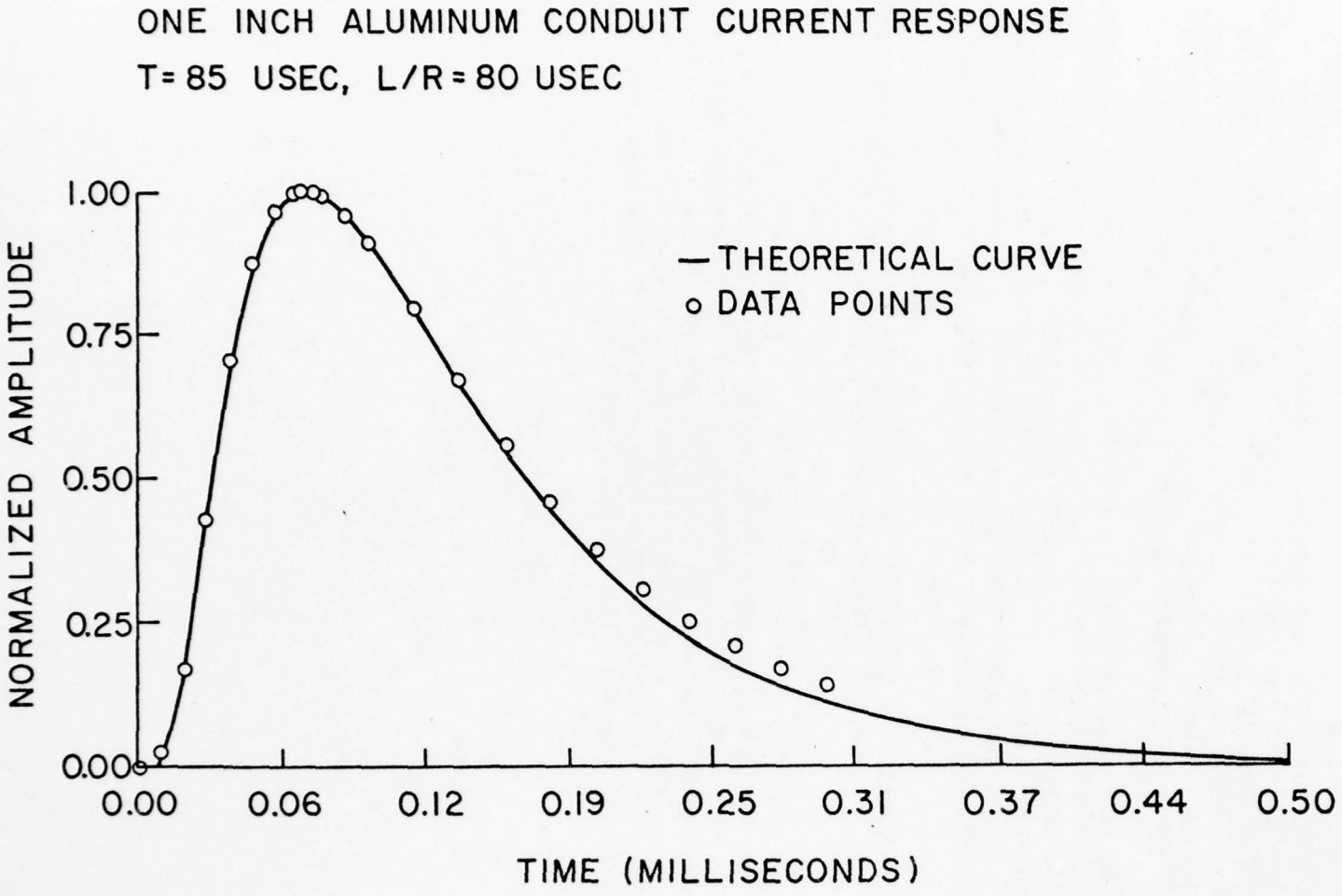

Figure H11. Theoretical curve vs. experimental data points for short circuit.

(Eq H7) was plotted to fit the data points; the value of L/R was selected to be 65 μsec and T was selected to be 85 μsec to achieve the best fit of the theoretical curve to the data. Figure H12 shows the plot. The value of the inductance was measured to be 1.8 μH, so the experimental value of L/R was 62 μsec. The theoretical expression is thus in excellent agreement with the experimental data.

The resistance was then increased to .11 ohms, and the theoretical expression was plotted to fit the data. The parameters L/R and T were selected to be 17 μsec and 85 μsec, respectively. The plot of the curve and the data is shown in Figure H13. The inductance was measured to be 1.7 μH, so the experimental value of L/R is 15.5 μsec. Again the theoretical expression is in excellent agreement with the experimental data.

To demonstrate the effect of changing the value of L/R, the theoretical curve for various values of L/R was plotted (Figure H14).

Summary

The calculated induced current due to the impulse current has a relatively simple series solution which involves parameters dependent on conduit dimensions and the resistance and inductance of the conduit sense wire system. It was demonstrated that experimental data could be put in the form of the theoretical calculations with excellent agreement for nominal 1-in. (25-mm) aluminum conduit.

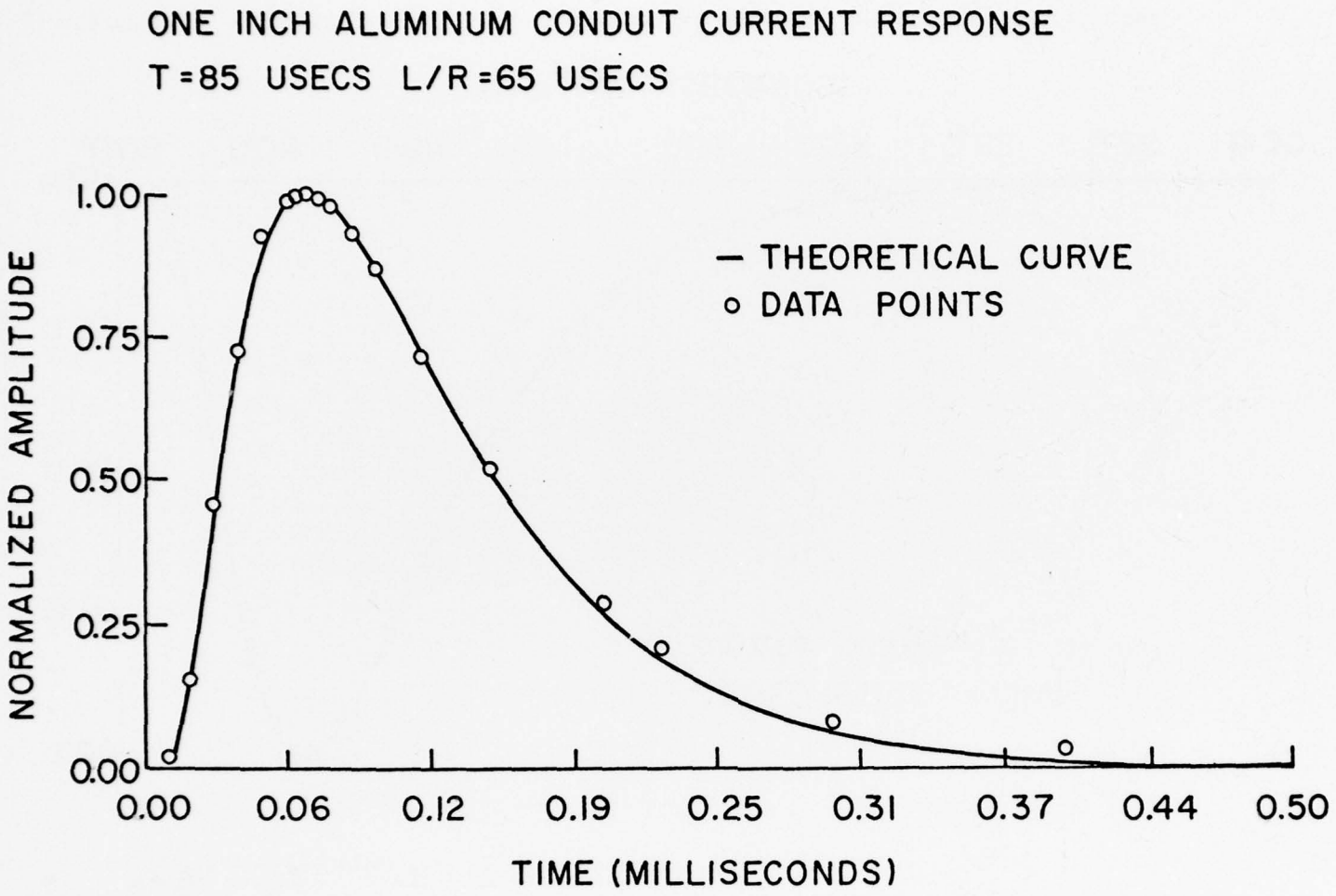

Figure H12. Theoretical vs. experimental data for resistance of .029 ohms.

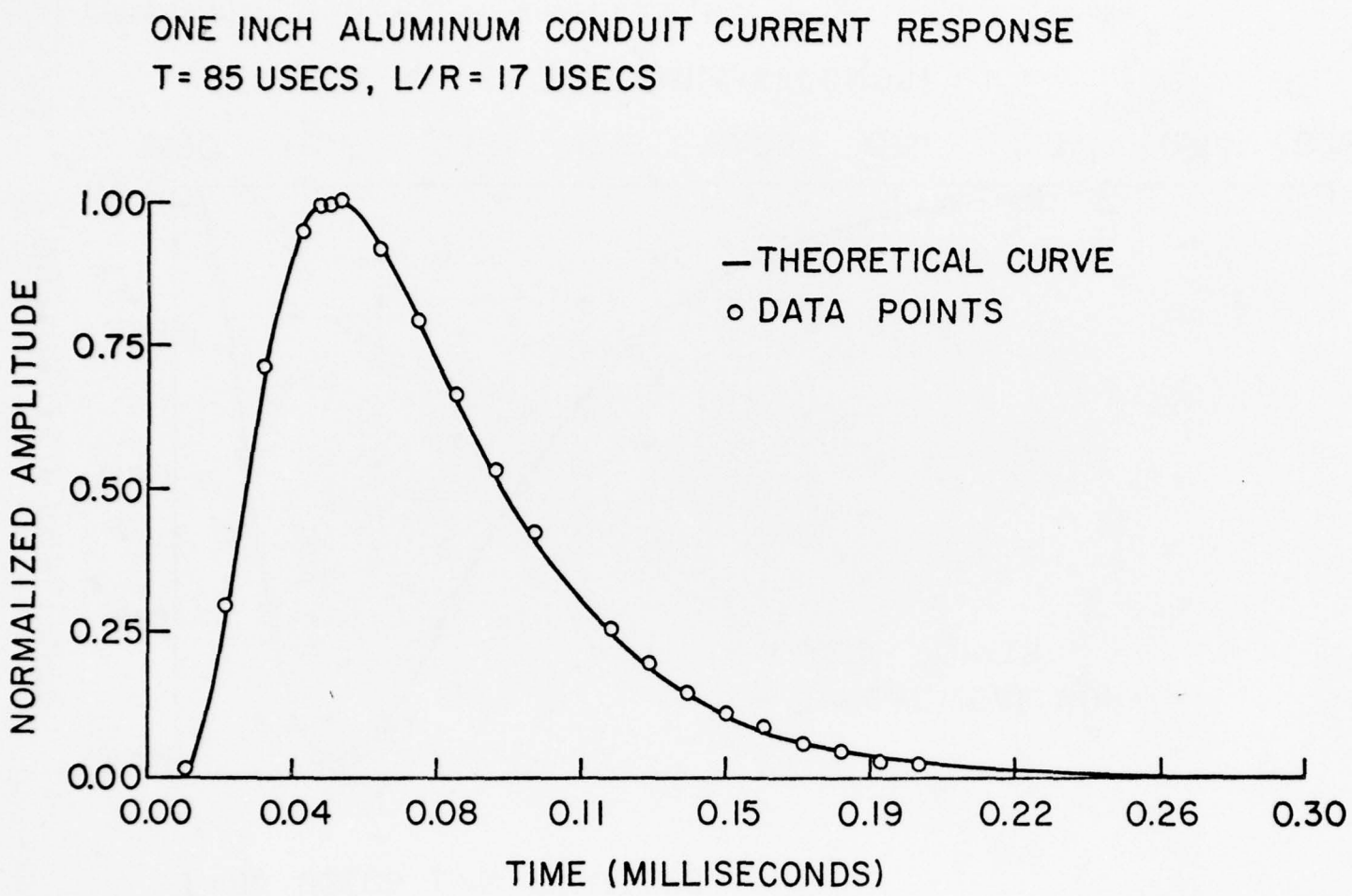

Figure H13. Theoretical curve vs. experimental data for resistance of 0.11 ohms.

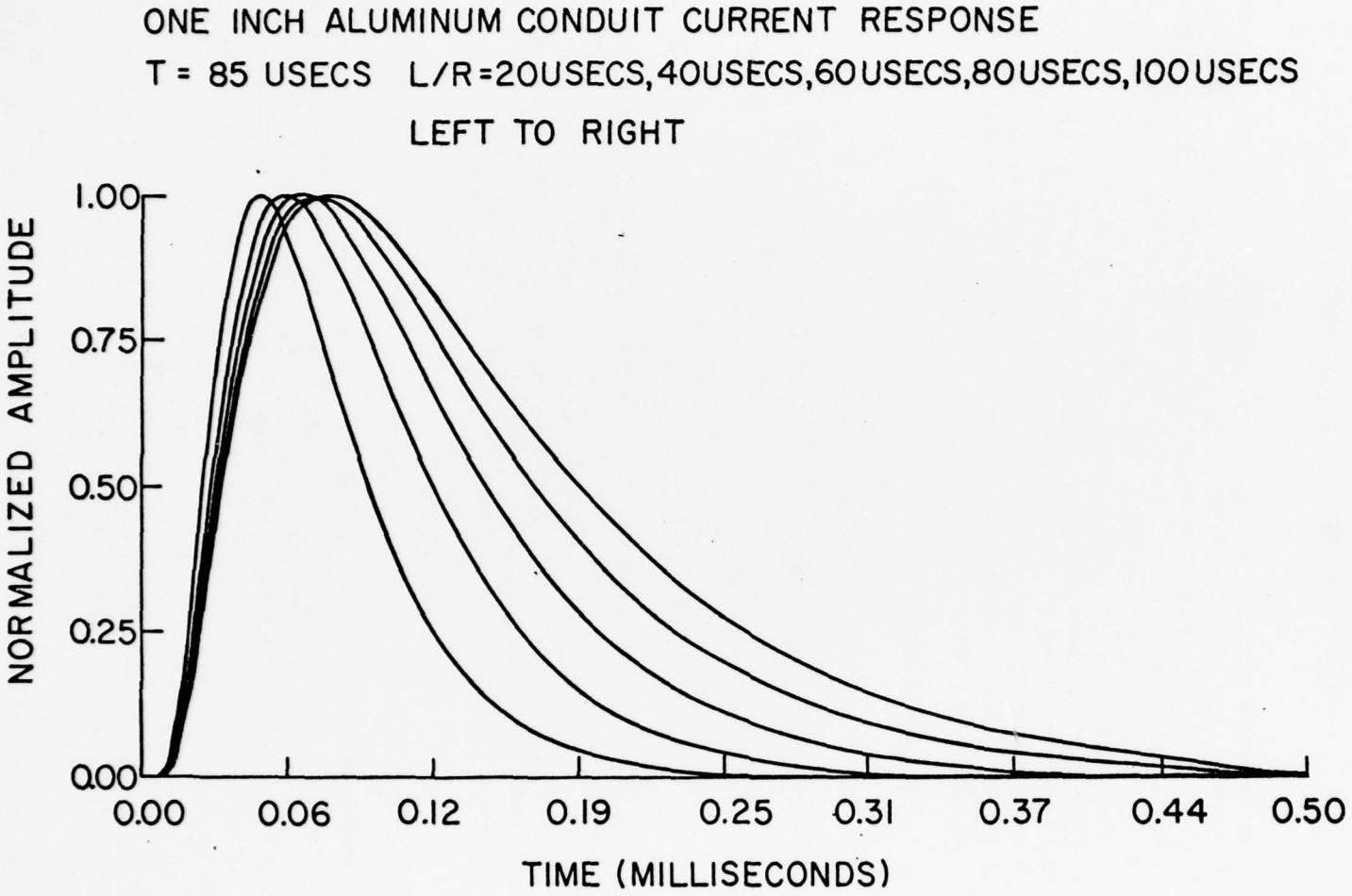

Figure H14. Effects of varying the value of L/R.

ANNOTATED BIBLIOGRAPHY

Considerable research has been conducted on many of the aspects of EMP interaction with electrical and electronic systems. While much of this research has been done specifically for aeronautical systems, the information is also useful in the design of ground facilities. This annotated bibliography lists the literature used as references in the development of the analytical procedure as well as other references which provide more detailed information on some of the important related factors. None of the references are required for use of the analytical procedure, but they provide the interested reader with a source of additional information. The documents are divided, by topic, into the following categories:

a. Induced currents

b. Signal coupling to internal wires

c. Coupling between wires

d. Saturation effects

e. Transmission line effects.

The documents either appear in the referenced literature, are available from the Defense Documentation Center (DDC) using the AD number given, or, in the case of the Protection Engineering and Management (PEM) notes published by the Lawrence Livermore Laboratory, can be obtained from the National Technical Information Service, U.S. Department of Commerce, 5285 Port Royal Road, Springfield, VA 22151.

Induced Currents

Brown, Glenn L., *Bulk Current in an Insulated Cable Lying on the Surface of the Earth,* PEM-30 (Lawrence Livermore Laboratory, February 1975). This note presents a method of predicting the bulk current that will be generated by an EMP field in an insulated cable lying on the surface of the earth. The technique could also be applied to conduit.

Burrows, M. L., *Measurements of Electromagnetic Pulse Propagation in Various Soils,* AD675292 (Lincoln Laboratory, Massachusetts Institute of Technology, August 1968). This report describes measurements of propagation velocity and attenuation of 2.5, 5, and 10 nsec pulses in various soils with varying water contents. The measurements were made by packing the soils into a specially built coaxial line. The soils tested included pure sand, various loams, and pure clay.

Mohr, R. J., "Coupling of Transient Radiated Fields into Lines," *International Electromagnetic Compatibility Symposium Record 1973*, IEEE CHO 751-8EMC (1973), pp 19-26. This report presents a method for calculating the current on an infinite conductor resulting from an incident field of general incidence, in free space and on the air-earth interface.

Pirjola, Risto, "On the Current Induced Within an Infinitely Long Circular Cylinder (or Wire) by an Electromagnetic Wave," *IEEE Transactions on Electromagnetic Compatibility*, Vol EMC-18, No. 4 (November 1976), pp 190-197. This report presents a direct method for determining the current on a wire (or conduit) in an arbitrary infinite homogeneous medium induced by a harmonic electromagnetic plane wave.

Stepanoff, Serge, "EMP Analysis of TACFIRE Systems," Paper No. 6-1-6, *Joint EMP Technical Meeting (NEM 1973): Proceedings*, DNA-3 609P-6 (Defense Nuclear Agency, June 1975). This report presents transmission line and loop antenna approaches for determining sheath currents for cables subjected to radiated EMP. These approaches could also be used for determining conduit currents. An analysis for internal conductors is also given using the cable transfer function and the transmission line characteristics of the cable-conduction system. An EMP computer program flow chart using fast Fourier transforms and frequency-dependent transfer functions is given.

Whitmer, R. M., and Wm. H. Robinetto, Jr., "Response of a Buried Cable to EMP From a High-Altitude Burst," Paper No. 3-1B-4, *Joint EMP Technical Meeting (NEM 1973); Proceedings*, DNA 3609P-6 (Defense Nuclear Agency, June 1975). This report discusses the internal leakage field in a buried communication cable from an incident EMP, and determines it to be the product of several transfer functions: soil-sheath, and sheath-internal field, internal field-conduction impedance.

Wilson, Monti R., *Transient Current Estimates for Finite Length Surface Cables*, PEM-34 (Lawrence Livermore Laboratory, February 1975). This report analyzes the problem of a cable lying at the earth-air interface. The transient response to a double-exponential incident pulse with 10-nsec rise time is obtained for various incident polarization, cable lengths, soil conductivities, and terminal impedances.

Signal Coupling to Internal Wire

Madle, P. J., *Cable and Connector Shielding Attenuation and Transfer Impedance Measurements Using Quadraxial and Quintaxial Test Methods*, PEM-45 (Lawrence Livermore Laboratory, November 1975). This report describes a frequency-dependent transfer impedance and admittance between cable shields and internal conductors which could also be applied to conduit-shielded cables. The following test fixtures and related test

procedures are listed: open wire, coaxial and inverted triaxial, triaxial, quadraxial, and quintaxial.

Vance, E. F., DNA *EMP (Electromagnetic Pulse) Handbook* (U), DNA-2114H-2, (Defense Nuclear Agency, December 1974), Chapter 11, "EMP Coupling to Cables," ADB001204. This chapter presents a detailed discussion of EMP interaction with soil and propagation through the soil. An analysis to determine the induced current on a base cable transmission line, which is analogous to an uninsulated conduit, is presented. This analysis can be used to determine current flow on conduits. Transfer impedances for solid tubular shields and braided shields are given. The *EMP Handbook* is classified confidential; however, Chapter 11 is available in an unclassified version from DDC as ADB001204.

Vance, E. F., *Electromagnetic Pulse Handbook for Electric Power Systems,* ADA009228 (Defense Nuclear Agency, February 1975). This handbook provides formulas and data for evaluating coupling of the high-altitude EMP to electric power systems and to facilities served with commercial electric power. The subjects covered include coupling to power transmission and distribution lines, transient coupling through transformers, lightning-arrester firing characteristics, and coupling through the service entrance. Grounding, EMP protective measures, and testing are also discussed.

Vance, E. F., *Treatment of Penetrations Entering Communications Facilities,* ADB007076 (Defense Nuclear Agency, August 1975). The EMP-induced transients on conductors such as power lines, communication cables, and waveguides are described. The theory and practice of treating those conductors that penetrate communication facilities are developed to guide the communication system designer in providing EMP-resistant facilities. The use of current-diversion and voltage-limiting techniques and the role of building shields and facility ground systems in EMP-resistant design are described.

Wells, Wm. C., *Nuclear Electromagnetic Pulse (NEMP) Hardened Cables,* Report No. ECOM 0341-1/ADA006642 (U. S. Army Electronics Command, January 1975). Surface transfer impedance Z(t) was determined for 12 prototype cables constructed to measure the extent of reduction of Z(t) possible. Mechanisms for inducing current, antenna effects, and transmission line effects are discussed.

Coupling Between Wires

Center, J. M., et al., *Single-line Modeling of Internal Coupling for Complex Cable Systems,* AFWL-TR-75-164/ADB012188 (Air Force Weapons Laboratory, May 1976). This report presents an analysis of complex cable coupling. Thevenin's and Norton's equivalents are developed for cables in conduit, shielded or unshielded, for single and N wires in

cables. The EOPRM (Geometric Cable Parameter Determination) computer program developed for this application is described. The analysis was conducted for aeronautical systems, but is also applicable to fixed facilities.

Cross-Coupling in the SAFEGUARD System, Technical Memorandum TM-81 (Boeing Aerospace Company for Huntsville Division, U. S. Army Corps of Engineers, December 1974). Cross-coupling models for small enclosures and conduit runs based on comparisons with available test data were constructed. These models were used to calculate a variety of cross-coupling situations for the SAFEGUARD system.

Vincent, M. L., C. C. Sutter, and G. L. Maxam, *Guideline for Application of Single-Line Modeling to B-1 Internal Coupling*, AFWL-TR-75-135/ADB011208 (Air Force Weapons Laboratory, April 1976). This report describes the development of the SNGLIN program, in which coupling between conductors is determined from the basic transmission line equations and transfer functions between the conductors.

Saturation Effects

Dahlen, G., K. Daxberg, L. Hoglund, B. Sjoholm, and M. Wik, "A Survey of Swedish Nuclear Electromagnetics (EMP) Research," *International EMC Symposium Record 1973*, IEEE 73 CHO 751-8 EMC (1973), pp 12-18. This report surveys some of the completed and current research at the Research Institute of Swedish National Defense (FOA) on the EMP, its effects, and protection problems. Studies include tests of conduits and EMP-shielded cables. A curve showing pulse transmission through a saturated Fe cable shield is given.

Kozakoff, P. J., *Diffusion of Transient Electromagnetic Fields Thru Saturated Ferromagnetic Media*, AD721906 (U. S. Army Corps of Engineers, Huntsville Division, June 1970). This report describes a computer solution of the ferromagnetic saturation effects. The solution incorporates material characteristics directly into the field equations.

Transmission Line Effects

Brown, Glen L., *General Solutions and Simplified Formulas for Calculating EMP Induced Currents in Lossless Transmission Lines*, PEM-27 (Lawrence Livermore Laboratory, undated). This note presents the transmission line equation for EMP coupling, the general solution for currents in the frequency domain, useful formulas for calculation of currents in the lossless line, and some experimental comparisons. Examples shown are a transmission line long in relationship to pulse length and a transmission line short in relationship to pulse length.

REFERENCES

Aluminum Electrical Conductor Handbook (The Aluminum Association), pp 17-2 and 17-6.

Aluminum Standards and Data, 5th Ed. (Aluminum Association, 1976), p 39.

American National Standard Specification for Rigid Steel Conduit, Zinc Coated, ANSO 630.1-1971 (R-1966) (American National Standard Institute [ANSI]).

As-Built Survey and Evaluation of EMP/RFI Protection Features, Vol 2, HND-SP-72-145-ED-R (Huntsville Division [HND], U. S. Army Corps of Engineers, August 1973).

Brown, S. S. and F. W. Anney, *Electrical Resistivity of Line Pipe Steels*, Paper No. 69, 20th Annual Conference of National Association of Corrosion Engineers (1964).

Cowdell, R. B., R. A. Hupp, and J. N. O'Leary, *RFI Attenuating Materials and Structures*, Technical Report AFAPL-TR-69-89 (Air Force Aero Propulsion Laboratory, Air Force Systems Command, 1969), p 125.

Erskine, J. L. "Calculation of the Fields in a Closed Cylinder Resulting from an Electromagnetic Pulse," *IEEE Electromagnetic Compatibility Symposium Record* (1968), pp 291-297.

Favaudo, B. D. and L. C. Martin, *Review of Factors for Application in Component Damage Analysis*, Protection Engineering and Management (PEM) note, PEM-52 (September 1976).

Federal Specification Conduit, Metal, Rigid; and Coupling Elbow, and Nipple, Electrical Conduit: Zinc Coated, WW-C-Bld (Federal Supply Service, General Services Administration, June 5, 1962).

Federal Specification Conduit, Metal, Rigid: Electrical, Thin-Wall Steel Type (Electrical Metallic Tubing); Straight Lengths, Elbows, and Bends, WW-C-563A (General Services Administration, December 1973).

Fink, E. G., Editor-in-Chief and J. M. Carroll, Associate Editor, *Standard Handbook for Electrical Engineers*, 10th Ed. (McGraw Hill, 1968), p 4-8.

Gray, D. E., *American Institute of Physics Handbook*, 3rd Ed. (McGraw Hill, 1972), p 9-39.

Harrison, Charles W., "Transient Electromagnetic Field Propagation Through Infinite Sheets," *IEEE Transactions on Antenna and Propagation*, Vol AP-12, No. 3 (May 1964), pp 319-334.

Interim Federal Specification Conduit, Metal, Rigid: and Coupling, Elbow, and Nipples, Electrical Conduit: Aluminum, WW-C-00540c (GSA-FSS) (Federal Supply Service, General Services Administration, 1967), p 2.

King, R. W. P. and E. W. Harrison, "Cylindrical Shields," *IEEE Transactions on Antenna and Propagation*, Vol AP-9, No. 2 (1961), pp 166-170.

Leverenz, D. J., W. Croisant, and J. Verdeyen, "Electromagnetic Induced Diffusion Signals on Conduit Protected Cables," *IEEE-EMC Symposium Record*, IEEE CHO 803-7 EMC (1974).

Leverenz, D. J., R. G. McCormack, and P. H. Nielsen, *Development and Evaluation of Repairs and EMP Leaks in Conduit Systems*, Technical Report C-17/ADA011223 (U. S. Army Construction Engineering Research Laboratory [CERL], April 1975).

Leverenz, D. J., R. G. McCormack, and P. H. Nielsen, *EMP Shielding Properties of Conduit Systems and Related Hardware*, Technical Report C-19 ADA012729 (CERL, June 1975), p 11.

Lyman, T., Ed., *Metals Handbook*, Vol 1, 8th Ed. (American Society for Metals, 1961).

Miller, D. A. and P. P. Toulias, "Penetration of Co-Axial Cables by Transient Fields," *IEEE Electromagnetic Compatibility Symposium Record* (1968), pp 414-423.

National Electrical Code, 1975 Edition, NFPA No. 70-1975, National Fire Protection Association. This has been approved by the American Standards Institute and is also known as ANSI C1-1975.

Nuclear Electromagnetic Pulse Protection, TM 5-855-5 (Department of the Army, February 1974).

Reference Data for Radio Engineers, 6th Ed. (H. W. Sams & Co., 1975), p 4-32.

Roberts, H. A., J. Capobianco, and F. Agee, *SAFEGUARD Buried Conduit Studies* (Harry Diamond Laboratories [HDL], undated).

SAFEGUARD EMP/RFI Lessons Learned (SAFEGUARD Ground Facilities), HND-SP-75-350-ED-SR (31 December 1975).

Schelkunoff, "The Electromagnetic Theory of Co-axial Transmission Lines and Cylindrical Shields," *Bell System Technical Journal*, Vol XIII (1934), pp 532-579.

Standard for Electrical Metallic Tubing, UL797 (Underwriters' Laboratories [UL], Inc., 20 June 1973). Approved as ANSI 33.98-1973, 20 June 1973).

Standard for Rigid Metal Conduit, UL6, 8th Ed. (UL, 1976), p 5.

Standard Handbook for Electrical Engineers, Reference Data for Radio Engineers, 6th Ed. (H. W. Sams & Co., 1975), p 4-21.

Underwriters' Laboratories, Standard 6 (1976), Table 5-2. *Revised Outline of Proposed Investigation for Intermediate Metal Conduit* (1976), Table 8.1.

USA Standard Specification for Electrical Metallic Tubing, Zinc Coated, USAS C80.3-1966 (American National Standards Institute).

USA Standard Specification for Rigid Aluminum Conduit, USAS C80.5-1966 (ANSI).

Vance, E. F., *Coupling to Cables*, DNA Handbook Revision, Chapter 11, ADB001204 (Defense Nuclear Agency, December 1974).

Vance, E. F., *Design Guidelines for the Treatment of Penetrations Entering Communications Facilities*, ADB007076 (Defense Nuclear Agency, August 1975).

Vance, E. F., *Electromagnetic - Pulse Handbook for Electric Power Systems*, ADA009228 (Defense Nuclear Agency, February 1975), pp 145, 26.

Vance, E. F. *(Electromagnetic-Pulse)* Handbook DNA-2114H-2 (Defense Nuclear Agency, December 1944), Chapter 11, ADB001204. The total document, DNA-2114H-2, is classified confidential; however, Chapter 11 is available in an unclassified version from the Defense Documentation Center using the reference AD number.

Vance, E. F., *Treatment of Penetrations Entering Communications Facilities*, ADB007076 (Defense Nuclear Agency, August 1975), p 2.

Vance, E. F. and J. E. Nanvicz, "Internal Voltages and Currents in Solid Shielded Cables," *IEEE Electromagnetic Compatibility Symposium Record* (1968), pp 198-209.

Whitson, A. L., *Engineering Techniques for Electromagnetic Pulse Hardness Testing*, Report DNA 332F/AD786722 (Defense Nuclear Agency, September 1974), p 150.

CERL DISTRIBUTION

Chief of Engineers
ATTN: DAEN-ASI-L (2)
ATTN: DAEN-MCE-D/H. McCauley
ATTN: DAEN-RDL
Dept of the Army
WASH DC 20314

US Army Engr Div, Huntsville
ATTN: Library (2)
ATTN: Chief, HNDED-SR
PO Box 1600, West Station
Huntsville, AL 35807

Defense Documentation Center
ATTN: TCA (12)
Cameron Station
Alexandria, VA 22314

Croisant, William
Development of conduit design analytical procedure / by W. Croisant ... (et al.). -- Champaign, Ill. : Construction Engineering Research Laboratory ; Springfield, Va. : available from National Technical Information Service , 1978.
147p. : ill. ; 27 cm. (Interim report. Construction Engineering Research Laboratory ; M-234)

1. Electric conduits. 2. Shielding (electricity) I. Nielsen, Paul. II. Sieber, David. III. McCormack, Raymond G. IV. Title. V. Series: U.S. Construction Engineering Research Laboratory. Interim report ; M-234.